C E S R

A Design Report for the

CORNELL ELECTRON STORAGE RING

This report is an appendix to a
proposal submitted to the National Science Foundation

April 1977

CORNELL UNIVERSITY
Laboratory of Nuclear Studies
Ithaca, New York 14853

CESR DESIGN REPORT

Table of Contents

CESR Design Progress Report

September 1976

The purpose of this report is to serve as an update for CLNS-345, the design report of October 1976, and to present a description of the prototype work accomplished.

The principal features of the design have been well established for some time and many of the details are in hand. Prototypes of the economically important and technically difficult components are already in an advanced stage. We anticipate that by October 1977 the design and prototyping of the major individual components will be complete so that manufacture could begin were funds available.

1. General Features of CESR

The proposed CESR project (Cornell Electron Storage Ring) has as its goal the modification of the existing 12 GeV Synchrotron facility to provide high luminosity colliding beams of electrons and positrons. The initial beam energy is 8 GeV (16 GeV in the center of mass) with the possibility for extension to 10 GeV being included in the design. The major modification of the present facility required is the addition of a second ring of guide field magnets to the tunnel housing the Synchrotron. Figure 1-1 shows an artists conception of the present tunnel and laboratory building complex. Figure 1-2 is a photograph of the synchrotron with a prototype of one storage ring magnet unit in place. In the tunnel the separation of the two beam lines is about 1.6 meter.

In the added storage ring, single bunches of electrons and positrons will collide in the South experimental hall, now used for synchrotron

experiments, and at a diametrically opposite point on the North side. Fig. 1-3 is a schematic plan view of the existing South area with the colliding beam storage ring and its 8x8 meters experimental pit added. Figure 1-4 is a photograph of the South experimental hall with the projected crossing point indicated.

The floor of the pit will be 3.8 meters below the beam line while the distance between synchrotron and storage ring beam lines at the crossing point will be 5.6 meters. Figure 1-5 is the corresponding schematic diagram for the north area together with a vertical section. While the north area will be relatively undeveloped for colliding beam experiments in the beginning, it would be possible to add access from the surface, laboratory space and a pit at a future date should that become desirable. It is estimated that interruption of colliding beam operation for this purpose could be kept to a maximum of 4 months.

Besides the addition of the storage ring to the tunnel, other modifications are required. As can be seen in Fig. 1-3, a flare must be constructed at the East end of the south hall to allow the storage ring to separate from the synchrotron. In conjunction with this flare we intend to provide space and access so that the synchrotron light emerging from the high field bending magnets adjacent to the interaction region can be used. This feature is described in more detail in a later section. In addition to this modest construction, two new cooling towers must be installed to accommodate the additional magnet and RF power load and the linac injector must be upgraded to provide sufficient positron intensity. The linac upgrade, being necessary for development studies of the proposed injection method, is well along and is being accomplished by the addition of the former CEA linac to our present injector.

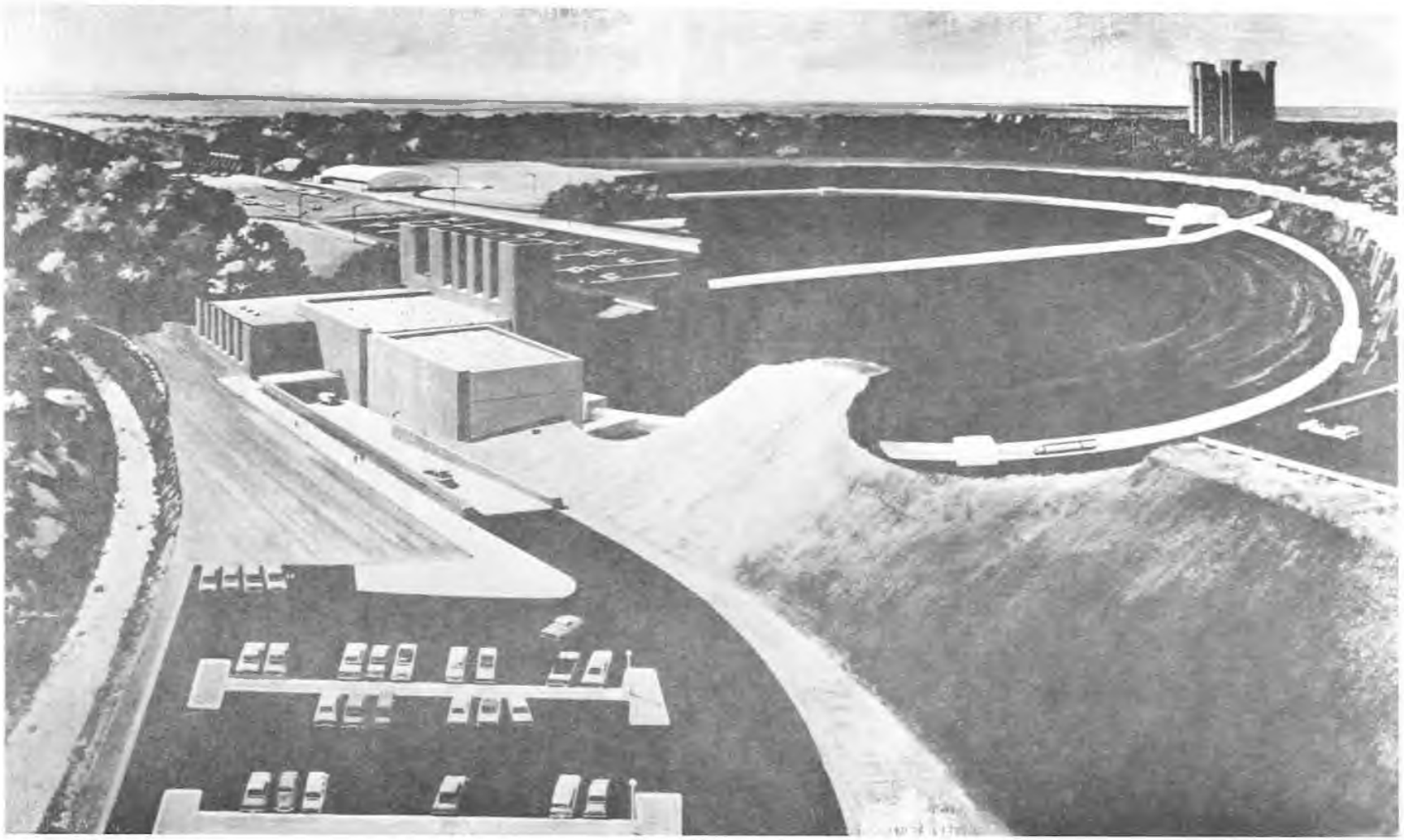

Fig. 1-1 Artists conception of present tunnel and laboratory complex

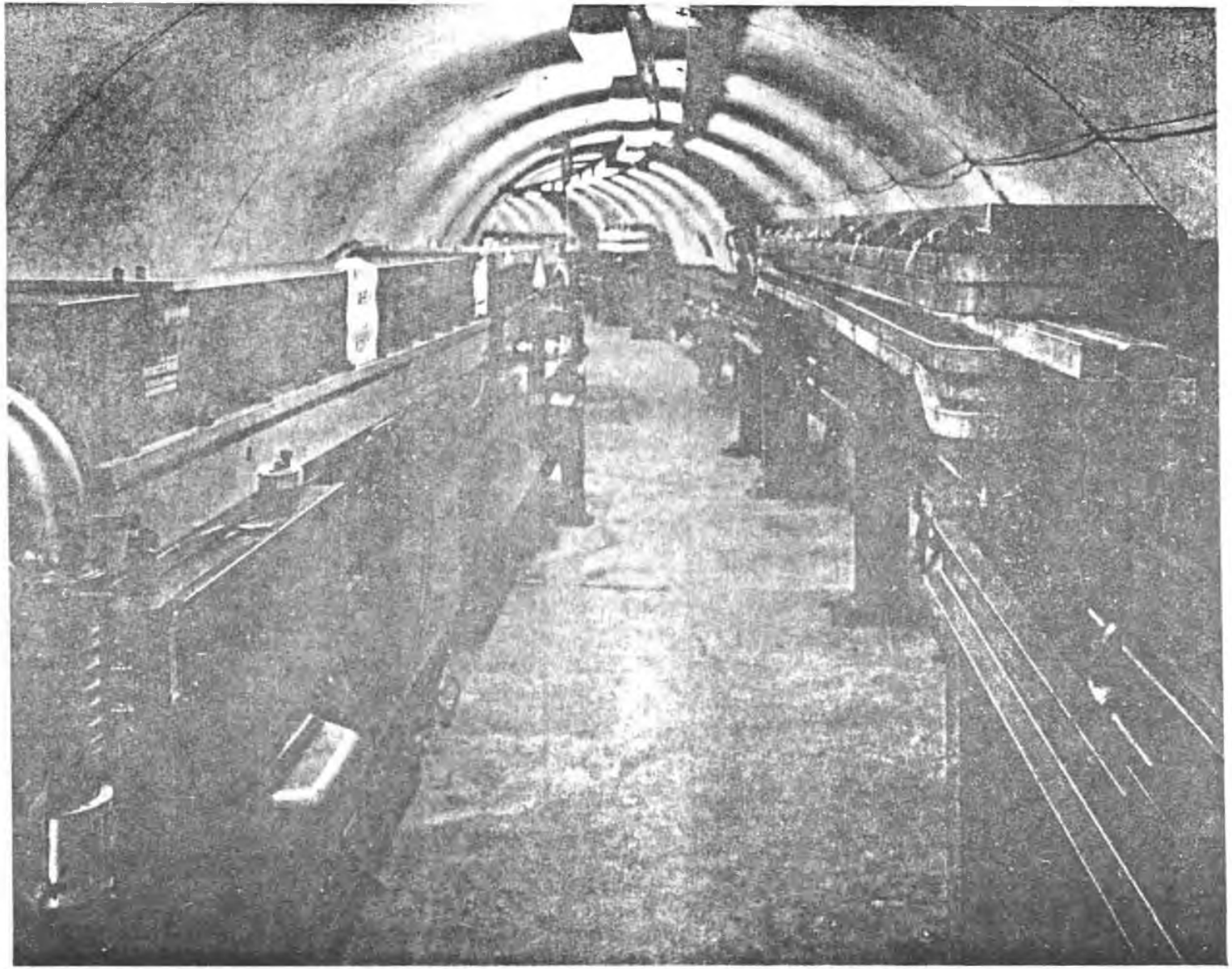

Fig. 1-2 Synchrotron tunnel with a prototype of storage ring dipole magnet in place.

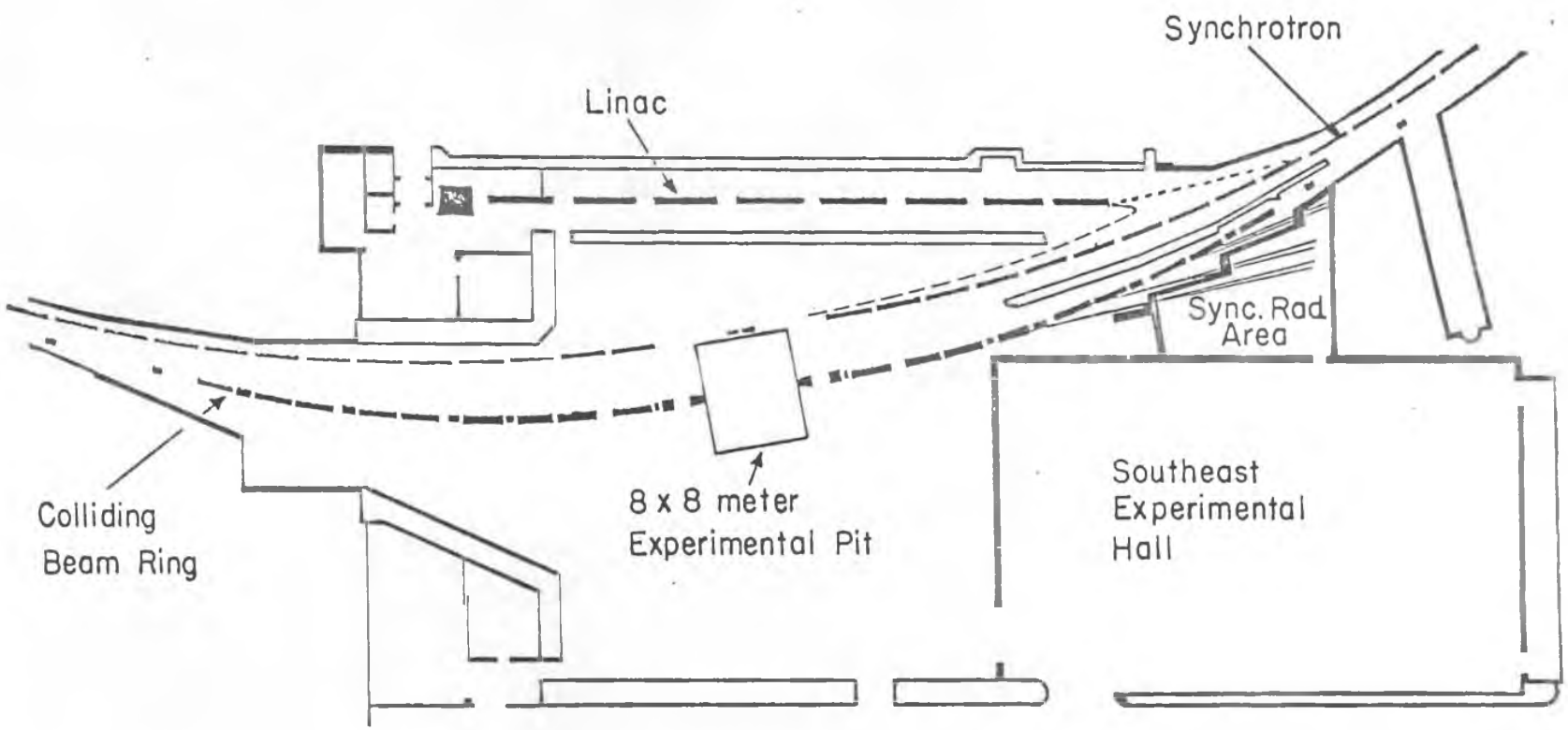

Fig. 1-3 Schematic plan view of south experimental area including new experimental pit modified east flare with synchrotron radiation area.

Fig. 1-4 South Experimental Hall - "X" indicates projected beam crossing point.

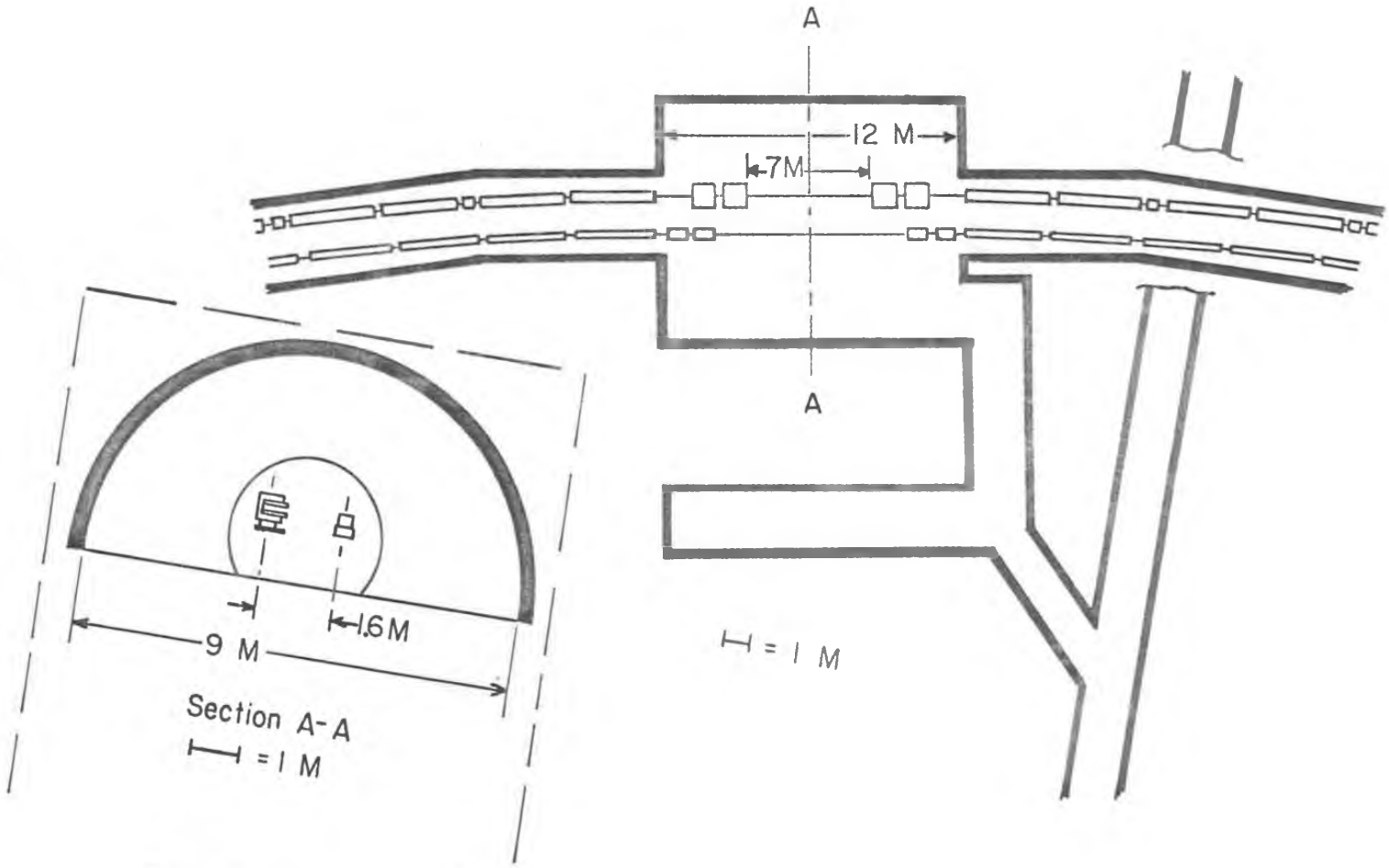

Fig. 1-5 Schematic plan and elevation view of intersection area in the north room.

2. General Machine Parameters

The table below is a list of parameters characterizing the principal features of CESR. Figure 2-1 is a plot of design luminosity vs. energy for 2 MW rf power. Figure 2-2 is a line diagram of the overall geometry and component disposition.

TABLE I

Design luminosity at 8 GeV	$10^{32}\text{cm}^{-2}\text{sec}^{-1}$
Number of interaction regions	2
Free space between quadrupoles at IR's	7 meter
South IR pit dimensions (tentative)	8x8x3.8 meter
Synchrotron-storage ring beam line separation at south IR	5.3 meter
Detector magnet power available at south IR	2 MW
Number of bunches per beam	1
Number of particles per bunch (8 GeV)	$1.5\text{x}10^{12}$
Circumference	768.429 meter
Revolution time	2.56 μsec.
Max. bending radius	87.89 meter
Min. bending radius	32.57 meter
Max. bending field at 10 GeV	1.02 T
Cell length	16.40 meter
Cell type	FODO
Magnet power at 8 GeV	950 kW
RF power at 8 GeV	2000 kW
Beam separation at North IR	1.4 M

3. Orbit, Geometry, Optics and Beam Characteristics

a) Geometry

While the most basic geometry of the storage ring is fixed by the existing tunnel with its six straight sections, some modification is necessary to provide unemcumbered space for the physics experimental apparatus.

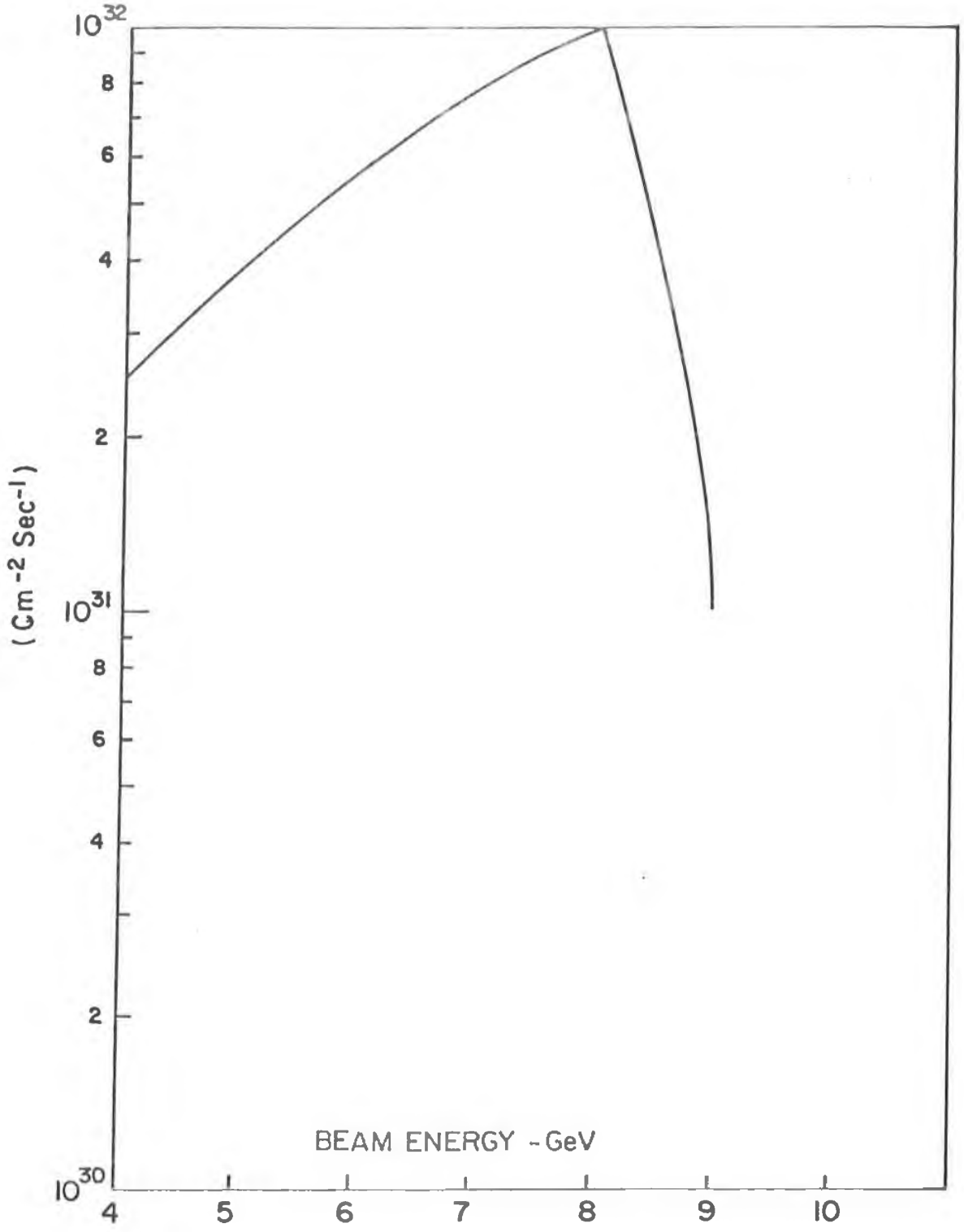

Fig. 2-1 Luminosity vs. Energy for 2 MW rf power

This is accomplished in the south area by putting a bulge into the storage ring orbit, increasing the distance between the synchrotron and storage ring to 5.6 meters at the crossing point. The bulge is engendered by inserting two 22.2 meter straights, called the "bulge straights", into the storage ring, allowing its equilibrium orbit to depart from the synchrotron orbit. These straights are symmetrically disposed about the south crossing point. At the ends of these straights nearest the crossing point, a series of four bending magnets of high field are placed to bring the storage ring equilibrium orbit parallel to the synchrotron again. The bending magnets immediately adjacent to the interaction region both have fields lower than the abrupt bends of the bulge to protect the crossing region from bombardment by the hard x-rays coming from synchrotron radiation in the high field magnets. Provision for alleviating the synchrotron radiation problem is discussed in a separate section.

The bulge straights will be used for the rf cavities and some wiggler magnets. The four 6 meter straights, associated in the synchrotron with rf acceleration, will be used for major injection equipment, some wigglers and for diagnostic and instability prevention equipment. The major part of the diagnostic equipment will be located in short spaces provided in each half cell (see Fig. 3-4) and in eight 1 to 2 m straights located at points shown in Fig. 3-3.

b) Optics and Beam Characteristics

Experience with colliding beam devices has shown that flexibility of the guide field optics is of prime importance. This flexibility is required for maximizing the luminosity over a range of energies and for the diagnosis and cure of instabilities.

The chief parameters which require control are the horizontal and vertical betatron amplitude functions at the interaction points, β_H^* and β_V^*, and the dispersion function at those points, η^*. In addition, it is necessary to control η and/or certain combinations of η and β around the ring to manipulate the beam size.

To allow maximum flexibility we have decided to provide the capability for varying each focusing element of the storage ring individually.

For designing the component dispositions and appropriate settings for the focusing elements we have developed a number of efficient computer programs for geometry calculations, manipulation of the transfer matrices of individual components, and computation of the relevant radiation integrals and luminosities including coupling. For design optimization these are combined with a highly efficient optimization routine developed in the Cornell Computer Science Dept.[1] For a given component disposition these combined programs can find the required quadrupole strengths by optimizing the luminosity subject to a series of weighting factors which limit the aperture, maximum β and η values and maximum quadrupole gradients. The beam energy is inserted as a fixed parameter. Figure 3-1 is a computer print out showing some of the results of these calculations for 8 GeV beam energy. The envelope functions , $\sqrt{\beta_H}$ and $\sqrt{\beta_V}$ are shown to scale as is the component disposition for 1/2 the ring.[2]

---

[1] J.E. Dennis and H. Mei, An Unconstrained Optimization Algorithm, TR 75-246, Dept. of Computer Science, Cornell University.

[2] Lateral dimensions of components are not to scale. "300" labels represent quadrupoles. "400" labels represent sextupoles.

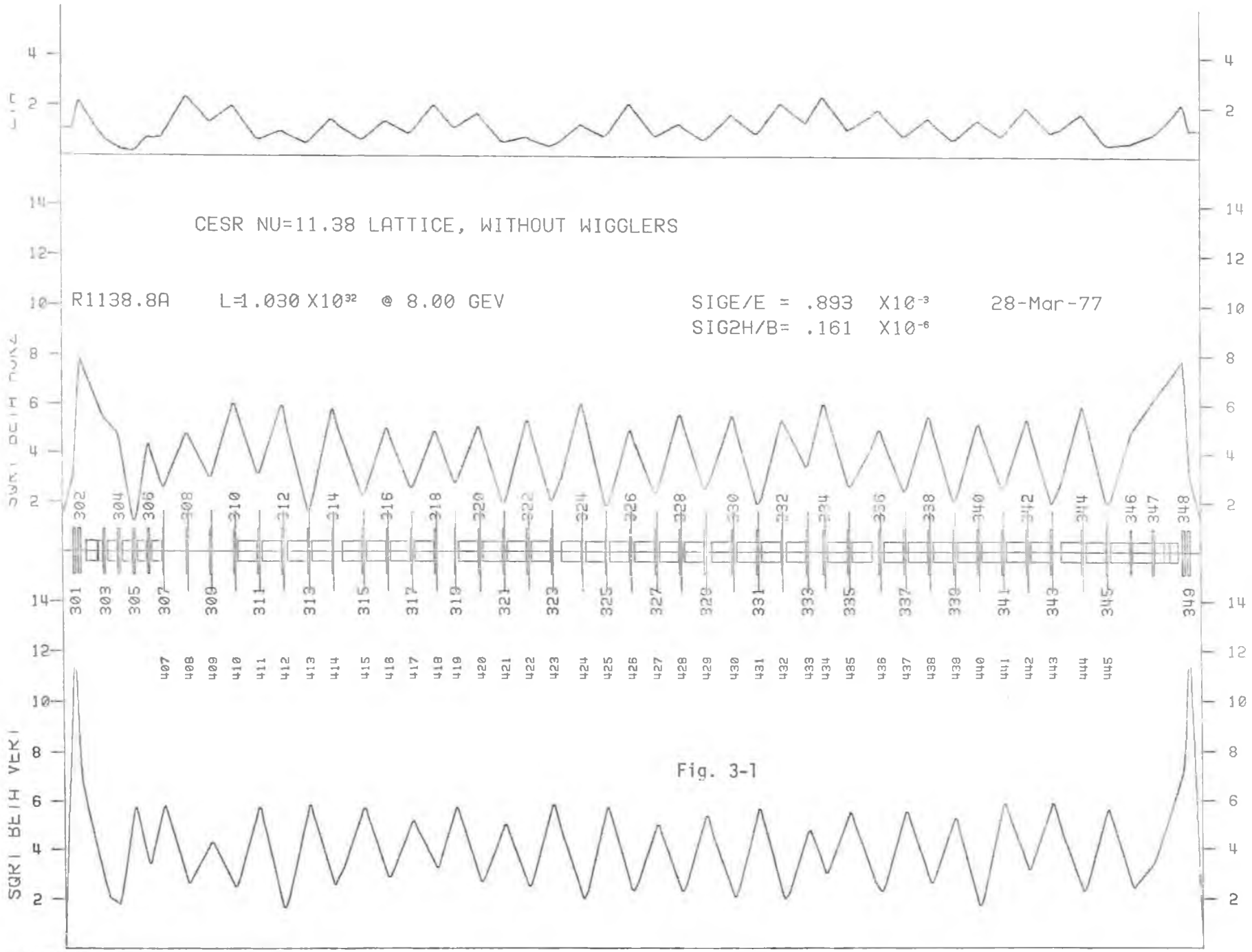
CESR NU=11.38 LATTICE, WITHOUT WIGGLERS
R1138.8A L=1.030 X10³² @ 8.00 GEV
SIGE/E = .893 X10⁻³
SIG2H/B= .161 X10⁻⁶
28-Mar-77
SQRT BETA H,V
(METERS)
1 INCH=100 WAVES AT 713.945 MHZ

Fig. 3-1

Figure 3-2 is a computer drawing of the horizontal beam envelope ($\pm 10\sigma$) as calculated for this 8 GeV lattice. Figure 3-3 is a detailed description of lattice and some beam properties at 8 GeV.

In the lattice geometry shown, a free space of 7 meters is provided at each intersection region. The quadrupole pairs flanking this region control the betatron amplitude functions at the crossing point. Beyond each pair, a group of quadrupoles matches the lattice functions to the rest of the ring while at the same time providing a means of independent adjustment of the dispersion function at the crossing point. The following 21 meter drift space (see Fig. 2-2) is part of this flexible matching section and will be the location for the rf cavities and some wiggler magnets as previously stated. Control of η around the ring can be exercised by varying the dispersion match between these sections and the rest of the lattice. The regular section of the lattice consists of standard FODO cells roughly 16m long; the schematic layout of a half cell is shown in Fig. 3-4.

The luminosity vs. energy of Fig. 2-1 is given presupposing that the beam size can be kept roughly constant throughout the energy range. Were the magnet currents simply scaled with energy this would not be the case, but rather the luminosity would vary as E^4. To keep the beam size or emittance large as the energy falls, two methods have been investigated. The first, called the method of η mismatch[3], which utilizes azimuthal variation of the dispersion function, tends to make the beam envelope

---

[3] R. Helm, M. Lee, J. M. Paterson, Proc. IX International Conference on High Energy Accelerators, p. 100.

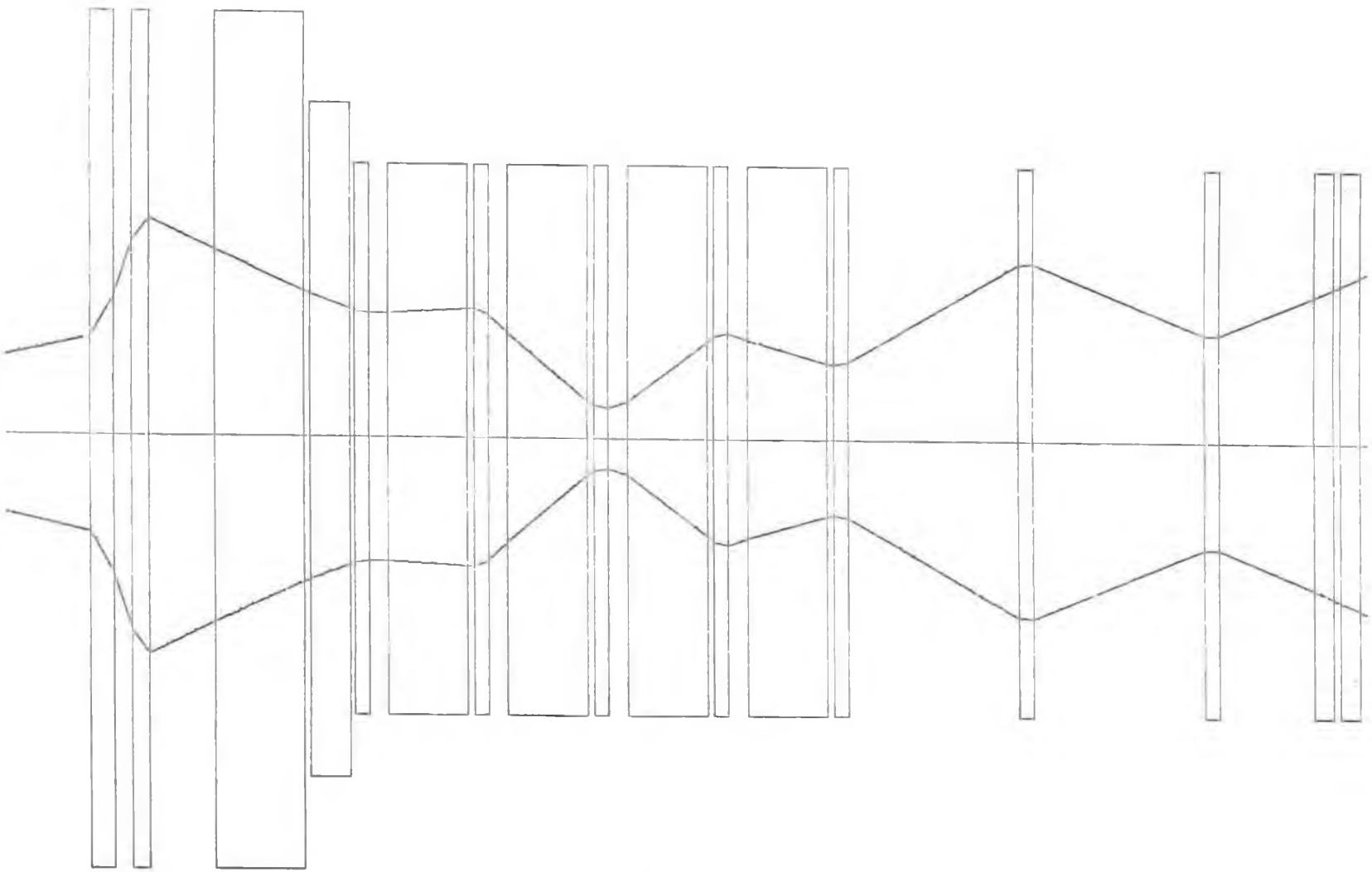

Fig. 3-2 Horizontal beam envelope.

```
BETA* VERT    HORZ     ETA     LUMINOSITY          NU     CHROMATICITY              PAGE        0          14:43  28-Mar-77
L0  .1001    1.7453  1.103   0.1030E+33    VERT   11.380  -31.032   SIG2H/B 0.16091E-06  ALPHA/P .00868450     CONFIG R1138.8A
L3  .1000    1.7111  1.105   0.1031E+33    HORZ   11.380  -18.249   SIGE/E  0.89270E-03  CIRCUM 1829.99991     LIST
                                                                                                              GEV=        8.0000
AREA:    L0 LARGE APERTURE    HIGH BEND (202)     BULGE STRAIGHT      NORMAL LATTICE    L3 LARGE APERTURE      MEV/TURN    5.0118
APER V    74.571  1TH 301     42.818  1TH 307     34.331  1TH 309     43.083  1TH 313    74.590  1TH 349     OPT COUP    0.5642
BETA V   129.556  1TH 301     33.467  1TH 307     18.396  1TH 309     34.009  1TH 313   129.633  1TH 349     PARTIC 0.1500E+13
APER H    83.543  1TH 302     53.537  1TH 202     69.649  1TH 310     74.101  1TH 334    83.301  1TH 348     LIMIT      L0
BETA H    60.956  1TH 302     27.580  1TH 202     35.947  1TH 310     36.350 35TH 201    60.858  1TH 348     POLIZ     26.6 MIN
 ETA       2.158  1TH 302      0.842  1TH 307      2.341  1TH 308      2.375  1TH 334     2.137  1TH 348
ODD,EVEN * SEXT STRENGTHS= -0.4698  0.1807
                                                                                                    (COMBINATIONS: / ENDS)
  (STARTING WITH 110)  L0 * ------
COMBINATION NOTATION EXAMPLE:
111 104 201 102 201 103 [0]  MEANS
IN LATTICE SEQUENCE AT RIGHT,
REPLACE 1 WITH 104 201 102 201 103
SEQUENCE STARTS AT L0 * AFTER FIRST

'/' AND ENDS IN L3* AFTER SECOND '/'

ELEMENT TYPE IS CODED BY HUNDREDS DIGIT
IE  3NN=QUAD  2NN=BEND   1NN=DRIFT
```

```
1 104 201 103 0  3 101 202 102 0/
110 301 400 111 302 400 112 203 102 204 103 303 400 3 304 400 3 305   ( (0) SEPARATE)
400 3 306 400 3 307 407 109 308 408 109 309 409 109 310 410 1 311
411 1 312 412 120 1 313 413 1 314 414 121 1 315 415 1
316 416 1 317 417 1 318 418 105 319 419 1 320 420 1 321 421 1
322 422 1 323 423 122 1 324 424 1 325 425 1
326 426 126 1 327 427 1 328 428 128 1 329 429 123 1 330 430 130 1          (1/2 MACHINE)
331 431 1 332 432 132 1 333 433 106 334 434
1 335 435 1 135 336 436 136 1 337 437 1 338 438 138 1
339 439 1 340 440 1 341 441 1 342 442 1 343 443 124 1 344 444 1
345 445 1 346 400     103 201 103 347 400 103 206 204 108 205
119 348 111 349 400 110/
                                                    ---------L3 *
```

(FOR .1% K CHANGE)

LABEL	DNU VERT	DNU HORZ
SUM	0.013164	0.013500
ABS	0.020761	0.019931
RMS	0.003895	0.003736
301	0.013489	-0.001266
302	-0.003622	0.003818
348	-0.003732	0.003598
349	0.013141	-0.001237

'SUM' =ALGEBRAIC SUM OF NU-SHIFTS FROM INDIVIDUAL K-ERRORS OF .1 % IN NORMAL QUADRUPOLES.

'ABS' =SUM OF ABSOLUTE VALUES FROM INDIVIDUAL K-ERRORS OF .1% IN NORMAL QUADRUPOLES.

'RMS' SQUARE ROOT OF SUMED SQUARES OF NU SHIFTS TAKEN AS ABOVE.

301 302 ARE L0 INTERACTION QUADS
348 349 ARE L3 INTERACTION QUADS

QUAD LABEL	LENGTH (METERS)	K 1/METER**2
323	0.6000	-0.2734740
325	0.6000	-0.2988810
327	0.6000	-0.2785810
329	0.6000	-0.2836630
331	0.6000	-0.3075060
333	0.6000	-0.2869510
335	0.6000	-0.2332940
337	0.6000	-0.2669330
339	0.6000	-0.3011870
341	0.6000	-0.2815690
343	0.6000	-0.2335300
345	0.6000	-0.2759190
347	0.6000	0.0101900

QUAD LABEL	LENGTH (METERS)	K 1/METER**2
301	1.0000	-0.5768110
302	0.7500	0.5573410
303	0.6000	-0.0372810
304	0.6000	0.2575730
305	0.6000	-0.3894480
306	0.6000	0.4786530
307	0.6000	-0.2847940
308	0.6000	0.2326520
309	0.6000	-0.2525090
310	0.6000	0.2333840
311	0.6000	-0.3128350
312	0.6000	0.2852810
313	0.6000	-0.3042450
314	0.6000	0.3047750
315	0.6000	-0.2321010
316	0.6000	0.2688080
317	0.6000	-0.2082120
318	0.6000	0.2580490
319	0.6000	-0.2490250
320	0.6000	0.2800770
321	0.6000	-0.2507170
322	0.6000	0.3161520
324	0.6000	0.2994810
326	0.6000	0.3109190
328	0.6000	0.2704610
330	0.6000	0.2816600
332	0.6000	0.2515520
334	0.6000	0.2652570
336	0.6000	0.2389210
338	0.6000	0.2878490
340	0.6000	0.2860320
342	0.6000	0.2906950
344	0.6000	0.3003770
346	0.6000	0.1171830
348	0.7500	0.5297670
349	1.0000	-0.5591430

LABEL	LENGTH (METERS)	RHO (METERS)	
101	0.80000		QUAD--HI-BEND SPACE
102	0.28000		HI-HI BEND SPACE
103	0.14180		BEND-QUAD SPACE
104	0.88838		SEXT,ETC SPACE
105	6.06000		20FT L5/L1 STRAIGHT
106	5.19800		20FT L4/L2 STRAIGHT
108	0.26000		BEND-BEND SPACE
109	7.40450		BULGE STRAIGHT
110	3.60000		INTERSECTION REGION
111	0.75000		(LARGE) QUAD-QUAD
112	2.06500		L0 SEP PLATES ET AL
119	1.56000		L3 SEP PLATES
120	0.46000		NEW STRAIGHT
121	1.92000		NEW STRAIGHT
122	2.00000		NEW STRAIGHT
123	1.08000		NEW STRAIGHT
124	2.10370		NEW STRAIGHT
126	0.22500		PART OF BUMPER SPACE
128	0.22500		PART OF BUMPER SPACE
130	0.22500		PART OF BUMPER SPACE
132	0.22500		PART OF BUMPER SPACE
135	2.14200		FAST KICKER SPACE
136	0.22500		PART OF BUMPER SPACE
138	0.22500		PART OF BUMPER SPACE
201	6.57273	87.891500	NORMAL BEND :CHEVRON
202	3.33042	32.573000	HI-FIELD BEND
203	3.75570	179.325600	L0 SOFT BEND
204	1.64350	87.891500	1/4 NORMAL BEND
205	2.65520	141.989000	L3 SOFT BEND
206	3.28698	87.891500	1/2 NORMAL BEND

Fig. 3-3 Detailed description of lattice and some beam properties at 8 GeV.

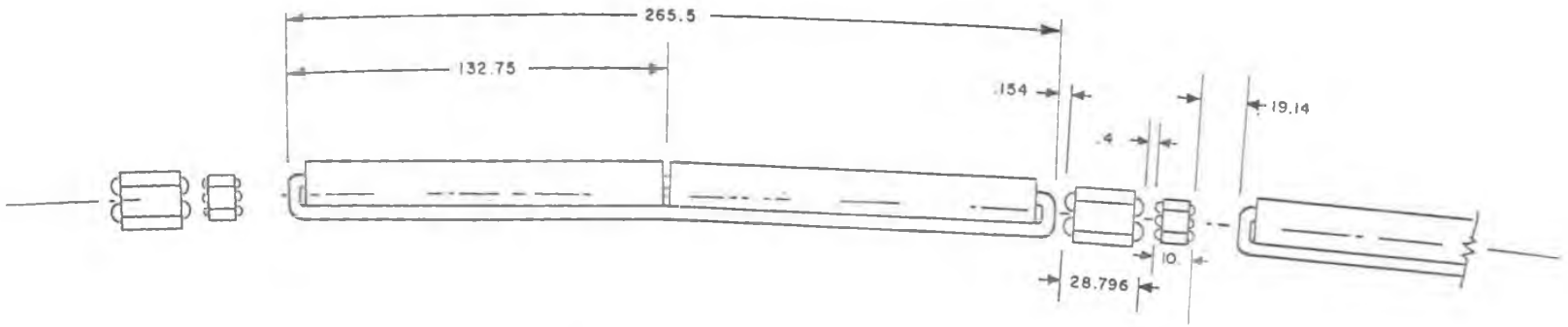

Fig. 3-4 "Half cell dimensions (inches)"

quite nonuniform and is limited in its power by requiring very large dispersions for the lowest energies. Nevertheless, it allows us, at least in principle, to keep optimum luminosity down to about 3.0 GeV beam energy. The second method, called the wiggler method,[4] works by adding localized and controllable radiation excitation to the beam, thereby increasing the incoherent phase space volume of the beam. This method has the advantage that it gives easy control and at the same time minimizes the radiation damping and polarization times and keeps the bunch length up. Both of these methods have been investigated at other laboratories but have had their primary development at SLAC. CESR will have the capability for employing both of these methods.[5]

Figures 3-5, 3-6, 3-7, and 3-8 show envelope functions for 5 and 3 GeV with eta mismatch or wigglers. The location of the wiggler magnets is shown in the component layout diagram. Table 3-1 is a list of principal orbit and beam parameters at 3 different energies. By combining powerful wigglers with eta mismatch it appears that in principle we could run CESR at as low a beam energy as 1.5 GeV. Below 2 GeV the useful luminosity will be limited by the Touschek lifetime.

The momentum dependence of quadrupole focal lengths gives rise to chromatic aberrations. It is well known that it is necessary to correct this chromaticity, or momentum dependence of the betatron tunes, to a

---

[4] Control of Beam Size and Polarization Time in PEP, J.M. Paterson, J. Rees, H. Wiedemann, PEP-125.

[5] One should note that the η mismatch method is peculiarly adapted to the CESR lattice with its high field magnets in the bulge. Small changes in dispersion in that region have large effects on the radiative excitation of the emittance. Indeed, in a generalized way, one might look upon the CESR lattice as a global wiggler where one controls η at the high field region rather than the field itself.

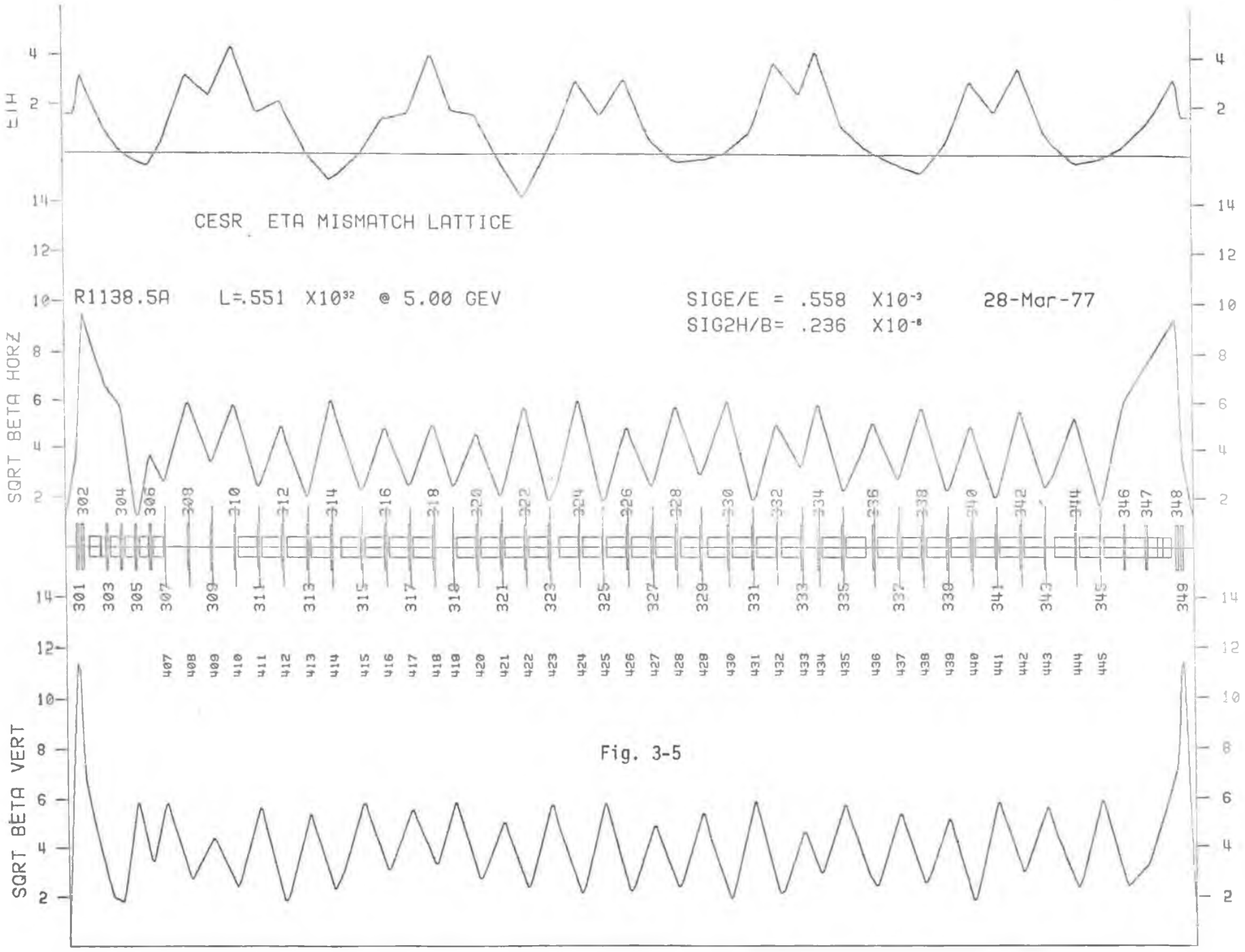
ETA H
CESR ETA MISMATCH LATTICE
R1138.5A L=.551 X10³² @ 5.00 GEV
SIGE/E = .558 X10⁻³
SIG2H/B= .236 X10⁻⁸
28-Mar-77
SQRT BETA HORZ
SQRT BETA VERT
(METERS)
1 INCH=100 WAVES AT 713.945 MHZ

Fig. 3-5

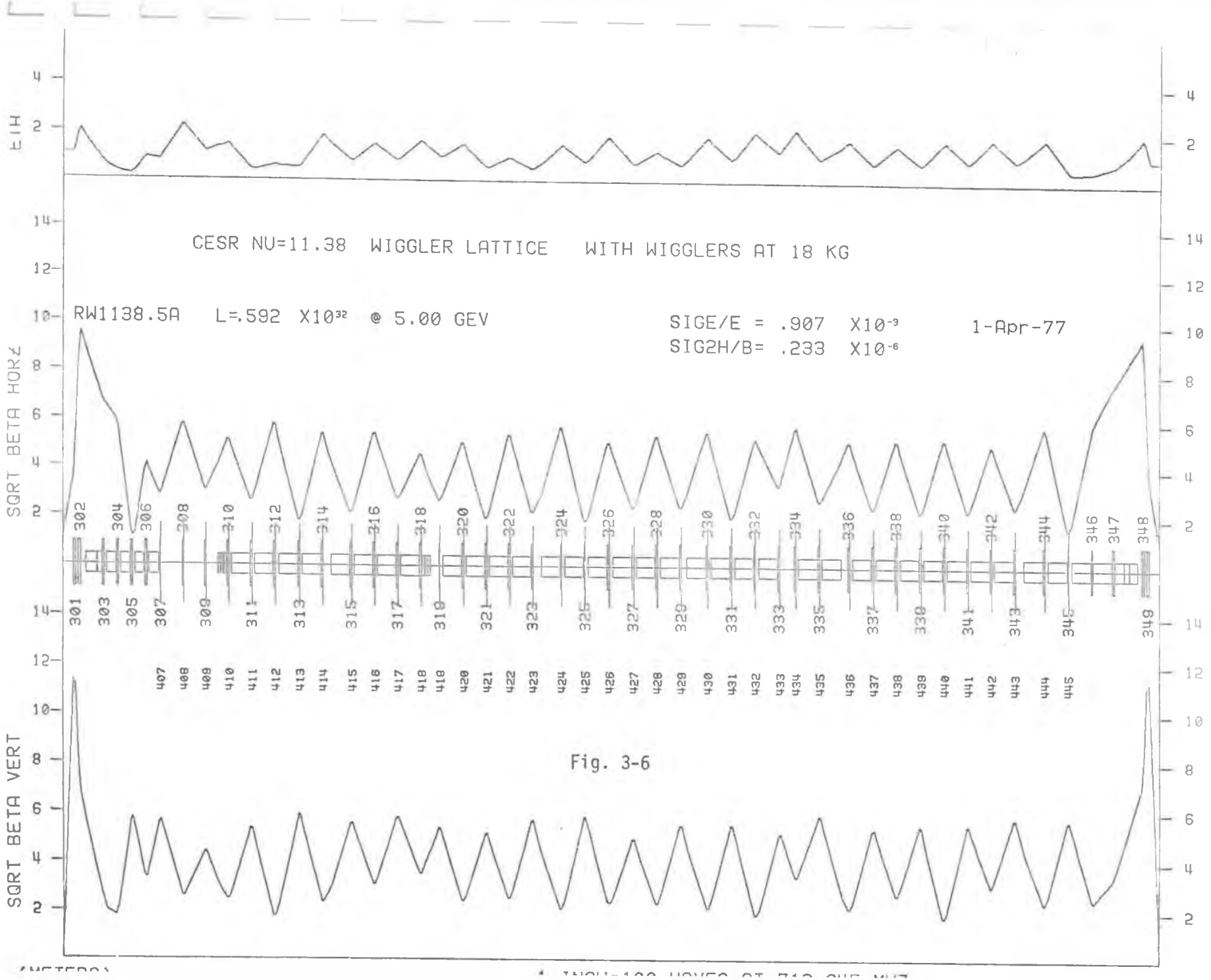
CESR NU=11.38 WIGGLER LATTICE WITH WIGGLERS AT 18 KG
RW1138.5A L=.592 X10³² @ 5.00 GEV
SIGE/E = .907 X10⁻³
SIG2H/B= .233 X10⁻⁶
1-Apr-77
SQRT BETA HORZ
SQRT BETA VERT

Fig. 3-6

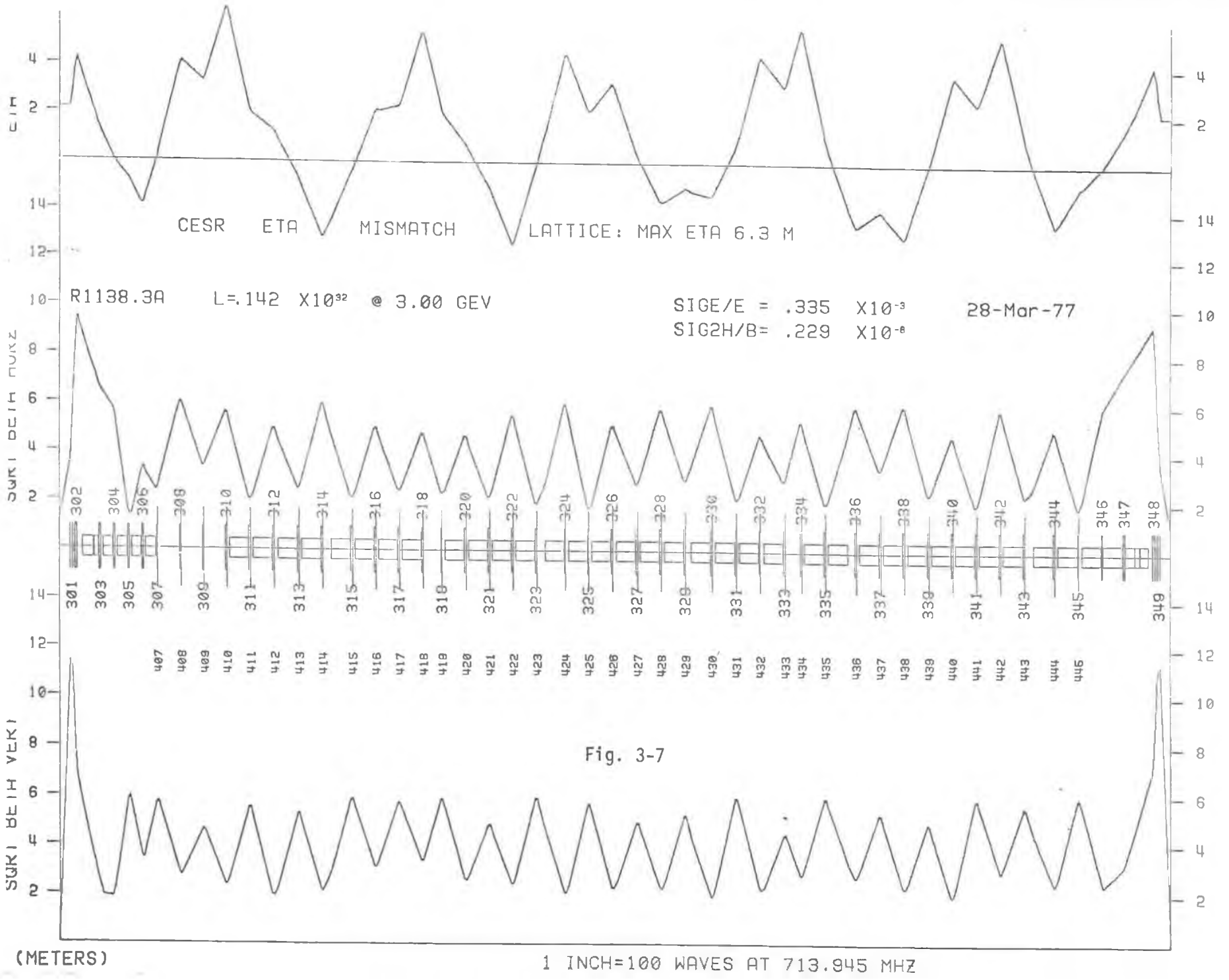
CESR ETA MISMATCH LATTICE: MAX ETA 6.3 M
R1138.3A L=.142 X10³² @ 3.00 GEV
SIGE/E = .335 X10⁻³
SIG2H/B= .229 X10⁻⁶
28-Mar-77
(METERS)
1 INCH=100 WAVES AT 713.945 MHZ

Fig. 3-7

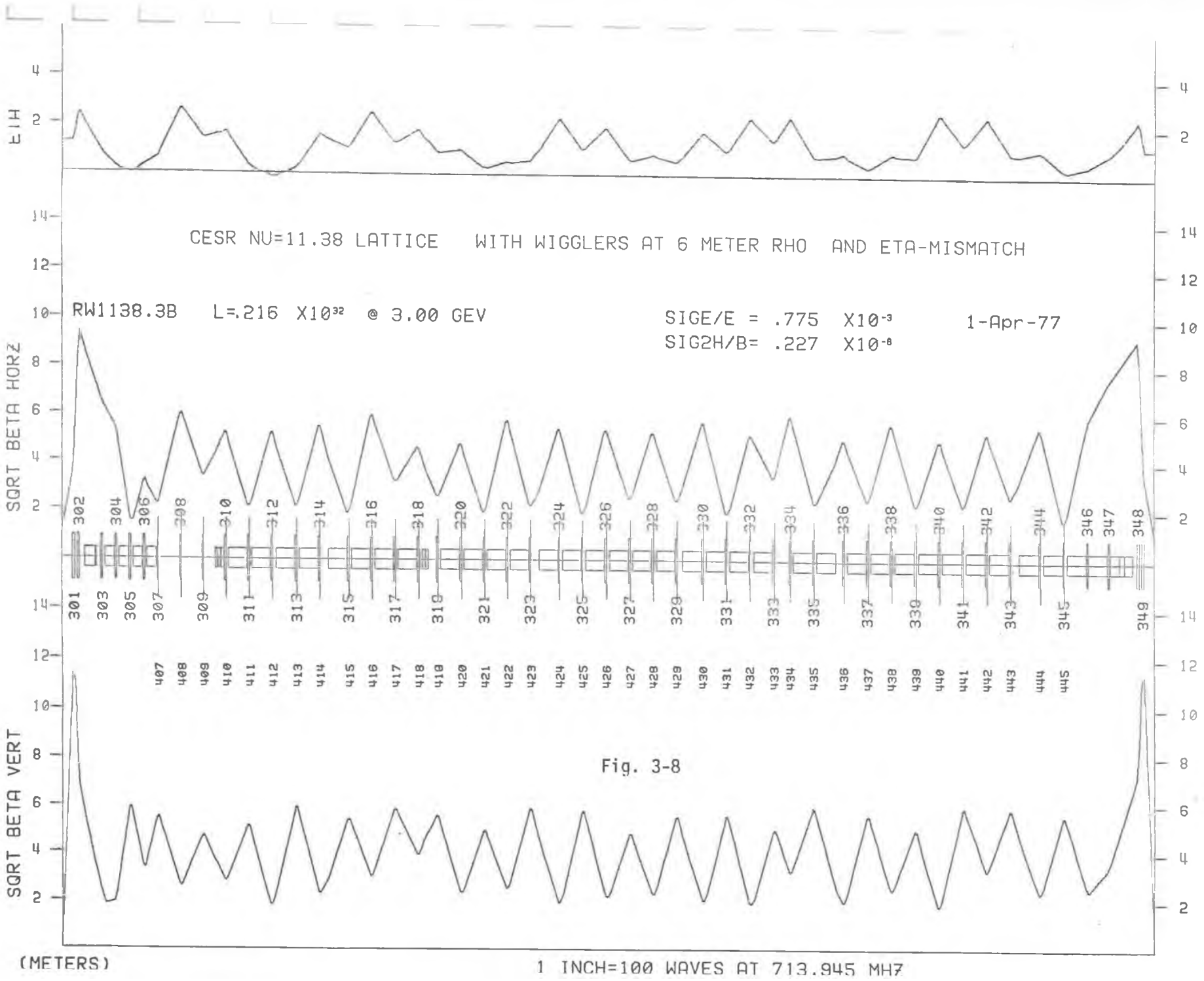
ETH
CESR NU=11.38 LATTICE WITH WIGGLERS AT 6 METER RHO AND ETA-MISMATCH
RW1138.3B L=.216 X10³² @ 3.00 GEV
SIGE/E = .775 X10⁻³
SIG2H/B= .227 X10⁻⁶
1-Apr-77
SQRT BETA HORZ
SQRT BETA VERT
(METERS)
1 INCH=100 WAVES AT 713.945 MHZ

Fig. 3-8

TABLE 3-1

Parameter	Unit	3 GeV	5 GeV	8 GeV
Luminosity	$cm^{-2}sec^{-1}$	$.21 \times 10^{32}$	$.59 \times 10^{32}$	1×10^{32}
β_V^*	m	.1	.1	.1
β_H^*	m	1.14	1.09	1.34
η_H^*	m	1.24	1.03	1.10
σ_H^*	mm	1.0	1.0	1.1
σ_V^*	mm	.09	.09	.06
$\sigma_H^2/$	mrad	1.43×10^{-7}	1.46×10^{-7}	1.22×10^{-7}
$\sigma_V^2/$	mrad	$.83 \times 10^{-7}$	$.86 \times 10^{-7}$	$.38 \times 10^{-7}$
K	-	.76	.77	.56
ν_H	-	11.38	11.38	11.38
ν_V	-	11.38	11.38	11.38
$\beta_{V,max}$(normal cell)	m	35	34	34
$\beta_{H,max}$(normal cell)	m	39	38	34
α	-	8.4×10^{-3}	8.7×10^{-3}	8.7×10^{-3}
τ_ρ(wigglers on)	sec.	61×10^{-3}	20×10^{-3}	8.2×10^{-3}
$\sigma_{\varepsilon/E}$	-	$.77 \times 10^{-3}$	$.91 \times 10^{-3}$	$.89 \times 10^{-3}$
η_{max}	m	2.6	2.2	2.4
β_{max}	m	129	128	130
N_b	-	$.82 \times 10^{12}$	1.34×10^{12}	1.5×10^{12}
$\tau_{pol.}$	min.	419	93.6	26.7

value slightly greater than zero to avoid the head-tail instability. The chromaticity can easily be corrected by the addition of sextupole elements to the lattice. On the previous lattice drawings these are shown as elements with "400" numbers. However, the distribution of these elements can cause the excitation of third order resonances which effectively limit the momentum aperture of the machine. To minimize this effect, the distribution and excitation of the sextupoles must be carefully tailored. The ability to do this tailoring systematically has been incorporated into our lattice design programs, the optimization being done by minimizing the variation of the β functions with momentum.

It has turned out that the most powerful method for maximizing the momentum aperture is by proper disposition of the sextupole elements rather than by elaborate groupings of the excitations. When that is done, i.e., certain key sextupoles are removed, it is found that two independent groups of sextupoles often give nearly as good results as those obtained by allowing each individual sextupole to have its own value. Nevertheless we have decided to provide individual powering of the sextupoles to be prepared for all eventualities.

Control of the coupling between horizontal and vertical betatron oscillations to the extent permitted by beam-beam interaction will be exercised by rotated quadrupoles and by close attention to the alignment of the focusing elements. The tunes of electrons and positrons will be separable by means of electric or rf quadrupoles and the beams themselves will be separated vertically by electric deflection plates during

injection. These deflection plates will be placed in short straights (labelled 119 and 112 in the lattice printout) especially provided for them near the interaction regions. Feedback systems to damp coherent oscillations of the beams will be provided.

4. Guide Field Magnet System

The collection of magnets making up the guide field for the storage ring contains 88 dipole bending magnets, 98 quadrupole magnets, 78 sextupole magnets, and a number of small miscellaneous correction magnets. The basic parameters for these magnets and the principal details of their construction are given in this section.

a) Dipole Magnets

Six different models of dipole bending magnets are required. The functions of these magnets and their major magnetic parameters are given in Table 4-1. All bending magnets and the eight quadrupole magnets nearest the interaction regions will be connected electrically in series. The quadrupole magnets and the high field magnets will have trim windings to correct for differences in saturation properties. The low field magnets as presently designed will also require trim windings, but these can probably be eliminated by small adjustments in the magnet lengths.

The profile of the dipole magnets is shown in Figure 4-1. The normal field and low field magnets have identical iron cores, but differ in the number of turns in the coils. The magnet cores are assembled from 1.5 mm laminations of low carbon steel, which are contained between 6.4 cm end plates which are contoured to provide the proper field profile at the magnet ends. The laminations and end plates are stacked on a jig, then enclosed with a C shaped shell of 0.95 cm steel which is welded to the end plates and to the laminations along the edges of the C, above and below the open sides of the magnet poles. This arrangement provides adequate rigidity to permit supporting the magnet cores at their ends without excessive distortion. Our prototype magnets show

Table 4-1

CESR Bending Magnets

Model	Function
201	Normal Field Magnet. Two cores per magnet
202	High Field Magnet in Bulge
203	Low Field Magnet near L0 Interaction Region
204	Short Normal Field Magnet. Half core
205	Low Field Magnet near L3 Interaction Region
206	Normal Field Magnet. Single core

Model	201	202	203	204	205	206
# Required	70	8	2	4	2	2
Gap Height (mm)	65	65	65	65	65	65
Gap Width (mm)	190	190	190	190	190	190
Bend radius (m)	87.892	32.573	179.326	87.892	141.989	87.892
Length (m)*	6.573	3.330	3.756	1.644	2.655	3.287
B at 8 GeV (KG)	3036	8192	1488	3036	1879	3036
I at 8 GeV (A)	991	991	991	991	991	991
Turns in coil	16	44**	8***	16	10***	16

* Chord across effective length

** Plus 80 turn trim coils

*** Plus small trim winding unless magnetic length is adjusted.

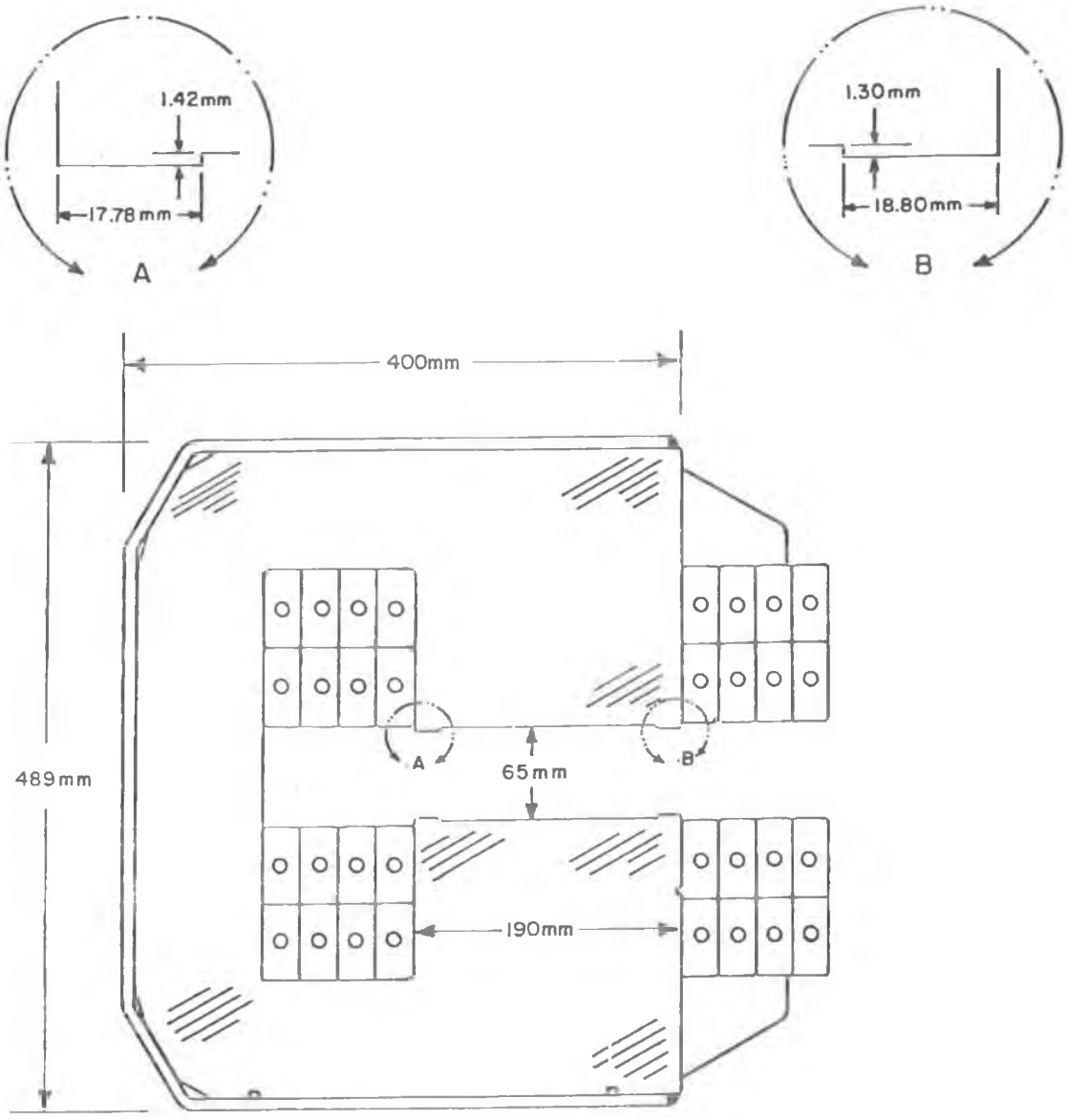

Fig. 4-1 Profile of normal field bending magnet

that the sag can be held to 0.6 mm, and the twist can be limited to less than 0.5 mrad. The C type configuration has been chosen to reduce the cost and complexity of the vacuum system and to provide direct access to it. The normal field magnets will be placed with their return yokes against the outer wall of the tunnel to provide access to the vacuum chamber from the center aisle and to simplify the design of the transfer lines between the storage ring and the synchrotron.

Our original magnet design called for normal bending magnets of 3.3m long. These magnets were arranged in pairs with quadrupoles between successive pairs. In order to maximize the space in the ring for other components the magnet pairs have been combined into single units each consisting of two cores within a single set of coils. The cores are straight but are arranged with an angle of 37 milliradians between their center lines to minimize the excursion of the central orbit from the pole centers. The reduction of the width of the good field region due to the sagitta is then negligible. The coils are formed to fit the poles of the two cores. A photograph of a prototype of this magnet assembly placed in the tunnel is shown in Figure 4-2.

The coils for the normal field magnets have 16 turns arranged in four pancakes, two on each pole. The conductors are aluminum bars with central holes for water cooling. In order to keep the magnet power consumption to a modest level the current density is held to about 80 A/cm^2 at the 8 GeV operating level. The amount of current bussing is reduced by connecting the magnet coils end to end around the ring. To do this the front conductor on the bottom pancake is replaced by the return bus, in order to equalize the total current on the two sides of the pole. This

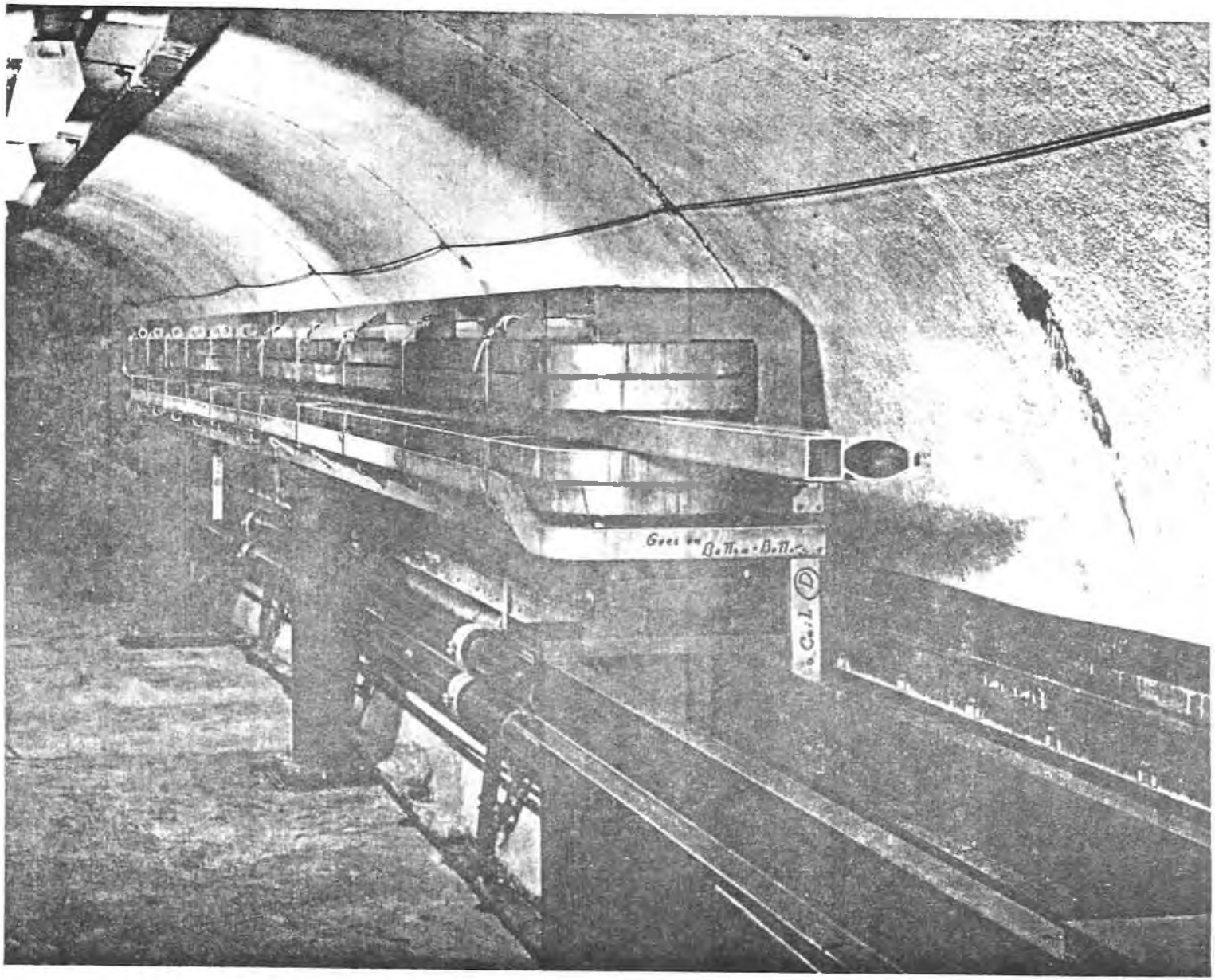

Fig. 4-2 Prototype of normal bending magnet (a positi

feature can be seen in the photograph of Figure 4-2. By using this arrangement, busses and bus bar supports are eliminated in most of the ring. At the long straight sections, the required bus bars will be made from the standard magnet aluminum conductor. Each normal field bending magnet coil will include a 9-turn steering coil of 0.25 x 5.0 mm copper ribbon to provide a maximum steering correction of ± 0.5 mrad at 8 GeV. The basic parameters of the normal field magnet coils are given in Table 4-2.

The profile of the high field bending magnets is shown in Figure 4-3. The coil window and the width of the return yoke must both be made larger than those for the normal field magnets to provide for the increased magnetic flux density. Both the main coil and the trim coil will be made of water cooled copper conductors. The shorter bending radius in these magnets requires that the cores be stacked on the arc of the orbit circle to eliminate the reduction in aperture by the sagitta. The stacking will be done directly on a structural base. Steel tie rods will be used to compress the stack between solid end plates. Partial laminations will be inserted as wedges to insure a solid stack.

These high field magnets will be located in areas where there is access to them from the outside of the ring. They will be oriented with their return yokes on the inside of the orbit to simplify the design of parts and vacuum lines for synchrotron radiation beams.

Parameters of the high field magnet coils are given in Table 4-2.

b) Quadrupole Magnets

The 90 quadrupole magnets in the normal lattice all have the same basic dimensions -- bore radius 40 mm and effective length 60 cm. In

Table 4-2

Parameters for Bending Magnet Coils
8 GeV

	Normal Field (Two cores)	High Field (Main coil)
Conductor material	Al	Cu
Conductor size (mm)	54.0 x 25.4	46.2 x 15.2
Cooling hole diameter (mm)	9.5	9.5
Resistance at 45°C (mΩ)	5.34	10.55
Current (A)	991	991
Current density (A/cm^2)	77	161
Voltage (V)	5.29	10.45
Power (KW)	5.24	10.36
Water flow, 30°C rise (GPM)	0.33	1.28
Pressure drop* (psi)	3.0	2.2
No. of water circuits	2	4
Weight of steel (Kg)	7470	7490
Weight of conductor (Kg)	772	1842

*No allowance for bends and fittings.

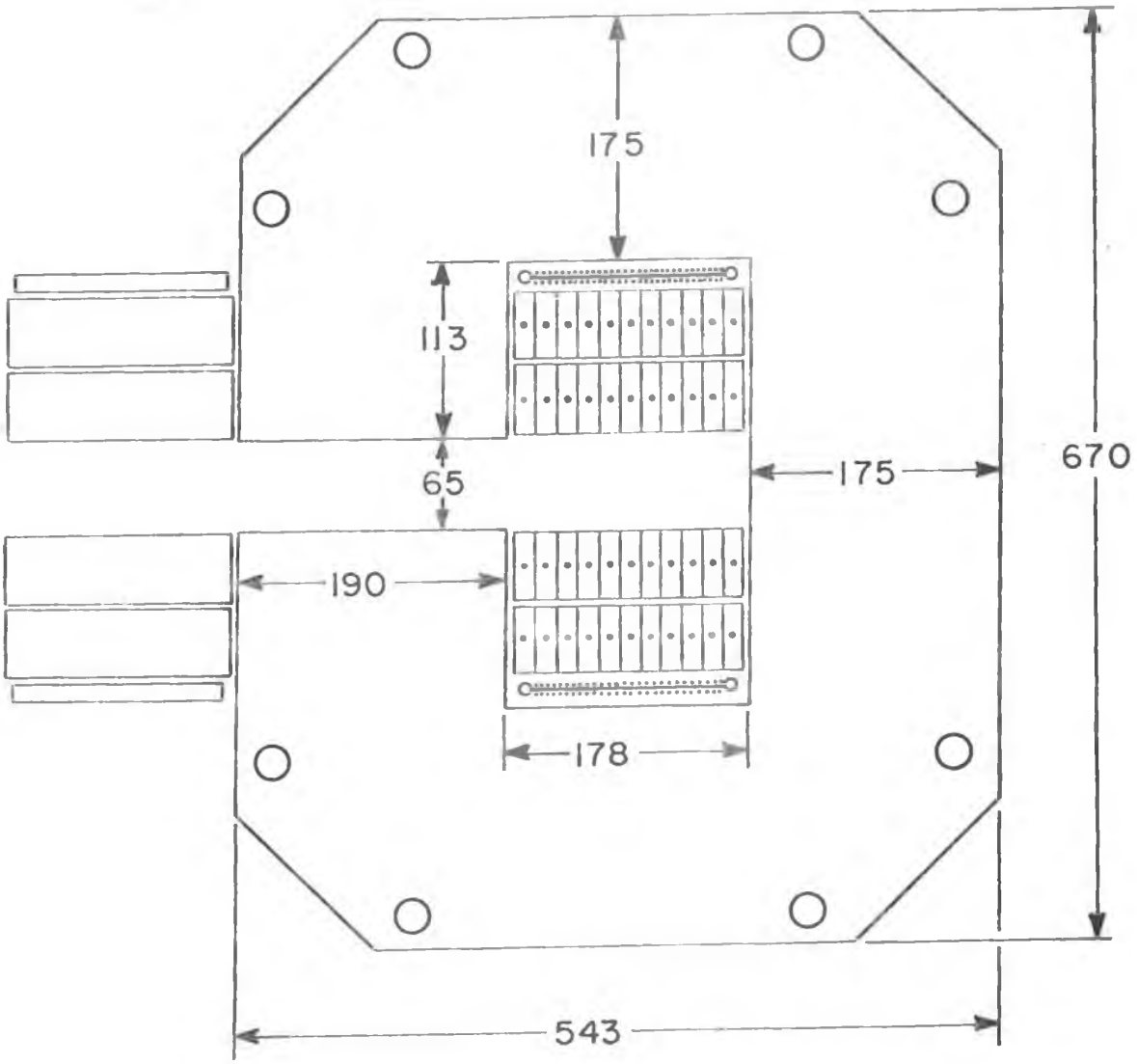

Fig. 4-3 Profile of the high field bending magnet. The pole configuration is identical to that shown in Fig. 4-1.

order to satisfy the lattice conditions they will be operated at strengths varying from K = 0.10 to 0.48 m^{-2}, corresponding to field gradients from 0.27 to 1.3 KG/cm at 8 GeV. Our first design for these magnets (Mark I) is shown in profile in Figure 4-4. The iron cores are stacked from 1.5 mm laminations with hard packs of epoxied laminations for end plates. The cores are assembled from four quadrants by bolting the sections together on the outside. The coils are wound with 95 turns of strip aluminum (0.041 x 9.53 cm) separated by 0.076 mm mylar insulating strips. Water cooled copper plates of 1.6 mm thickness are cemented to the edges of the current strips with thermal conducting epoxy. The cooling tubes are located as shown in the figure. These coils are fabricated in this manner to achieve a relatively high impedance and thus simplify the distribution of power in the tunnel. A photograph of the machine for winding these coils is shown in Figure 4-5. A photo of a prototype of a Mark I quadrupole with a field measuring coil in place can be seen in Figure 4-6.

We have also designed a two-section quadrupole magnet (Mark II) whose profile is shown in Figure 4-7. The iron and stamping costs for this model are less than that for Mark I. However, its main advantage is that the two piece magnet can be assembled easier and with higher reliability in maintaining the required magnetic field profile. The saving in iron is partly the result of having narrower poles (7.4 cm wide compared to 9.2 cm for Mark I). The pole faces are contoured to give a calculated field profile that differs from the ideal quadrupole field by no more than 3 parts in 10^4 within the aperture of ± 4.5 cm. The fringe field falls off more rapidly in the Mark II quadrupoles than in the Mark I. In the injection region, where a wider aperture is required, we plan to install Mark I units. Otherwise we expect to use Mark II quadrupoles throughout the lattice.

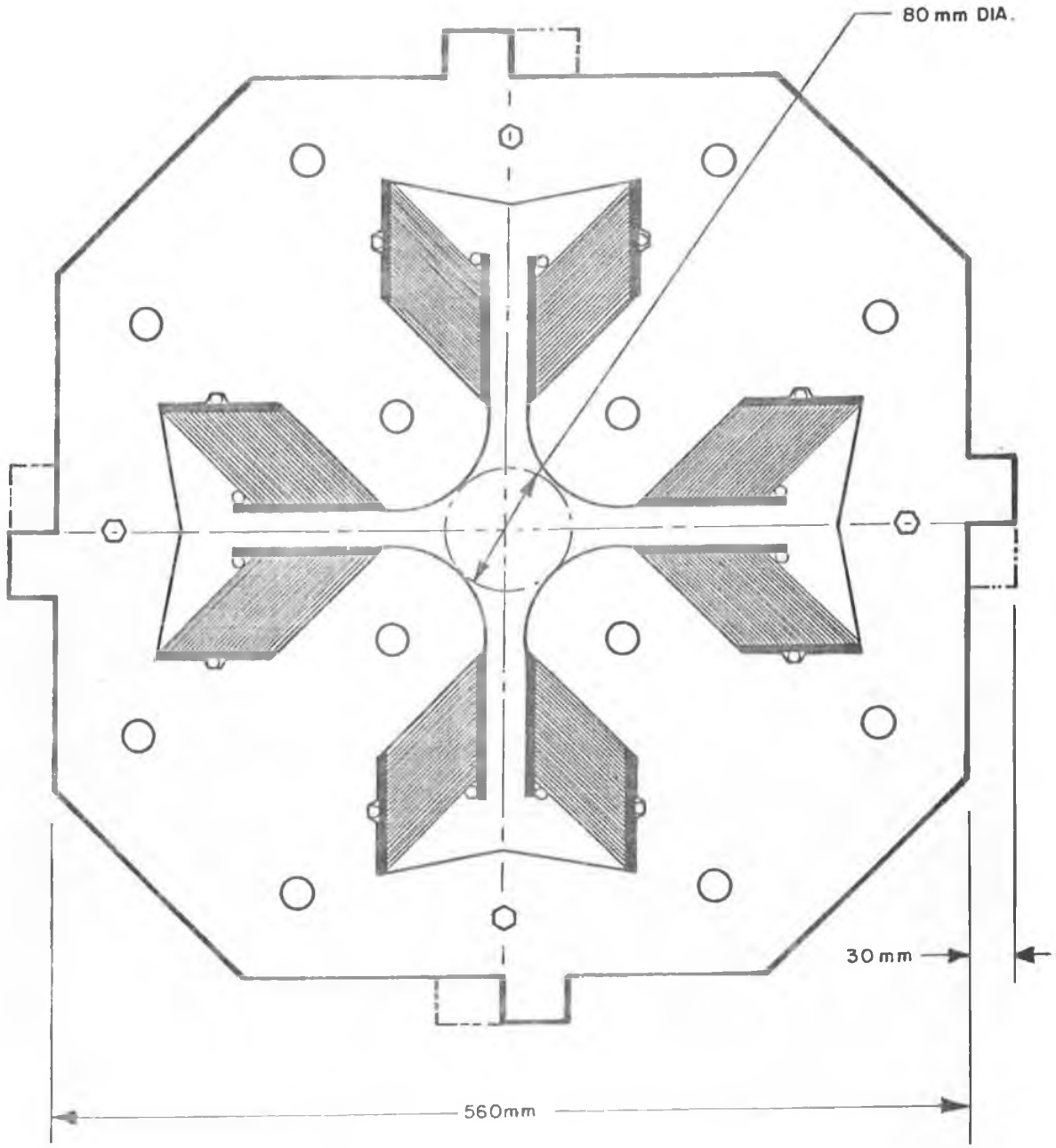

Fig. 4-4 Profile of the Mark I quadrupole magnet

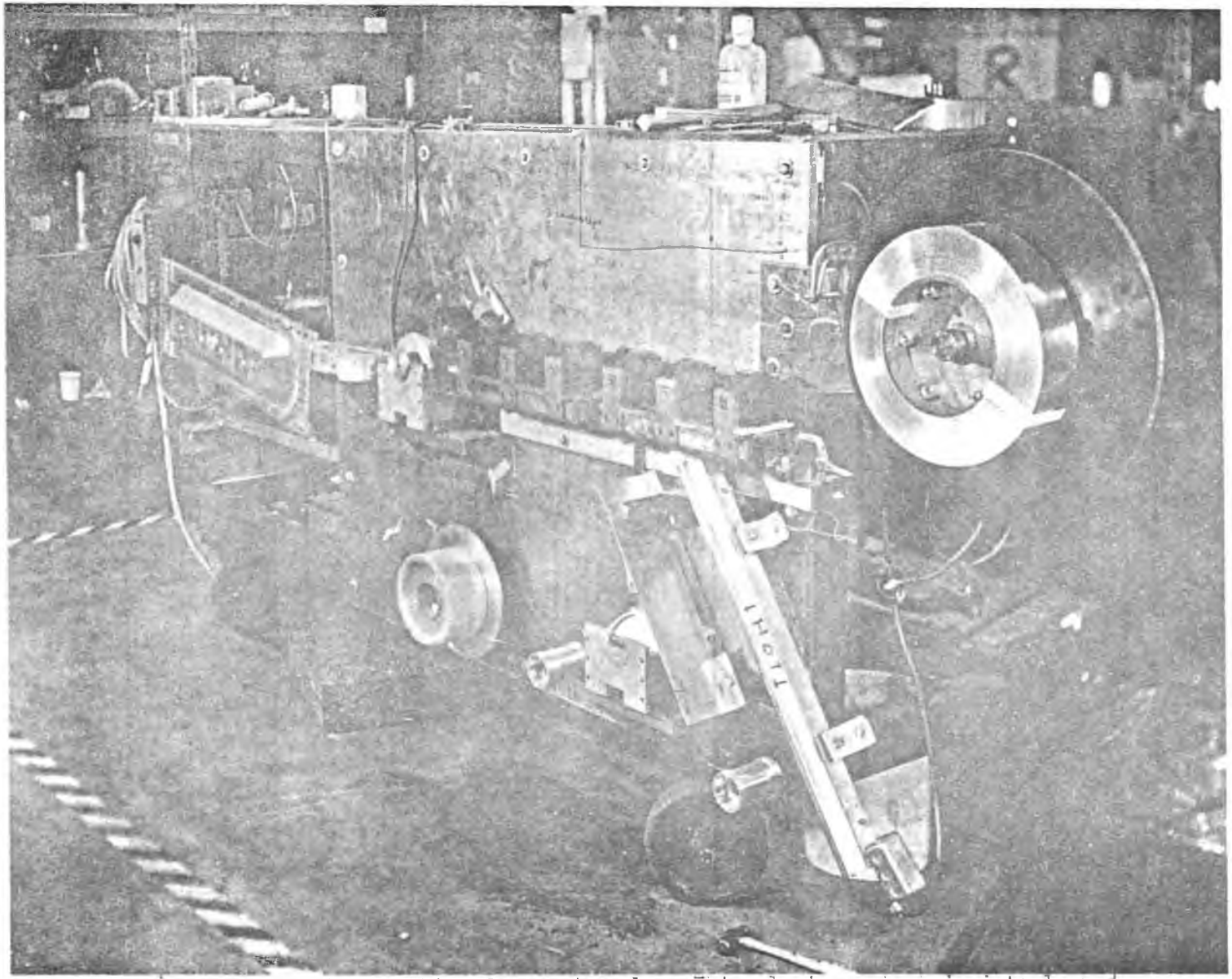

Fig. 4-5 Winding machine for quadrupole. Thin aluminum stock is interleaved with mylar insulation and wound on form at left.

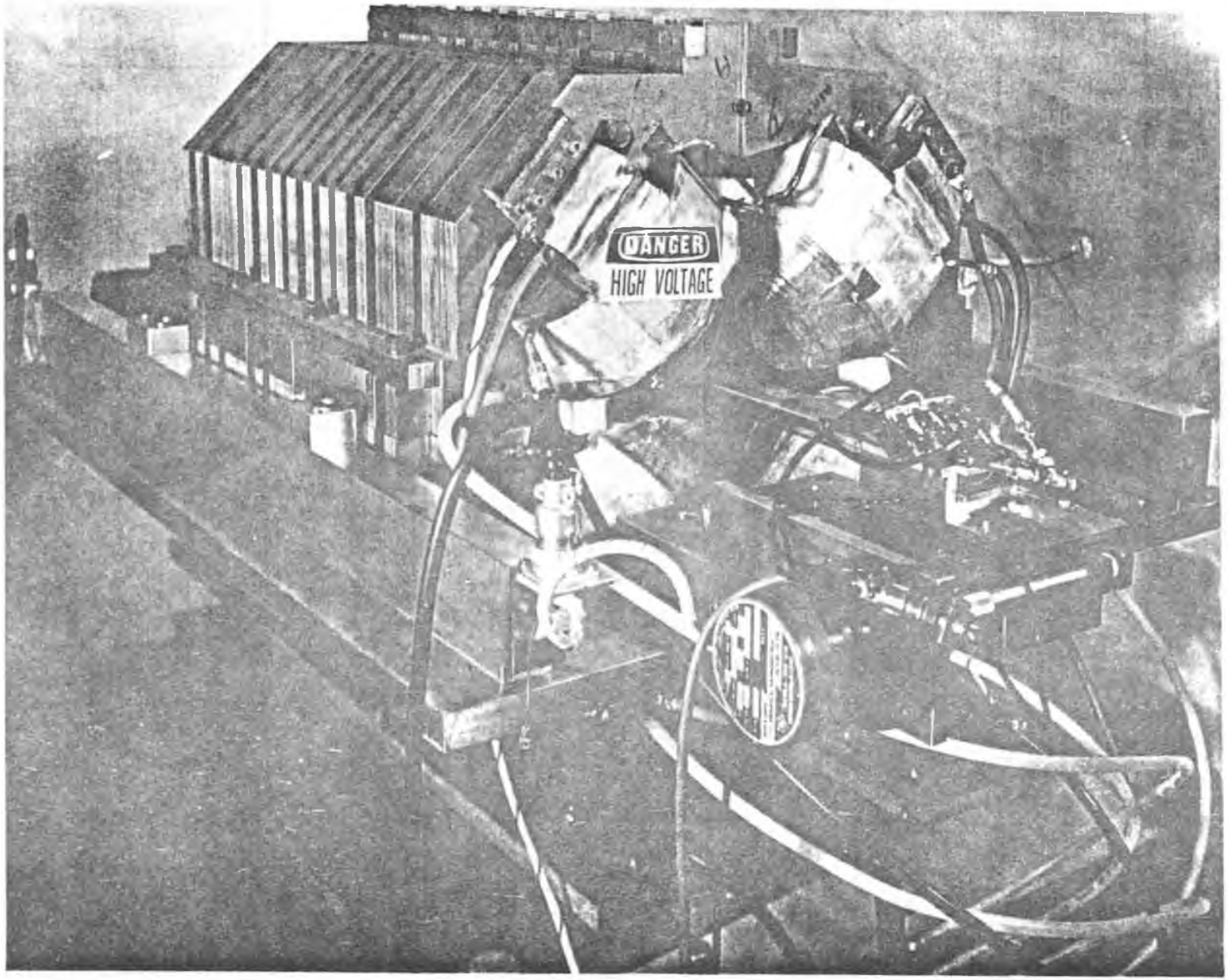

Fig. 4-6 Mark I quadrupole with field measuring apparatus in place.

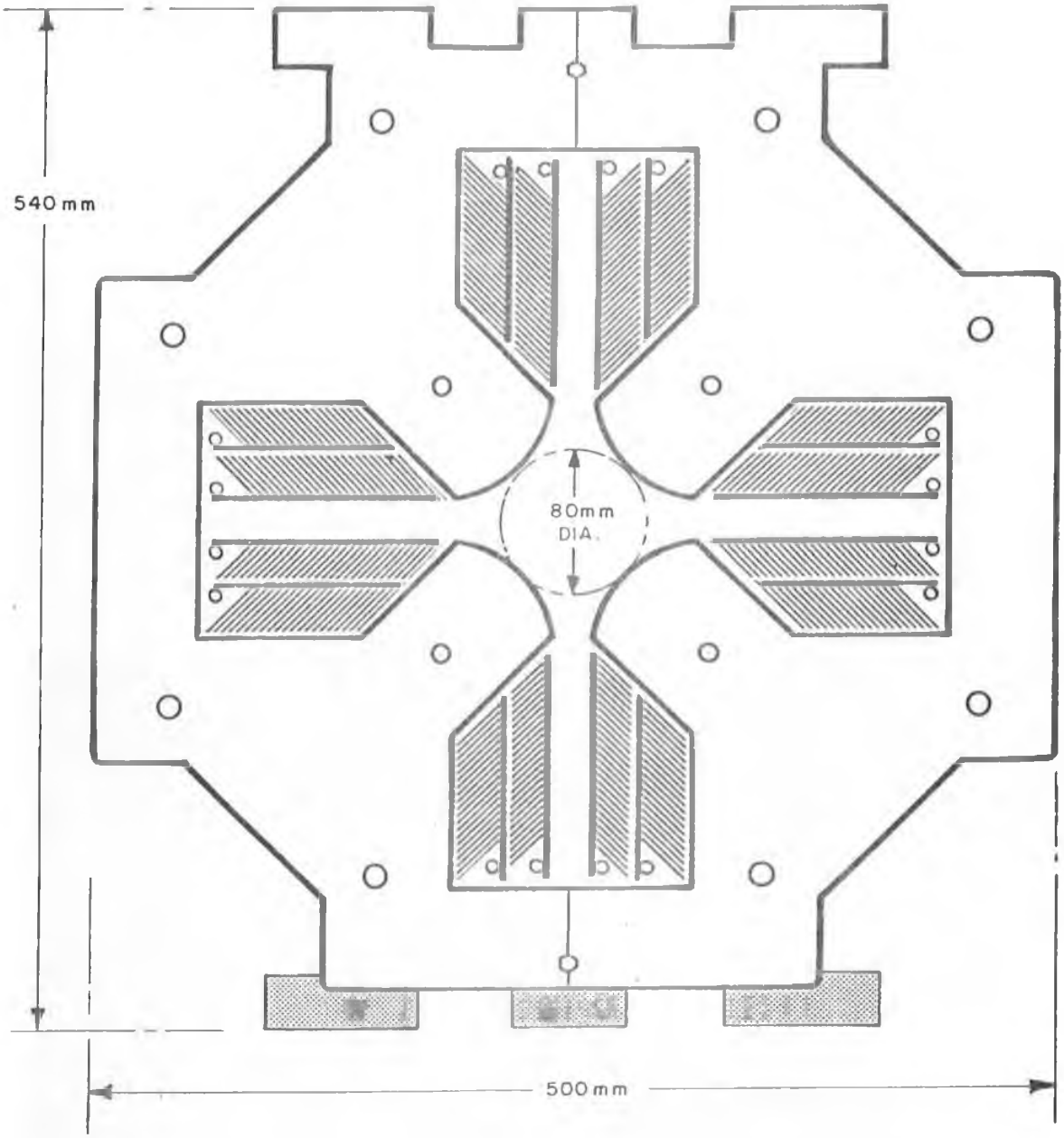

Fig. 4-7 Profile of the Mark II quadrupole magnet

The coils in the Mark II magnets are split into two sections to make it possible to insert them between the poles of the half section. The method of fabrication is similar to that for the Mark I coils, but the aluminum conductor will be 1.27 x 28.6 mm. There will be 41 turns in the coil section nearer the pole and 54 turns in the outer section. The coil winding machine can be readily modified to produce either the Mark I or the Mark II coils. Four quadrupoles will operate at appreciably higher levels than the others in the ring. The coils for these will be wound of copper strip to reduce the power dissipated in these units.

The pairs of quadrupole magnets on either side of the interaction regions will have a bore radius of 60 cm. A profile of these magnets is shown in Figure 4-8. The magnet cores are assembled from two half sections in a manner similar to that used for the Mark II lattice quadrupoles. Each pair consists of one magnet of an effective length 1.0 m and another of 0.75 m. These lengths are chosen to make the field gradients roughly equal to minimize the corrections that must be made for saturation. The coil assembly contains a main winding connected in series with the bending magnets and a trim winding to provide a fine adjustment. Both windings are made of hollow copper conductors. The coils are made in two sections to permit insertion into the half magnets.

A list of parameters for the quadrupole magnets is given in Table 4-3.

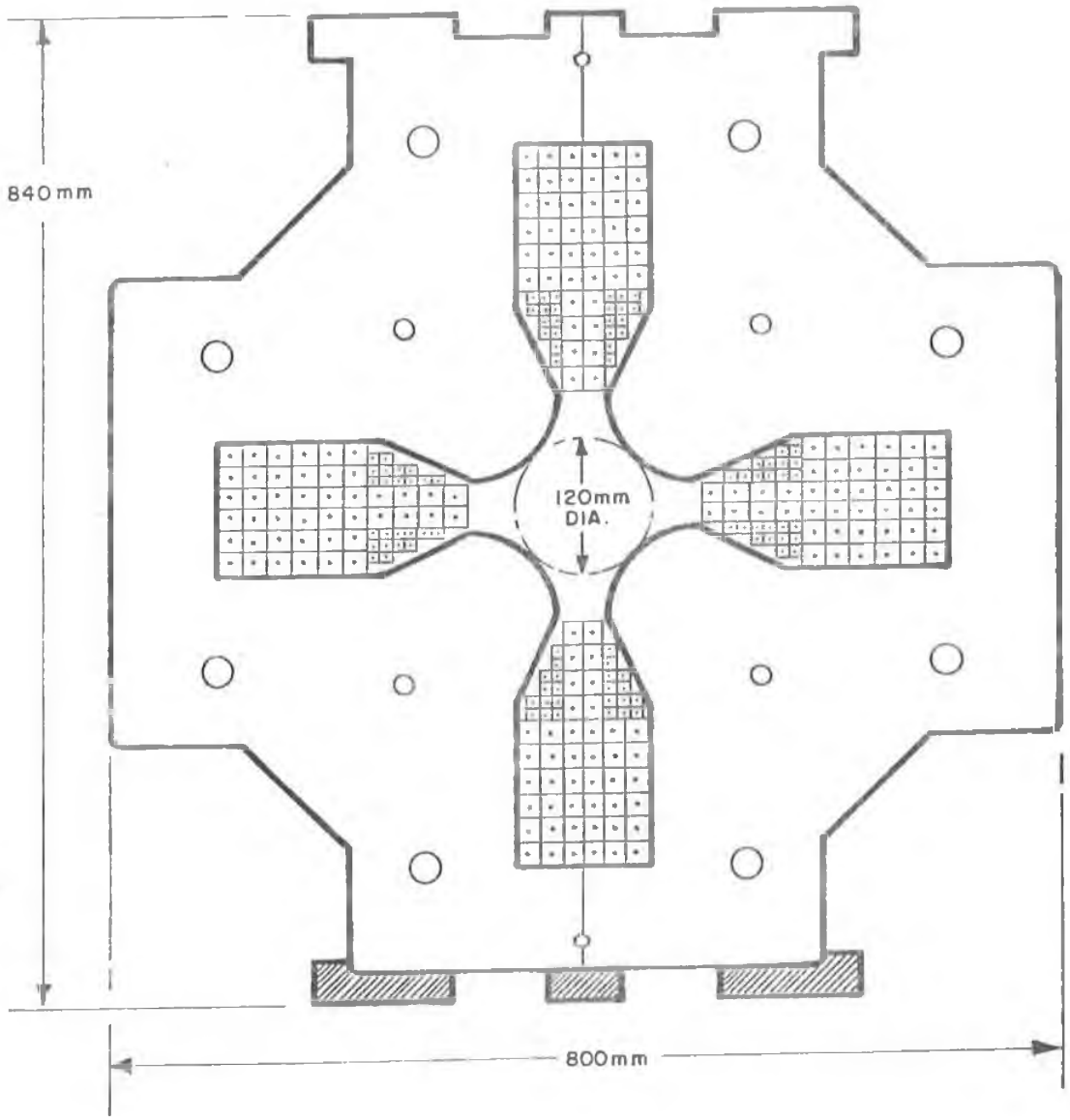

Fig. 4-8 Profile of the intersection region quadrupole magnet

Table 4-3

Parameters for Quadrupole Magnets

8 GeV

	Lattice		Interaction Region	
	Low Field	High Field		
Bore radius (mm)	40	40	60	
K (m^{-2})	.10 - .35	.35 - .48	0.57	
Field gradient (KG/cm)	.27 - .93	.93 - 1.28	1.52	
Field at pole center (KG)	1.1 - 3.7	3.7 - 5.1	9.1	
Effective length (m)	0.60	0.60	0.75, 1.0*	
			Main	Trim**
Number of turns (4 poles)	380	380	88	48
Conductor	Al	Cu	Cu	Cu
Conductor size (mm)	1.27 x 28.6	1.27 x 28.6	17 x 19.5	9 x 10
Cooling hole diam. (mm)	-	-	9.5	6.4
Resistance at 45°C (mΩ)	518	317	19.5	41.3
Current (A)	17 - 62	62 - 86	991	360
Voltage (V)	8.8 - 32	20 - 27	19.3	14.9
Power (KW)	.5 - 2.0	1.2 - 2.3	19.15	5.35
Water flow (GPM) (Max 30°C rise)	0.25	0.29	2.38	0.66
Pressure drop (psi)	5.2	6.7	4.9	2.0
No. of water circuits	1	1	4	4
Conductor weight (Kg)	55	182	611	65
Steel weight (Kg)	Mark I 885 Mark II 631		2970	

*All electrical quantities refer to 1.0 meter length.

**Maximum values for ± 20%.

Note: Electrical properties of the Mark I and Mark II coils are essentially identical.

c) Sextupole Magnets

Sextupole magnets will be located in the storage ring adjacent to nearly every lattice quadrupole magnet. Two views of the sextupole magnet design are shown in Figure 4-9. The magnet poles are extended beyond the cores to the outer faces of the coils in order to maximize the effective magnetic length in a limited space along the beam orbit. The cores will be assembled from 1.5 mm laminations. The poles will be machined from low carbon steel and will be mounted on the cores after the coils are in place, using the dovetail keying shown in the figure. In addition to the sextupole coils, the magnets contain a pair of dipole coils to provide vertical steering corrections. A list of parameters for the sextupole magnets is given in Table 4-4.

d) Magnetic Measurements

A magnetic measurement system has been set up to make a variety of measurements on the dipole prototypes which have been constructed. For this purpose, a stepping motor is used to rotate a flip coil and the voltage is integrated electronically using a Hewlett Packard integrating voltmeter. Relative measurements can be reproduced to better than one part in 10^4. Using calculational programs Trim and Linda the original profile of the magnet was established with wedge shaped lips at the profile edges to extend the useful field. The first attempt provided a field uniformity of about 15×10^{-4}, and the second attempt (using square lips) gave the uniformity of 2×10^{-4}. Figure 4-10 gives a graph of the measurements of the relative field intensity as a function of radial position in the median plane for the second attempt. There is a

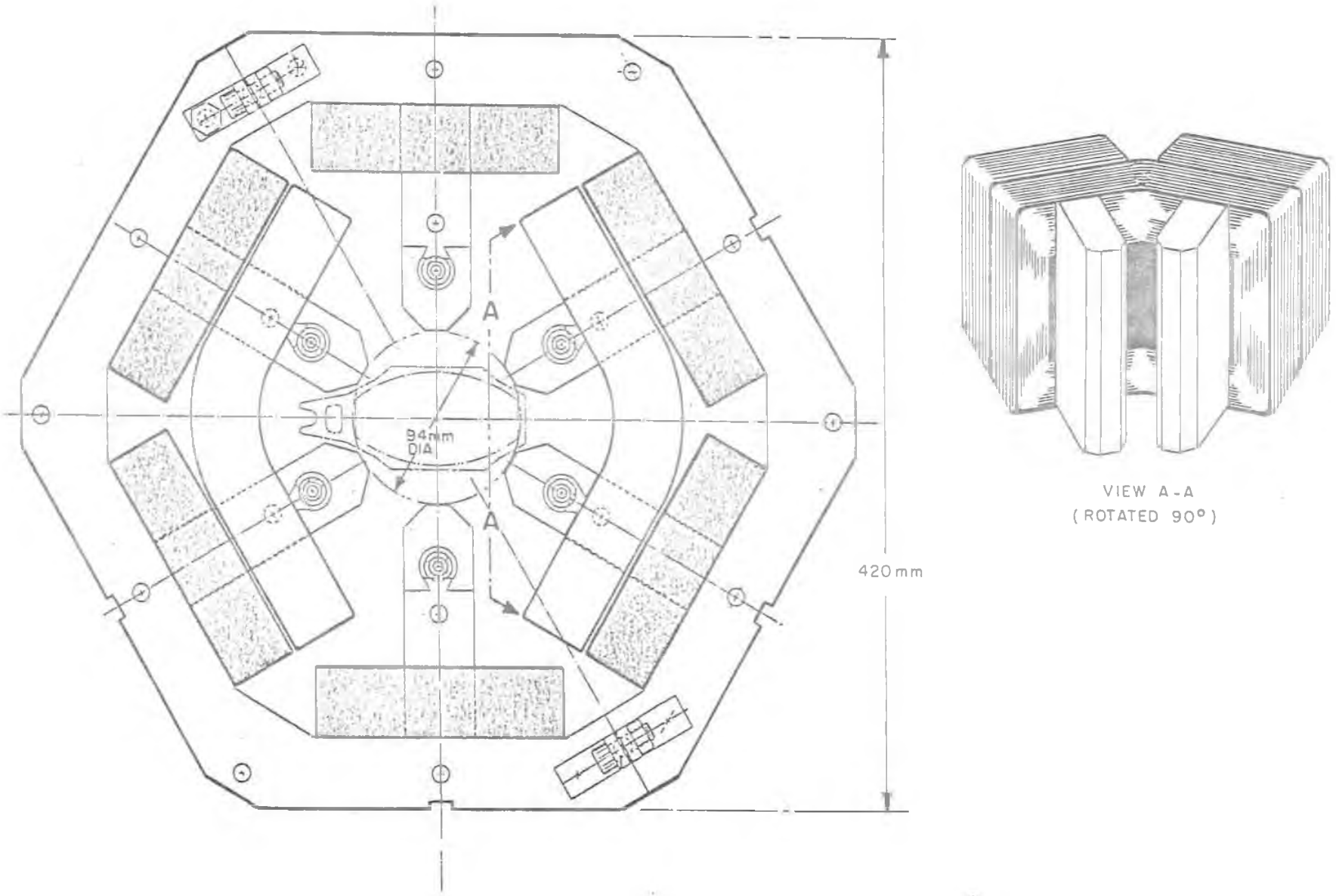

Fig. 4-9 Profile and cut-away view of the sextupole magnet

Table 4-4

Parameters for Sextupole Magnet

8 GeV

Bore radius (mm)	47
Effective length (m)	0.28
Maximum strength (KG/cm^2)	0.272
Field at pole tip (KG)	3.0
Sextupole coil	
Turns per pole	200
Conductor	#9 Cu
Resistance (ohm)	0.337
Maximum values	
Current (A)	25
Voltage (6 poles) (V)	50.5
Power (6 poles) (KW)	1.26
Steering Coil	
Turns	440
Conductor	#12 Cu
Resistance (ohm)	2.10
Maximum values:	
Steering angle (mrad)	± 0.5
Current (A)	11
Voltage (2 coils) (V)	46.2
Power (2 coils) (KW)	0.51

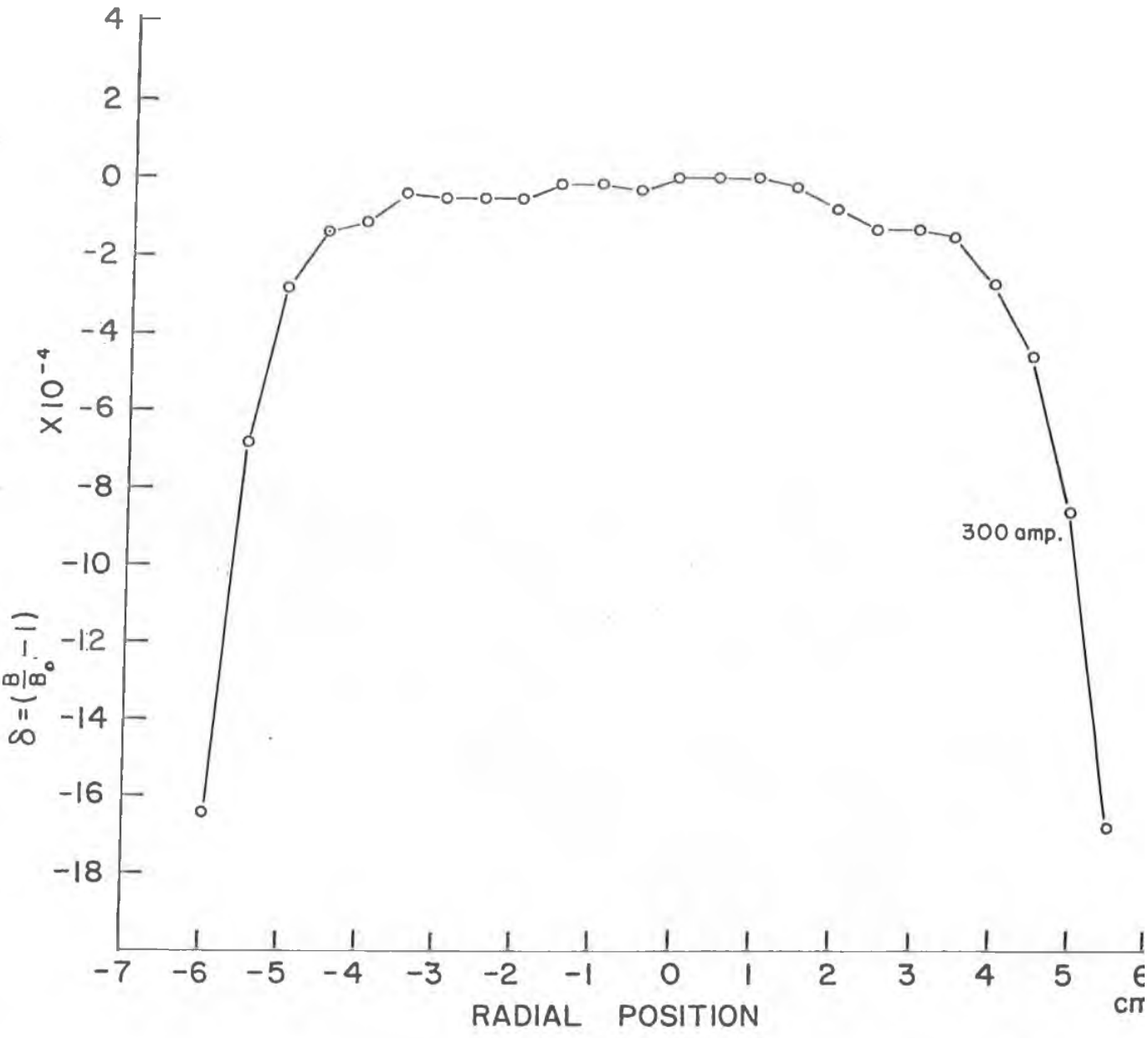

Fig. 4-10 Relative field intensity as a function of radial position. The relative deviation, δ, of the field from the central orbit value is shown in parts per 10^4.

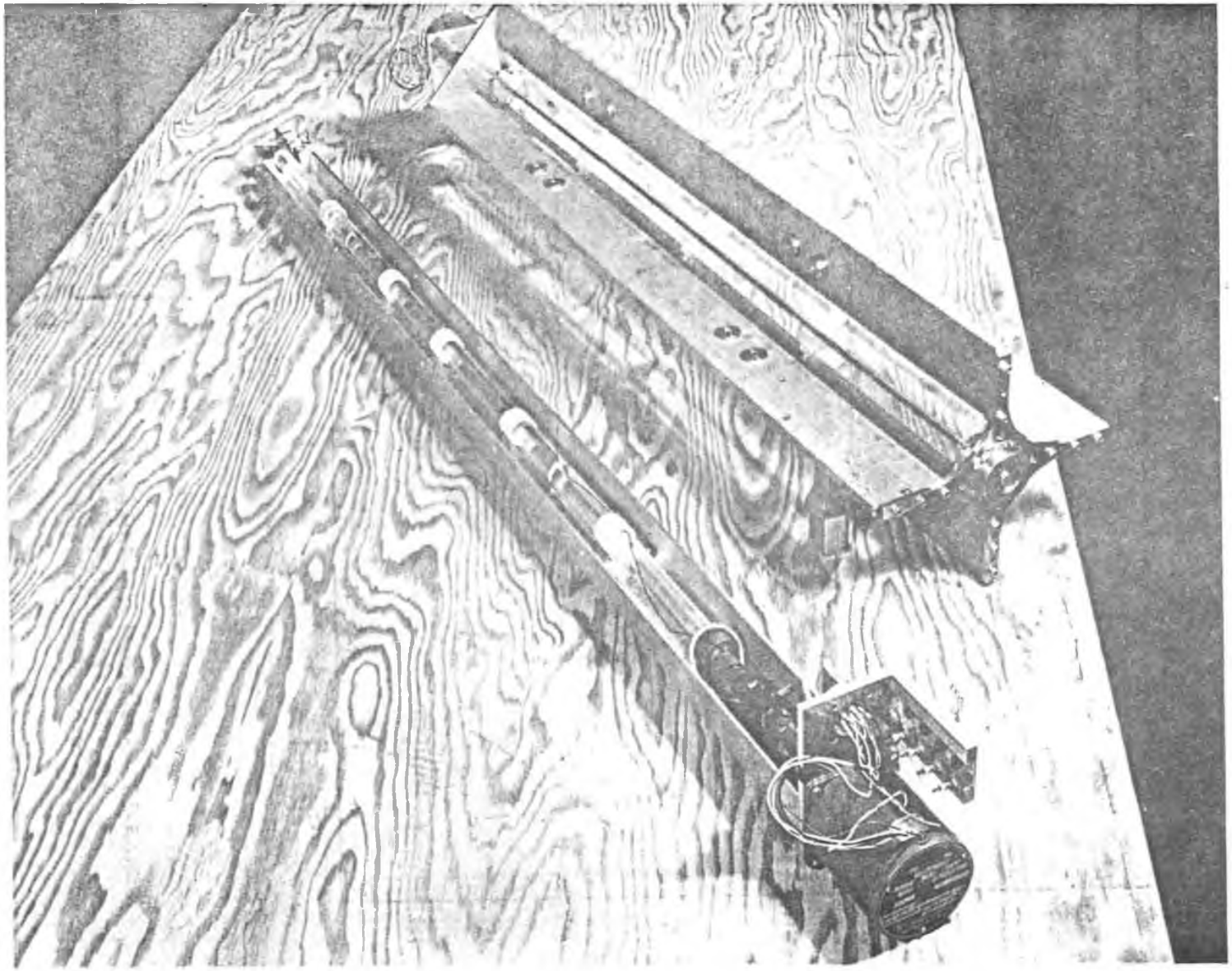

Fig. 4-11 Photograph of stepping motor, coils and coil holder for magnetic field measurements.

small quadrupole component of the field which is dependent on excitation. It will be compensated by the current settings used in the quadrupole magnets which are located at the end of every half cell. In order to correct for end effects of the magnets, the poles at the ends of the magnets were empirically contoured to provide a constant bending length over the ± 4.5 cm width of the pole. We believe the final profile can now be established.

A measurement program has also been set up for the quadrupole magnets. Two measuring techniques are being used. In one a coil is rotated step-wise to measure the field on a circle just inside the pole boundary. From this information one gets a multipole analysis of the field inside the circle. In the other technique a search coil is translated step-wise along the median plane to obtain the field gradient directly. This technique is essential to obtain results beyond the inscribed circle. Measurements on the first prototype Mark I quadrupole give agreement to within 5 parts in 10^4 among the two experimental results and a calculation of the field using the TRIM program. Further refinements in the technique are being made. Figure 4-11 is a photograph of a complete search coil for a short dipole test magnet and the rotating coil device for the quadrupole. The translation search coil can be seen in the photograph of Figure 4-6.

e) Magnet Power Supply System

Three Transrex power supplies presently used to power experimental magnets in the laboratory will be used to power the normal bending magnets, the high field bending magnets, and the large quadrupole magnets in the storage ring. Since these magnets must all be connected in series, the total power requirement is 991 amps at 675 volts for 8 GeV operation. Connecting the three Transrex power supplies in series will provide a maximum current of 1650 amps at 900 volts which is comfortably more than is required. In normal operation two of the supplies would be on voltage control while the third would be on current control. Small modifications to the current regulation loop must be made to accommodate computer control of these supplies. Tests on the supplies show that their stability is more than sufficient to meet the tune shift requirements of the storage ring. To cancel saturation effects in the high bend magnets and the large quadrupole magnets, which reach 15% at 10 GeV, separately powered trim windings will be added. These will be powered by small separate computer controlled power supplies. The overall power circuit is shown in Fig. 4-12.

Because of the broad range (a factor of three) of focal lengths required for the ninety normal quadrupoles, we have decided to use a separate switching type power supply for each quadrupole. Maximum power for one of these quadrupole magnets is 100 amps at 60 volts. Two of the laboratory's existing Meaker power supplies (150 volts at 3000 amps) would provide a very low impedance D.C. voltage source which would be regulated to approximately 0.5%. A variable duty cycle transistor switch in series with the magnet then controls the current through the quadrupole

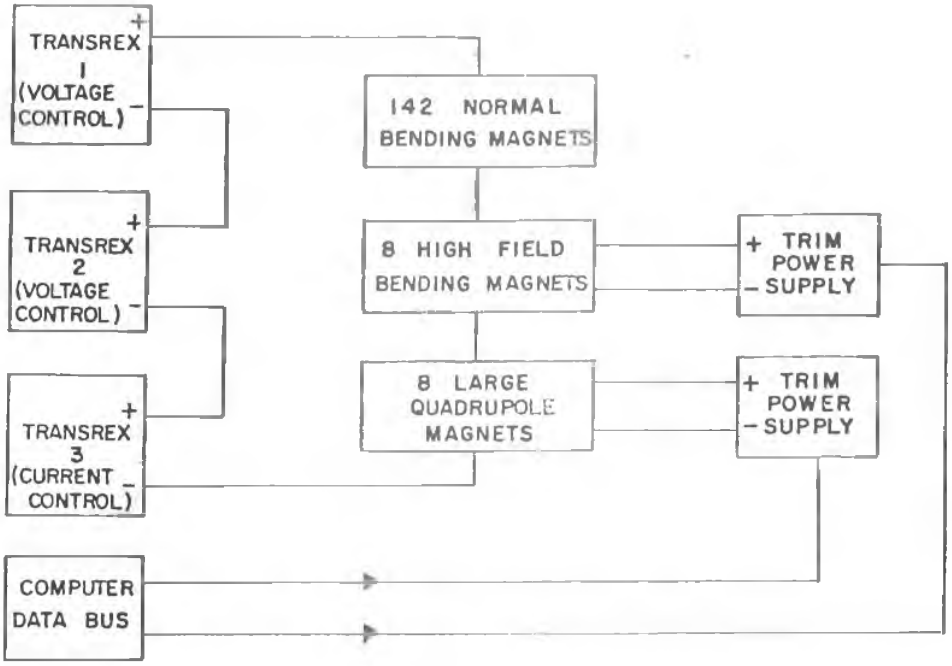

(a) BENDING MAGNET AND LARGE QUADRUPOLE MAGNET POWER CIRCUIT

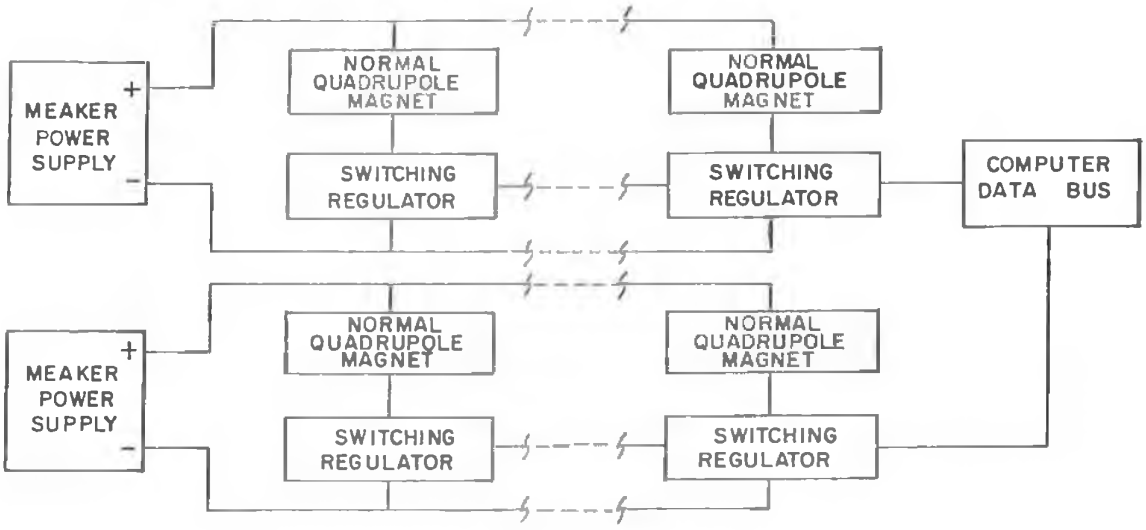

(b) NORMAL QUADRUPOLE MAGNET POWER CIRCUIT

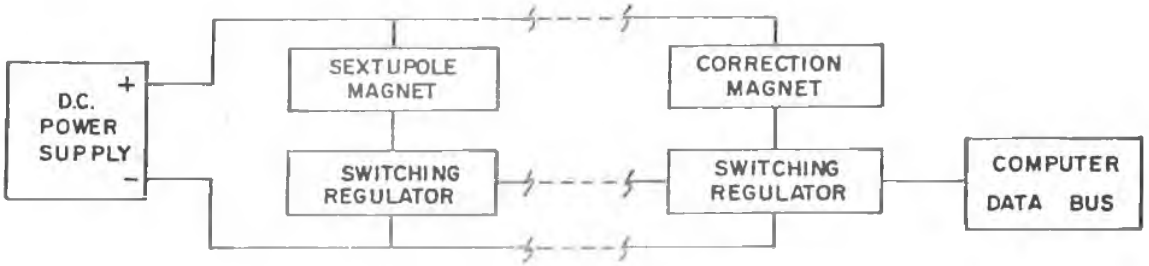

(c) SEXTUPOLE MAGNET AND CORRECTION MAGNET POWER CIRCUIT

Fig. 4-12

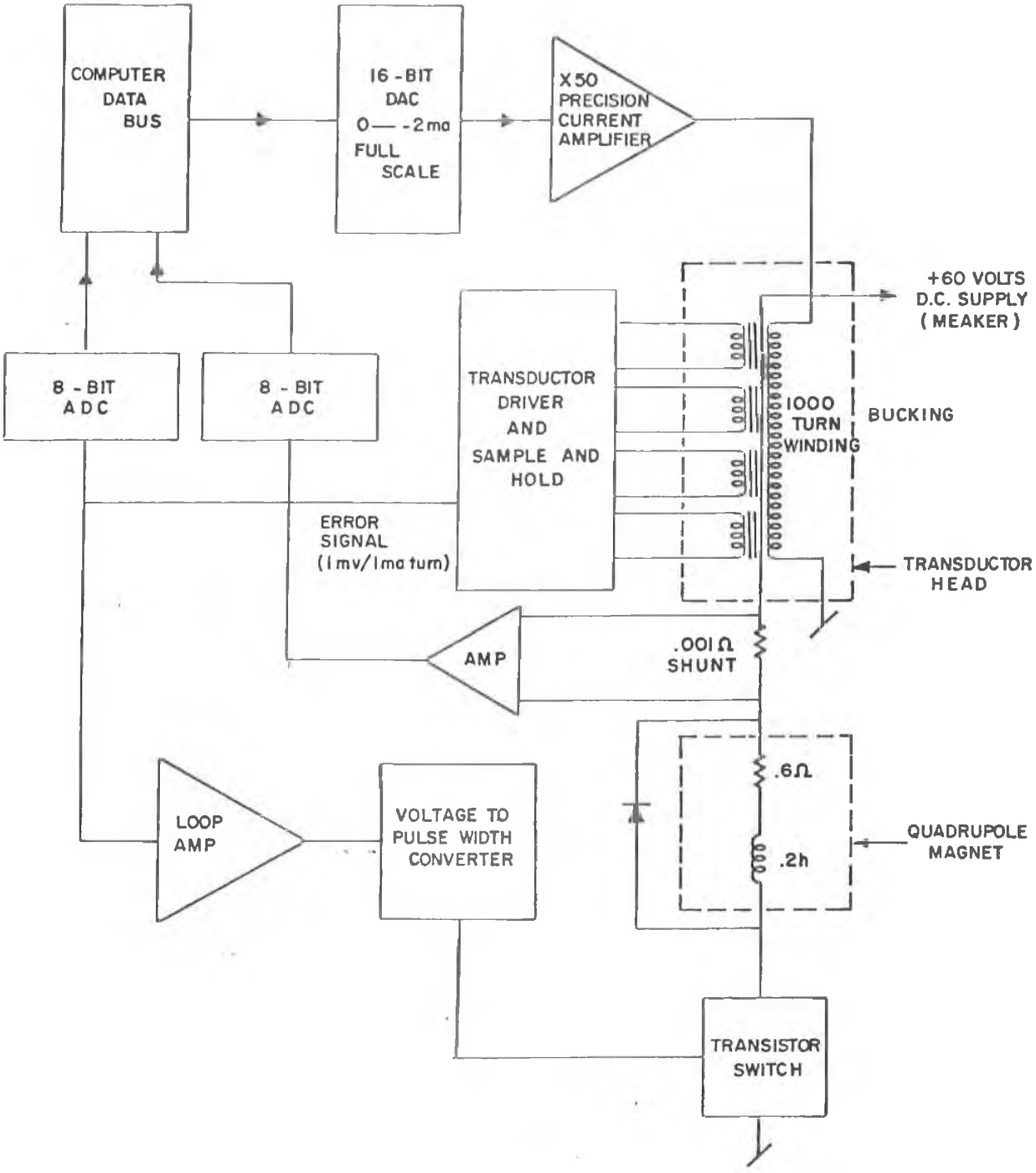

NORMAL QUADRUPOLE POWER SUPPLY (0-100 AMPS AT 60VOLTS NOMINAL)

Fig. 4-13

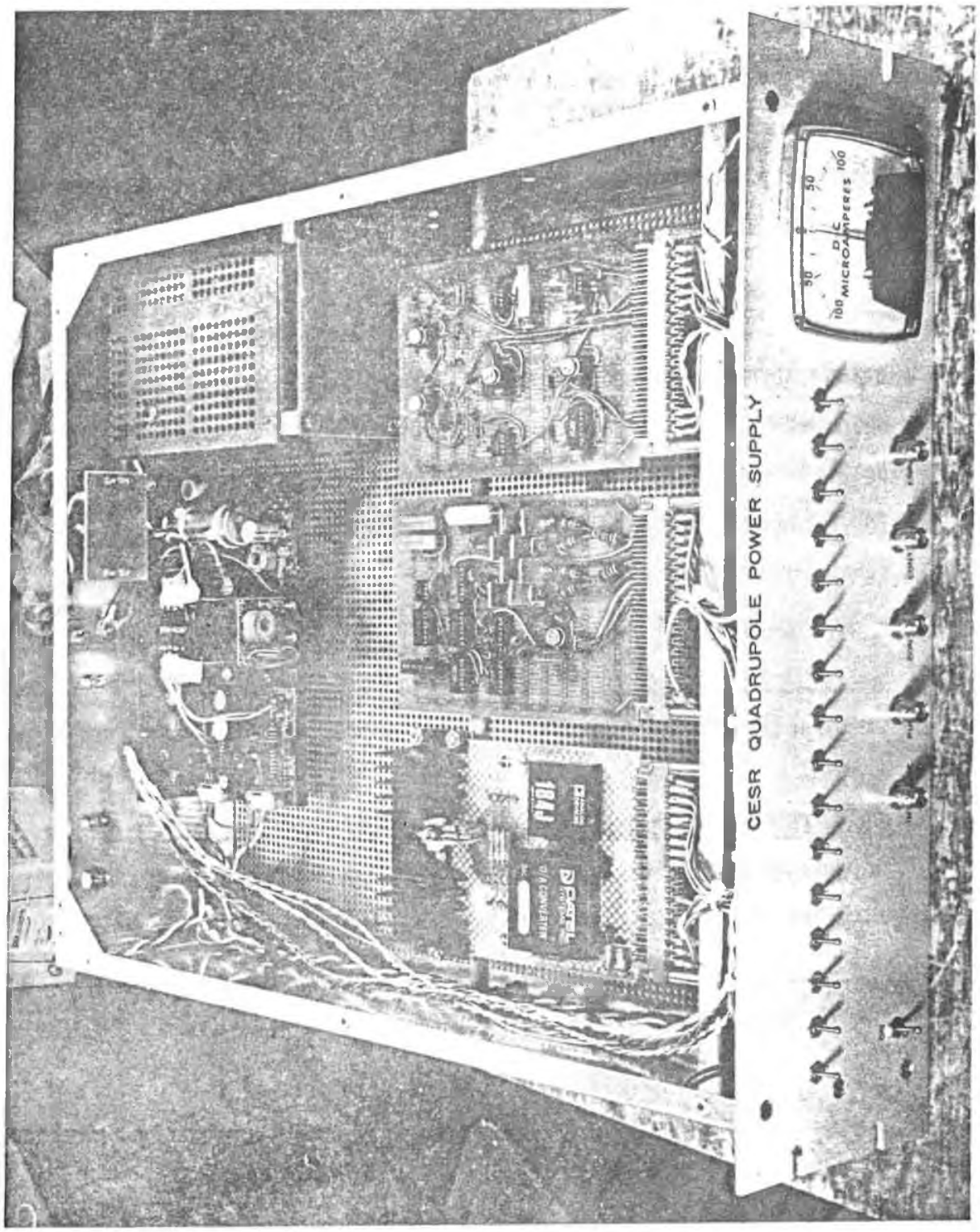

Fig. 4-14 Prototype of quadrupole power supply.

magnet to the required .01%. Since each of these currents must be set to this accuracy absolutely, a transductor has been chosen for measuring these currents. We have developed a new type of transductor which is very simple and inexpensive and has an rms noise level of 300 μA-turns with a long term stability of better than 2 mA-turns. It is basically a second harmonic type with the error signal between the current to be measured and the computer controlled current in the bucking winding being synchronously detected with a cheap CMOS switch and a capacitor as a sample and hold. The conventional second harmonic type transductors use a complicated filter amplifier system combined with a phase detector to provide the error signal. In our system this error signal is amplified and used to control the duty cycle of the transistor switch. Figure 4-13 is a schematic diagram of our normal quadrupole power supply. A complete full power prototype has operated with a current stability better than .01% for short periods. Figure 4-14 is a photograph of a quadrupole supply unit. Further tests of the long term stability and reliability are in progress.

The currents for the sextupole magnets and the correction magnets will be provided by similar switching regulated supplies. However, because of the much less stringent regulation requirements, a conventional shunt will replace the transductor and an inexpensive 12-bit DAC will control the current setting.

5. RF System

a) General Parameters

In order to supply the beam energy losses, a powerful rf system is required. Table 5-1 lists the parameters of this system.

At 8 GeV per beam the synchrotron radiation loss is 5 MeV per revolution. In addition to this loss there will be significant losses in the walls of the vacuum chamber, including rf cavities, due to beam induced currents. If the beam were surrounded by a perfectly smooth vacuum pipe, the characteristic impedance for losses would be of the order of 0.5 MΩ[1]. This impedance is substantially increased by irregularities in the vacuum chamber such as synchrotron radiation shields, interaction region chambers, joints, ports, etc.[2]

Using theoretical calculations[3] for cavities and bunch measurements for beam induced losses in various vacuum components, we estimate that these so called higher mode losses will require an additional 1.56 MeV accelerating voltage[4]. The total accelerating voltage required is thus 6.56 MeV per revolution. A cavity voltage in excess of this is required to provide long term containment of the beam in the face of radiation induced fluctuations of the individual particle energies. For a quantum lifetime in excess of 2 hours the nominal peak cavity voltage is 12.4 MV.

---

[1] A. Piwinski, DESY 72/72 Dec. 1972, p. 12.

[2] M. Allen, J. Paterson, J. Rees, P. Wilson, Beam Energy Loss to Parasitic Modes, 1975 Particle Accelerator Conference Proceedings.

[3] See, for example, E. Keil, C. Pellegrini, A. Turrin, A. Sessler, SLAC Publ. 1580.

[4] This vacuum passes 220 watt total lost at each of the 98 regular vacuum chamber joints, which have been made as smooth as possible, plus inavoidable irregularities equivalent to 15 of the accelerating cavity chambers.

TABLE 5-1

RF Parameters for 8 GeV Operations

Beam Energy Loss Per Revolution		
Synchrotron radiation		5 MeV
Higher cavity modes		1.15 MeV
Vacuum chamber		.41 MeV
	Total	6.56 MeV
Operating frequency		499.762 MHz
Cavity shunt impedance		535 MΩ
Effective cavity length		16.8 meter
Number of accelerator modules		4
Number of cells per module		14
Mode		Parallel coupled π
Power delivered to beam		1.23 MW
Total RF power		1.8 MW
Bunch length		4 cm
Bunch lengthening factor assumed		2.1
Number of Klystrons (250 kW nominal)		8

In computing the power that must be supplied by the rf source we must take into account the fact that a significant portion of the energy stored in the cavity is extracted each time a beam bunch passes through.[5] The resultant power required from the source is 1.8 MW. The power economy is shown in the parameter table.

In making the computation of higher mode losses a bunch length must be assumed. While no theory has as yet been proven to be reliable for the general case, we have made the assumption that the potential well distortion model[6] will give a lower limit for the bunch lengthening. It is this result that is given in the table. In this computation it is assumed that only the accelerating system is responsible for the lengthening.

b) Frequency

In computing the parameters given above it is assumed that the operating frequency will be 500 MHz. This choice is based upon economic factors. Were it possible to produce an economical and reliable system at a frequency in the range 50-100 MHz, experience to date seems to indicate that it would be desirable to do so. The major point is that at the lower frequencies, the amount of bunch field energy contained in the band of wavelengths which are comparable with vacuum chamber dimensions, would be relatively small so that beam induced reaction forces and heating would not be troublesome. The detailed technology for such a system

---

[5] P. B. Wilson, Proc. IX Int'n. Conf. on High Energy Acc. p. 57-61.

[6] See, for example, E. Keil, Bunch Lengthening and Bucket Distribution Due to Cavities, PEP note 126.

has not yet been developed for electron storage ring service and would require substantial effort. It is our belief that the heating and instability problems can be handled even when the rf system is operated at UHF frequencies. Therefore, we have decided to concentrate on solving these problems and to build the CESR system to operate at a frequency where the technology and economics are well understood[7]. Having made this decision, the exact value of operating requency was decided by the immediate commercial availability of a klystron at 500 MHz (250 kW units).

c) Cavity Design

Figure 5-1 is a cutaway view of the proposed cavity structure. It is a parallel coupled assembly of cavities with cavity profile optimized for shunt impedance and ease of fabrication. Coupling is effected by the resonant coaxial line which joins the cavities. Very little energy, even at higher frequencies, is transferred along the beam tube. All cavity components are constructed of rather thin walled members and cooling is accomplished by immersion of the entire assembly in a moving water bath. Coupling in the structure is strong enough that tuning can be accomplished by a single capacitively coupled, movable stub off the resonant coupling line. The structure is thermally stable, i.e., a detuning in a single cell results in a net decrease in the energy in that cell.

The structure design outlined above is somewhat different from that discussed in previous proposals and has resulted from a detailed examination of the particular needs of CESR. The injection scheme requires that

---

[7] Further details of our study of the instability and heating problems for short bunches are contained in the sections on cavity design and higher mode loss measurements.

CESR be stable under both multi-bunch, single bunch operation and various beam distributions in between. Experimental evidence from several accelerators show that beam-cavity interactions at frequencies other than the fundamental can cause serious instabilities in multi-bunch beams. It is clear from the theoretical analyses[8] that suppression of these instabilities requires control of the shunt impedance of many modes of the accelerating system. For this reason, we chose to make a cavity design which permitted strong coupling to each individual cavity chamber so that energy in modes other than the fundamental accelerating mode could be led away from the beam containing volume and dissipated harmlessly in a resistor. Such heavy coupling exists in the present cavity design, the unwanted energy being dissipated in a load coaxial with the coupling line but isolated from it by a rejection filter for the accelerating mode. The specifics of the design were arrived at by detailed consideration of the theory and each important cavity mode as measured in a multi-cell model at S-band. This is an iterative procedure, each step requiring a modification of the cavity and coupling to allow each of the important modes to be coupled to the line with sufficient strength to bring the instability threshold predicted for each mode to a beam current greater than that anticipated in CESR.

Fig. 5-2 is a photograph of a partially assembled prototype 14 cell cavity. The protruberances seen in the figure serve the dual purpose of symmetrizing the fields in the fundamental mode against perturbations due to the coupling iris and fixing the polarization of degenerate cavity

---

[8] See, for example, F. Sacherer, "A Longitudinal Stability Criterion for Bunched Beams" IEEE NS-20, 3, 1973 pp. 825 ff. R. Kohaupt, Longitudinal Instabilities, etc.., DESY H1-73/1 Sept. 1973. R. Kohaupt, Excitation of a Transverse Instability by Parasitic Cavity Modes, DESY H1-74/2 May 1974.

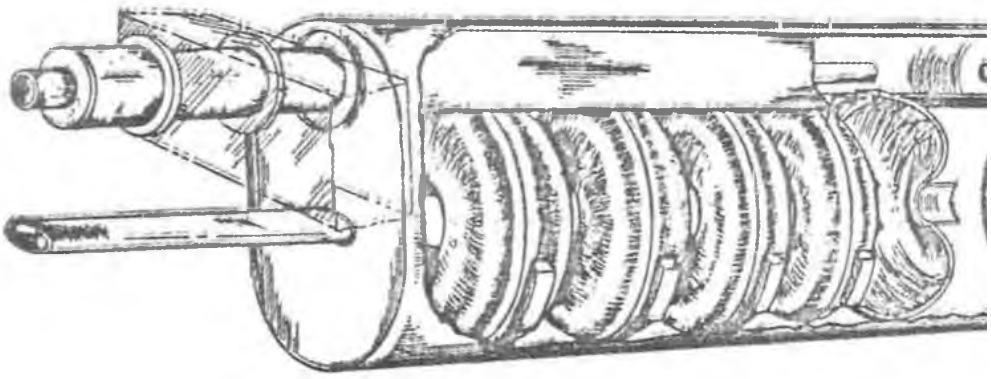

Fig. 5-1 Cutaway view of cavity structure

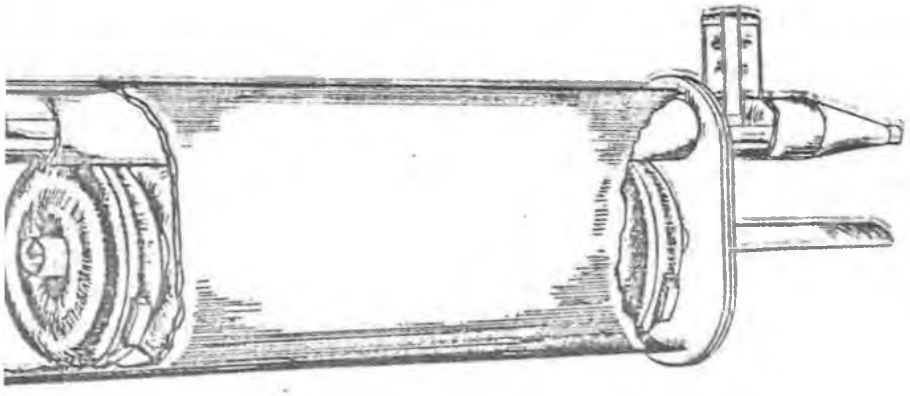

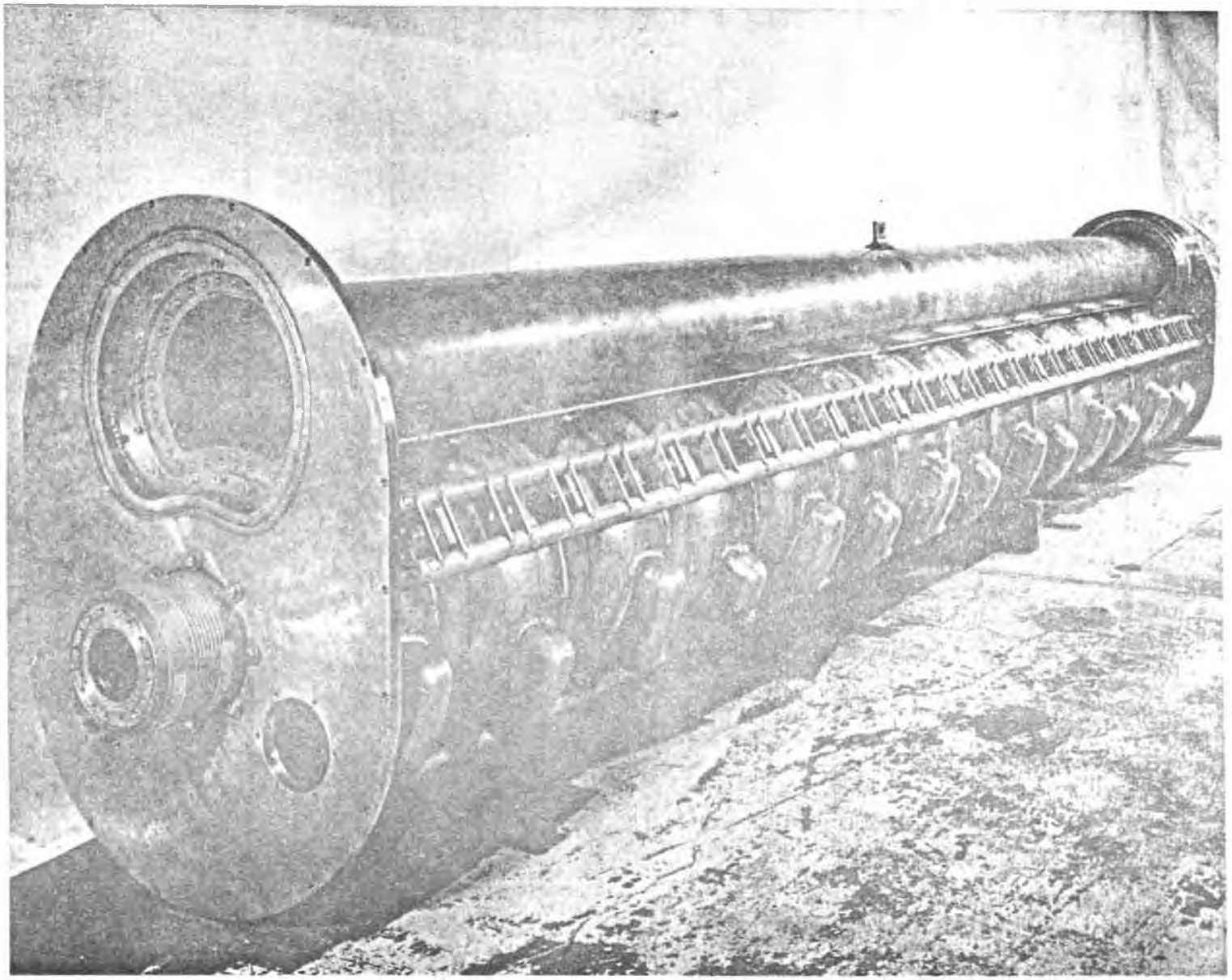

Fig. 5-2 14 cell cavity prototype

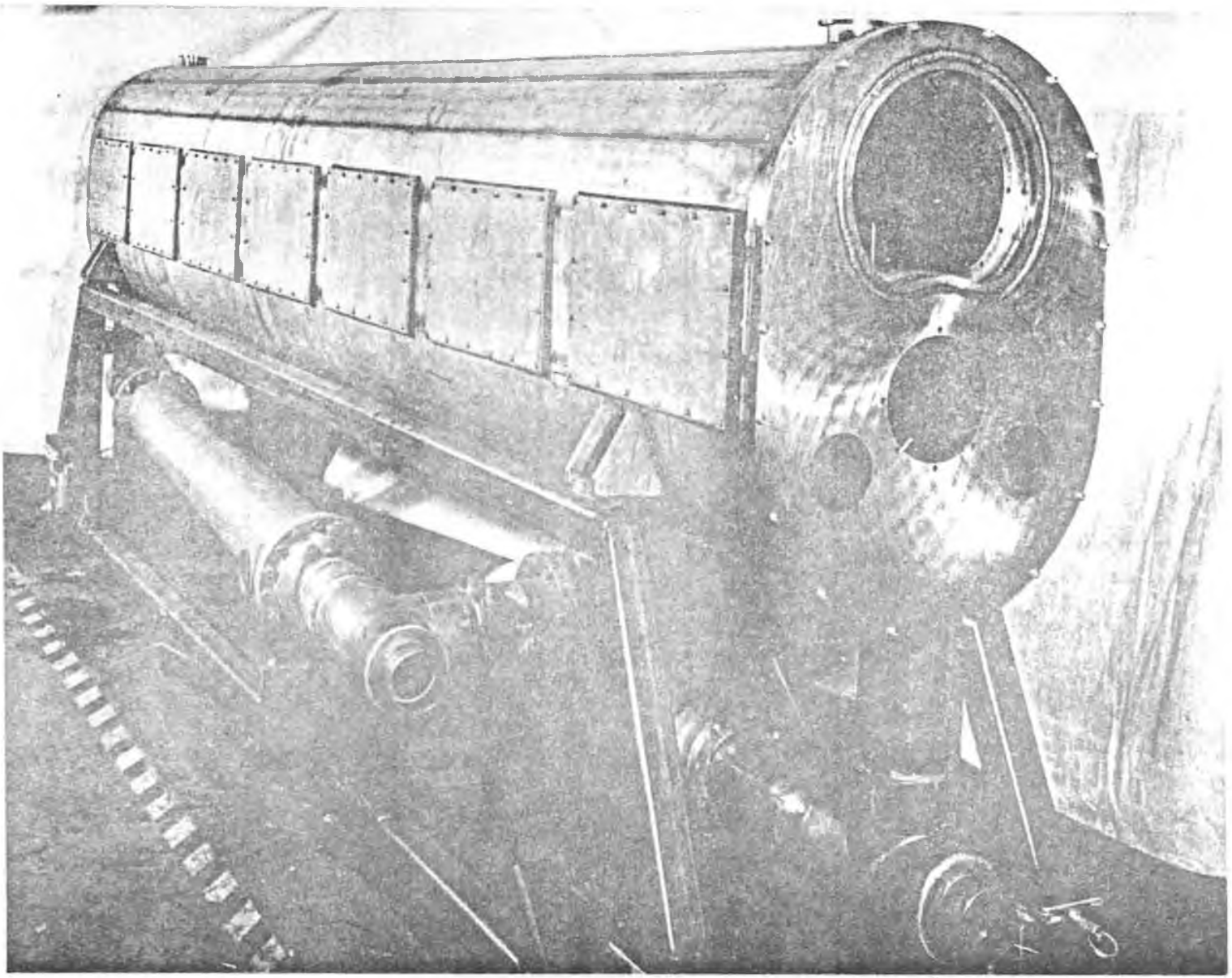

Fig. 5-3 Water jacket for 14 cell cavity unit.

modes split by the coupling iris so that both members are heavily coupled to the coupling line. Fig. 5-3 is a photograph of the water jacket for the 14 cell cavity unit.

d) RF Power Source and Control

In the frequency range selected for CESR, klystrons offer the only proven means of producing the requisite rf power. There are at present two commercial sources of 500 MHz klystrons capable of producing about 250 kW cw. A third firm is actively developing a 500 kW tube. The circuit diagram of Fig. 5-4, showing the rf circuit, is based upon the presumption that 250 kW units will be utilized. Should the more efficient and somewhat less costly 500 kW units become available in time, we will use them. The cavity units are designed for 500 kW input so that combiners will be necessary in the 8 tube (250 kW each) configuration. The output of the combiners will be fed to the input of the coupling lines through reflectometers. In addition, we may find it necessary to include ferrite isolators in the circuit to protect the tubes from the high "reflected" power pulses engendered by the beam. This matter is still under study.

The klystrons are of the modulating anode type and that control electrode will be used for smooth power control. The mod anode control circuit is shown in Fig. 5-5. A prototype of this circuit is now under construction.

In order to maintain correct phase and amplitude control of the accelerating voltage during operation of the storage ring, fast and slow feedback loops on these quantities will be necessary. In addition,

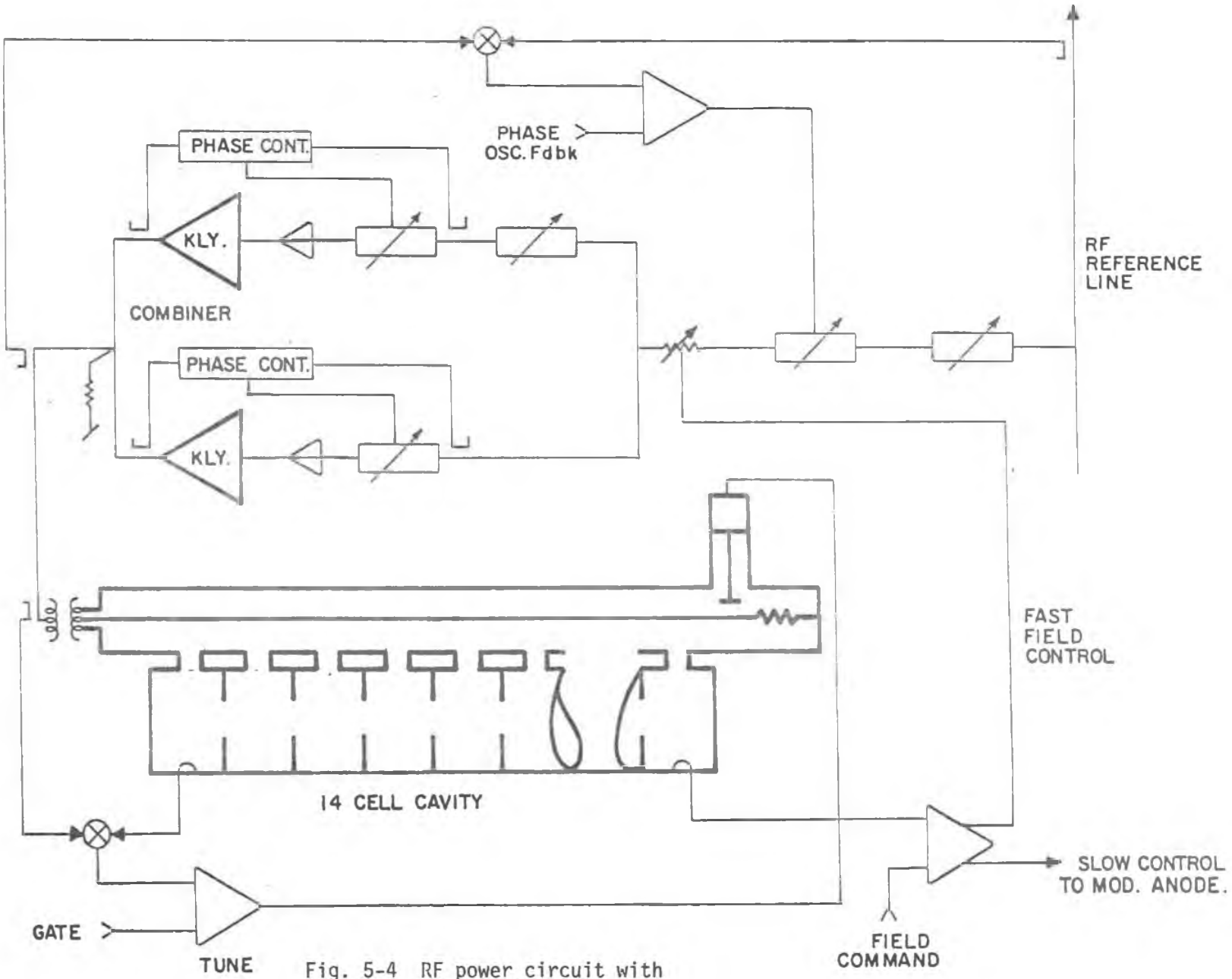

Fig. 5-4 RF power circuit with 250 KW klystrons

provision is made for controlling the phase to damp coherent phase oscillations of the beam. Protective circuits will be provided to shut off high voltage and drive for the klystrons in case of faults. Figure 5-4 is a schematic circuit diagram of the system showing the principal components. The phase shift across the klystron and its drive amplifier is controlled by a closed loop. The tuning of the cavity units is also controlled by a closed loop with an externally controlled offset which can be set manually or placed under feed back control to minimize the power reflected from the cavity. Monitor signals of all important variables will be multiplexed and transmitted to the control room.

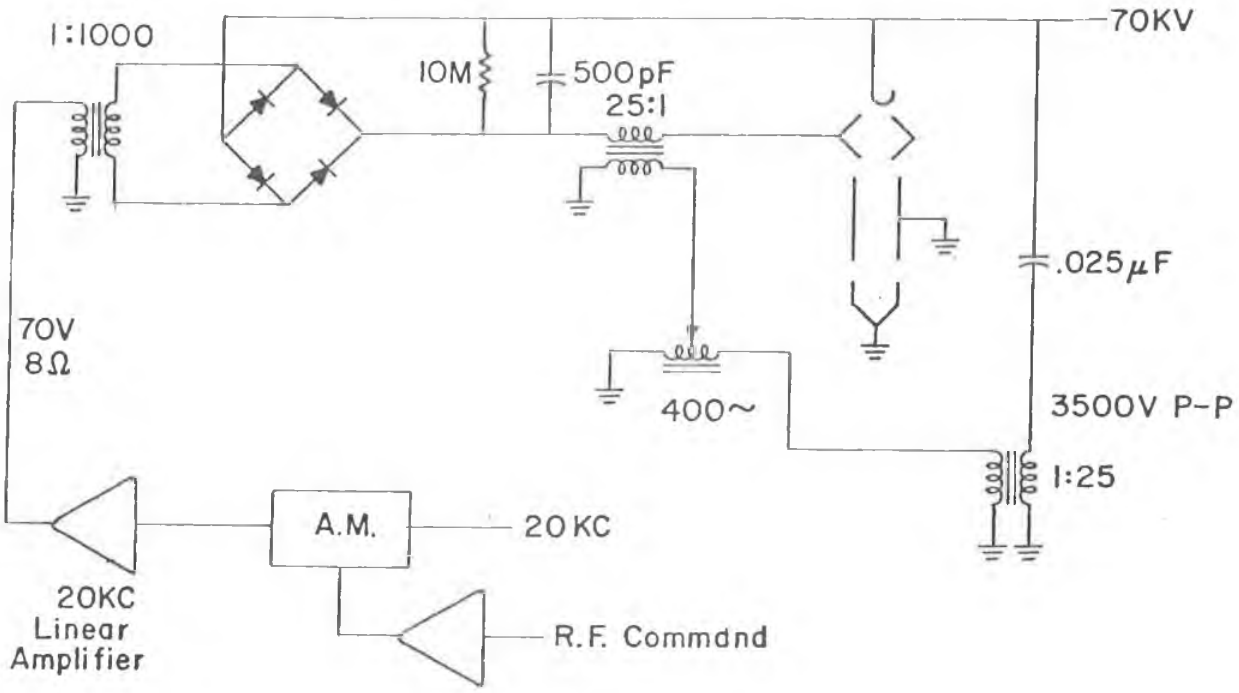

Fig. 5-5 Mod Anode Control Circuit

6. Vacuum System

The vacuum system is designed to maintain an average pressure of about 10^{-8} Torr with both beams circulating, so that the beam lifetime due to beam-gas bremsstrahlung is about ten to twelve hours. The main gas load is gas desorption from the walls of the vacuum chamber due to synchrotron radiation (SR). Table 6-1 shows the relevant parameters and the resultant total gas load. In the high-field regions, the linear energy flux on the outer wall of the chamber is 11 kW/m at 8 GeV with both beams circulating. The system is designed for adequate operation at 10 GeV with about 2 MW in synchrotron radiation. The spectral distribution of synchrotron radiation is shown in Fig. 6-1. The total gas load due to radiation is estimated to be 1.2×10^{-3} Torr-ℓ-sec^{-1} at 8 GeV. The gas load due to thermal desorption is estimated to be 2×10^{-5} Torr-ℓ-sec^{-1}.

The average pressure in various sections of the rings is shown in Fig. 6-2. The pumping speed of the distributed ion-pumps (see below) varies with the magnetic field, so that at low energy, extra 400 ℓ/s pumps are required near the low-field magnets around the interaction region. The average pressure seen by the beams is also shown in the figure.

a) Vacuum Chamber and Associated Components

The vacuum chamber in the curved regions will be made of extruded aluminum, with a cross-section as shown in Fig. 6-3. A water channel is built into the extruded sections for cooling the wall exposed to synchrotron radiation. The chamber will be curved to follow the orbit in the bend sections. The profile of the extruded aluminum vacuum chamber is designed so that a single continuous chamber can be used for both main bend magnets and the quadrupole in a half-cell, without troublesome joints. This requires

TABLE 6-1

VACUUM SYSTEM

		Beam Energy 8.0 GeV
I, Beam Current (Two beams)	(mA)	200
$<\varepsilon_c>$, Critical Energy in Normal Bends	(keV)	12.7
Radiated Synchrotron Power	(kW)	1000
Average Linear SR Intensity		
High Field Sections	(kW/m)	11
Normal Lattice	(kW/m)	1.5
Total gas load due to Synchrotron Radiation	(Torr-ℓ-s^{-1})	1.6×10^{-3}
Total gas load (no beams)	(Torr-ℓ-s^{-1})	2×10^{-5}
Base pressure (no beams) (holding pumps only)	(Torr)	5×10^{-9}
(all pumps and magnets on)	(Torr)	$\sim 10^{-10}$
Operating pressure (Average)	(Torr)	1.6×10^{-8}
Estimated pressure at Interaction point	(Torr)	1.4×10^{-10}
Lifetime due to beam-gas bremsstrahlung	(Hrs.)	12
Distributed ion pumps total speed	(ℓ-s^{-1})	$1.3 \times 10^{+5}$
Holding ion pumps†	#	65
Holding ion pump speed	(ℓ-s^{-1})	140

†Does not include ion pumps for intersection regions.

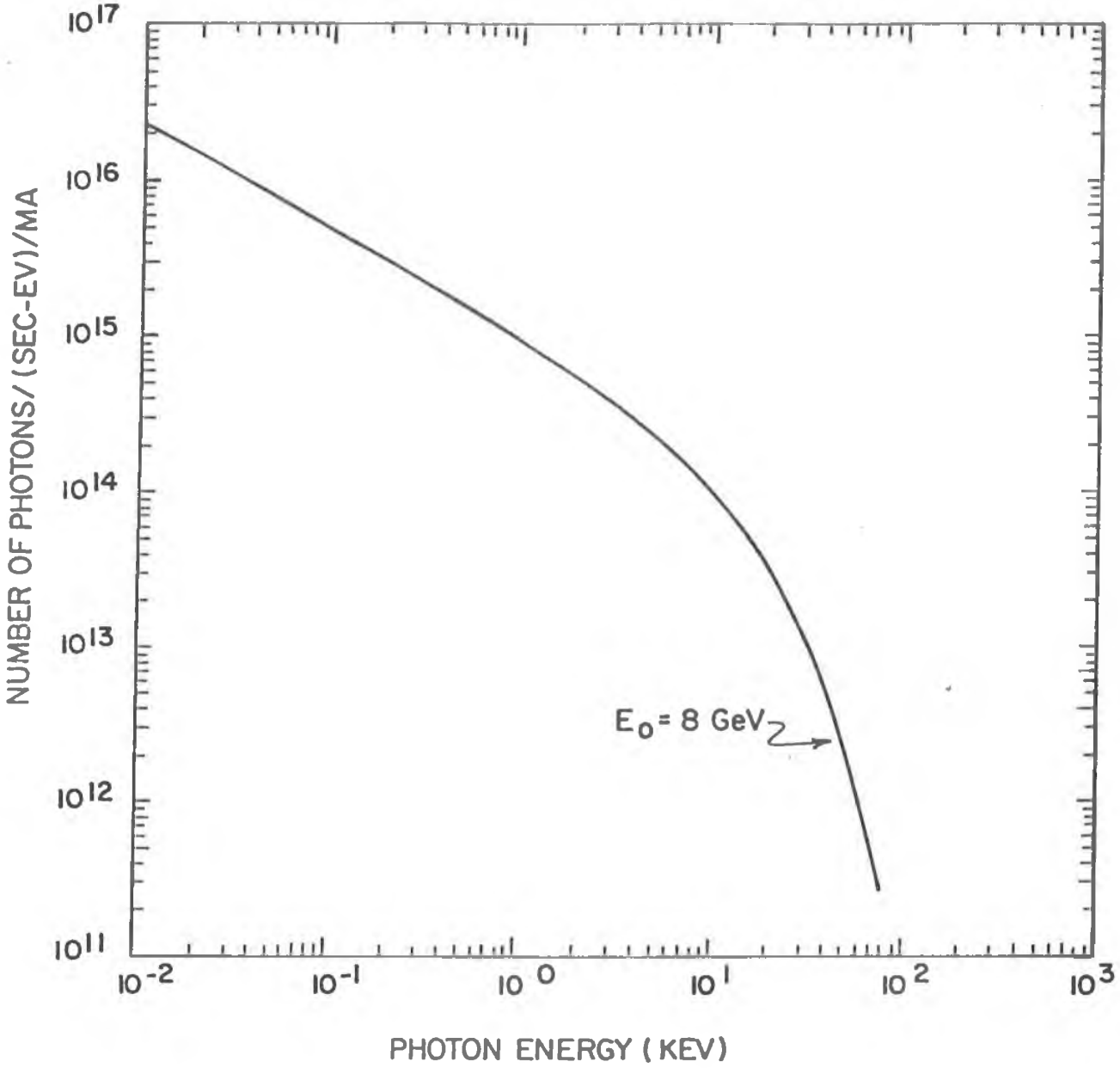

Fig. 6-1 Spectral Distribution of Synchrotron Radiation.

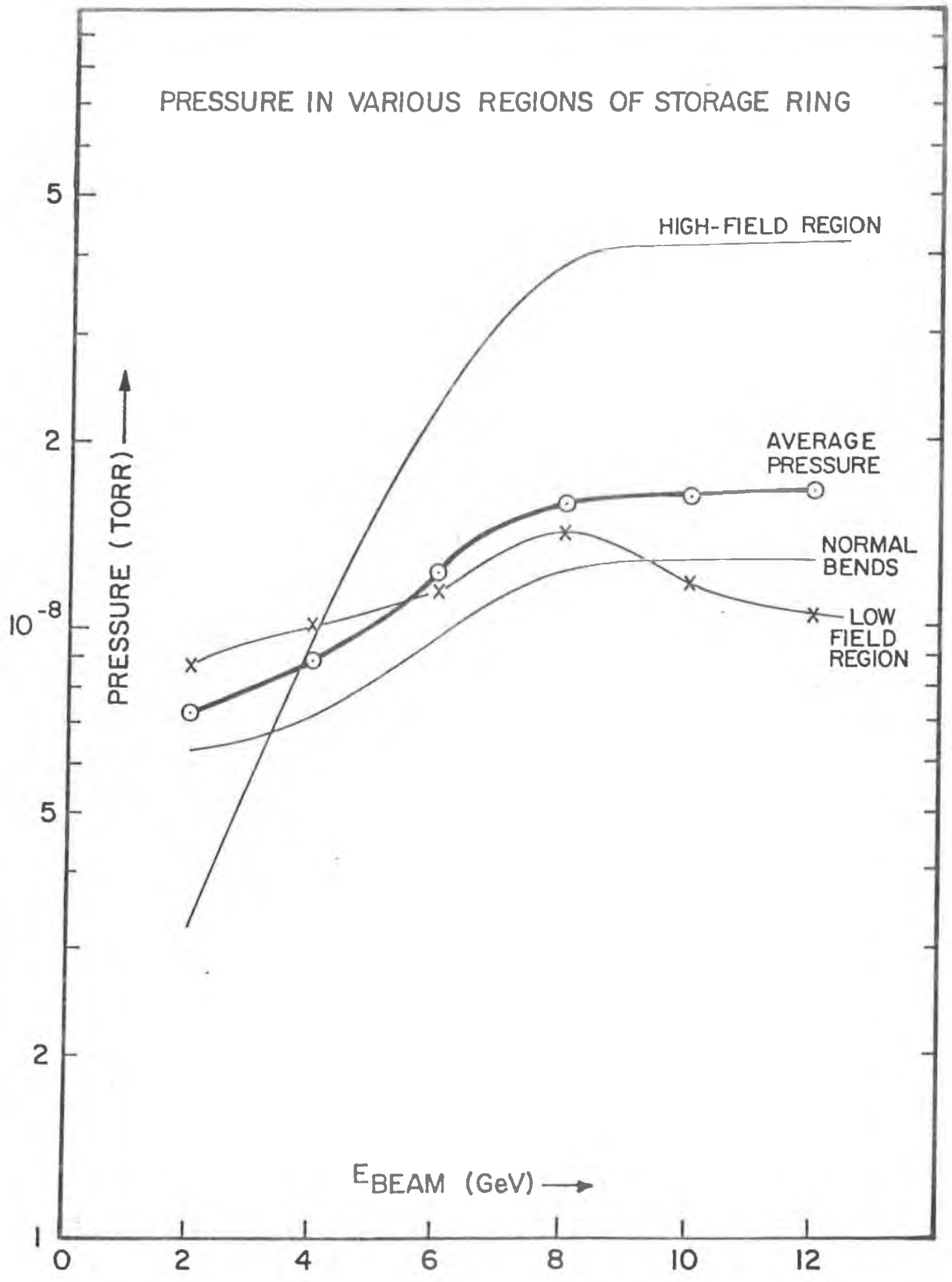
PRESSURE IN VARIOUS REGIONS OF STORAGE RING
HIGH-FIELD REGION
AVERAGE PRESSURE
NORMAL BENDS
LOW FIELD REGION
PRESSURE (TORR) ⟶
5
2
10⁻⁸
5
2
1
0
2
4
6
8
10
12
E BEAM (GeV) ⟶

Fig. 6-2

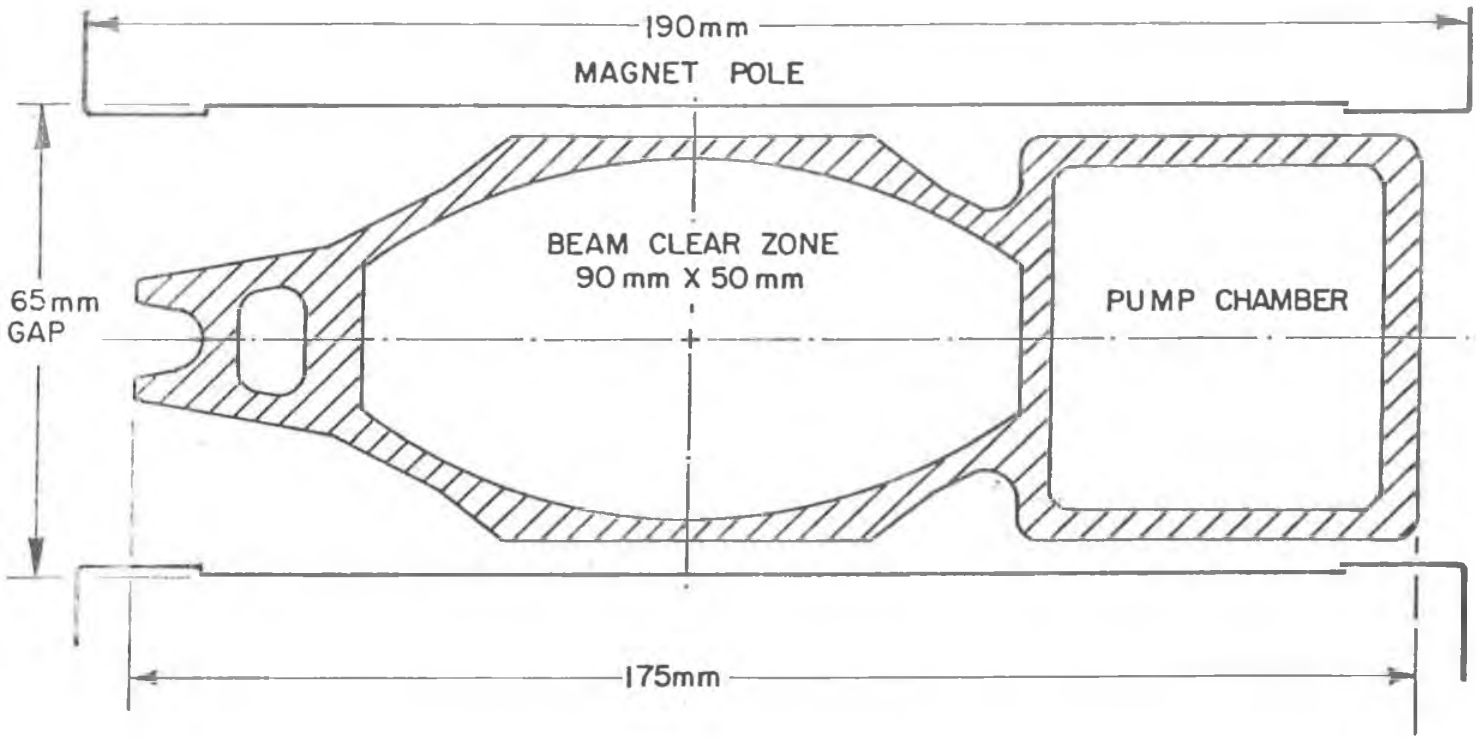

Fig. 6-3 Cross-section of aluminum extrusion for the vacuum chamber

the pump-chamber, as extruded, to be isolated by a solid wall instead of an open space. The pump chamber will then be cut away for the section through the quadrupole. The solid wall between the pump chamber and the beam chamber will be perforated to provide pumping slots. Two methods for making the slots were considered: Electrical discharge machining (EDM) and mechanical punching of slots using a punch and die combination which travel through the chambers. The second method appeared more feasible. A slot punching machine has been designed and fabricated, and has been successfully used for punching chambers up to 11 m long. A bending machine has also been made, and prototype chambers have been bent to the correct (88m) radius.

Nineteen 11 m long aluminum extrusions have been received. Twelve of these will be used in the protosector (one-sixth of the ring). The rest will be used for prototype development. Chambers for the protosector are being punched and will be bent to the correct radius in April. After all the required machining is completed, the chambers will be degreased and chemically cleaned before welding and assembly.

Figure 6-4 shows the details of a typical bellows joint between chamber sections. These joints are quite intricate, to avoid problems arising from the intense synchrotron radiation hitting the thin bellows, etc. Various inexpensive methods of producing vacuum-tight connections between aluminum chambers and stainless-steel bellows, etc., are being tried out, to assure good performance under heat cycling stresses, etc. In the design of all joints and transitions involving the beam chamber, care is taken to avoid steps larger than 0.5 mm in the interior profile of the chamber, in order to minimize higher-mode losses. Figure 6-5 shows an apparatus for testing the sliding-joint described above. High-power RF tests have been performed to determine the suitability of various RF gasket configurations and materials.

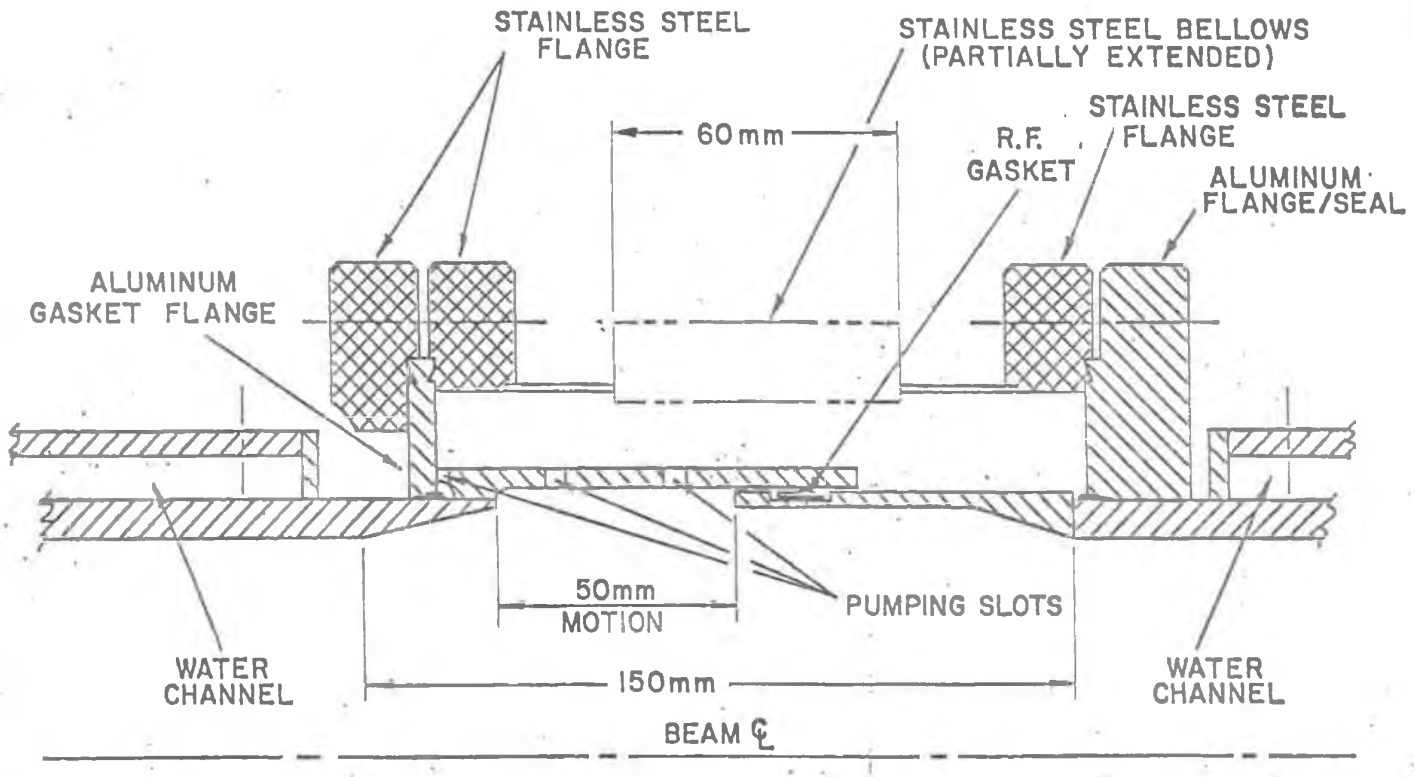

Fig. 6-4 Detail of bellows joint between vacuum chamber sections

The complicated design of a sliding joint may be avoided if a simple bellows could be designed such that higher-mode losses are reasonably low. Measurements have been made on a model elliptical welded bellows having an interior profile matching the beam-chamber profile. "Fine-tuning" of the bellows losses is possible by tapering the beam chamber to match the impedance of the bellows. Under these conditions a loss of 50 watts is expected for a beam bunch of about twice the natural bunch-length. A very steep rise of the power loss is expected with decreasing bunch length. We are studying the possibility of scaling down the bellows convolutions in order to reduce the power losses further.

Fast acting isolation valves will be used to divide the ring into sectors and to isolate the transfer lines to the synchrotron. In addition, manually operated isolation valves will isolate every major piece of equipment in the straight sections. Design modifications of commercially available UHV gate valves are being worked on, to provide a smooth unbroken chamber wall through open gate valves. This is necessary because of the problems due to large beam-induced RF fields in a non-uniform vacuum chamber. Figure 6-6 shows a modified valve, where the gate is extended to form an opening which, when the valve is "open", forms a smooth wall for the beam chamber. RF gaskets are used to make positive contact. This prototype valve has been successfully operated for over 4000 cycles under vacuum.

All parts of the vacuum chamber will be cleaned and baked out before assembly. Argon glow discharge cleaning of the vacuum chamber is being studied, both as a method of final cleaning after assembly and for cleaning in place in the ring if necessary. Provision will also be made for bake-out of all components in place in the ring. For the extruded chamber

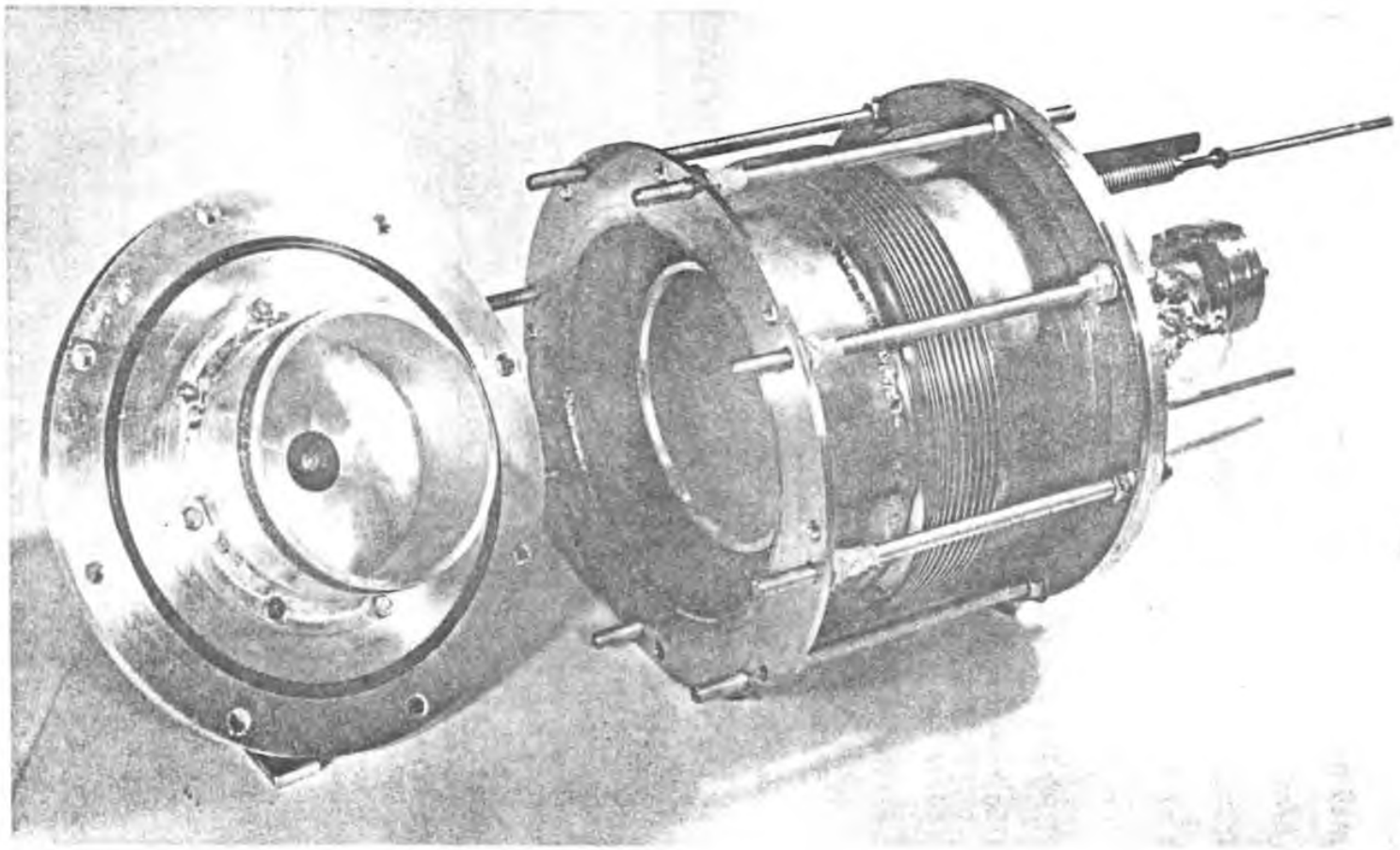

Fig. 6-5 Apparatus to test sliding joint between vacuum chambers shown in Figure 6-4.

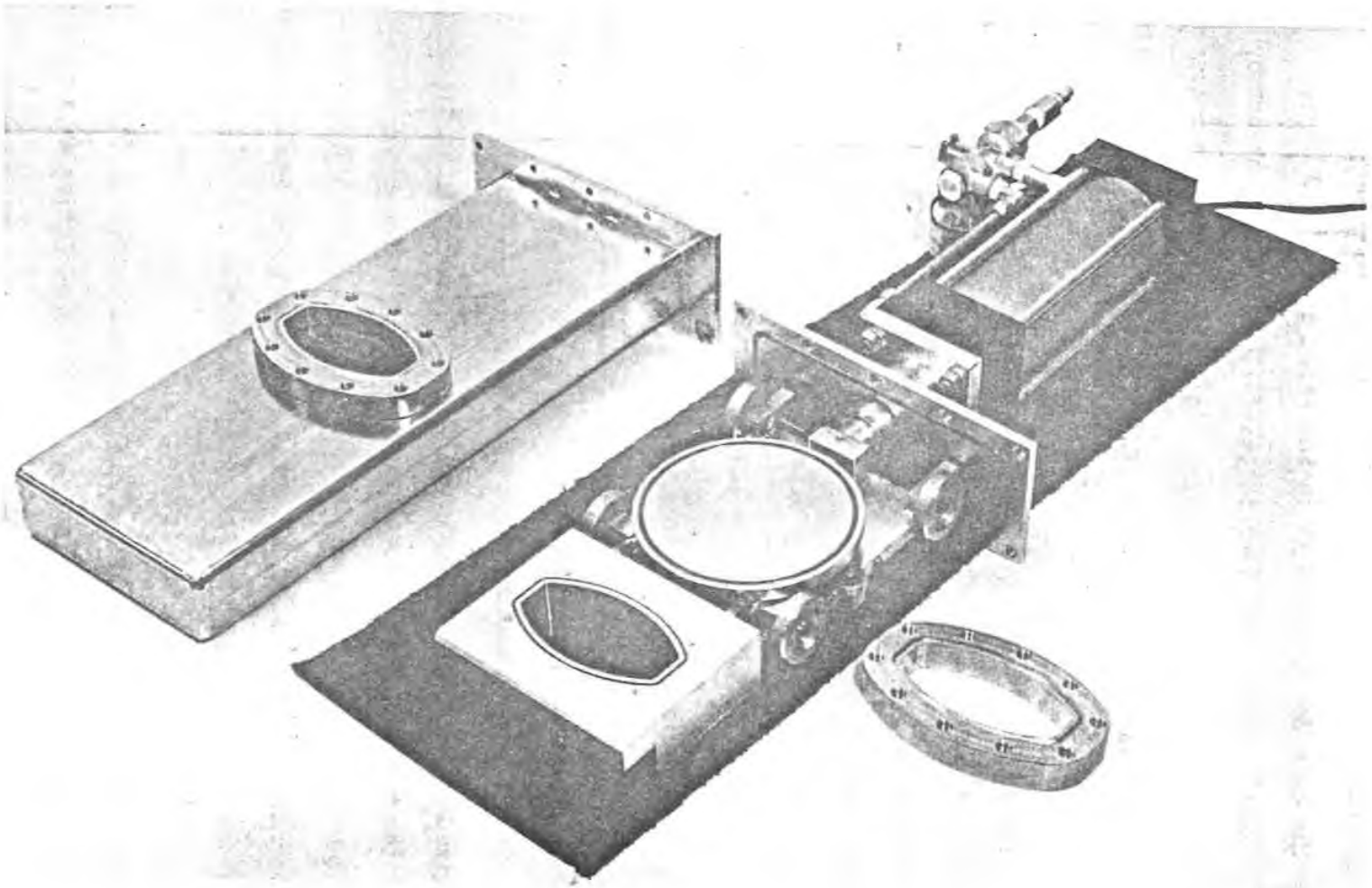

Fig. 6-6 UHV gate valve, modified to provide smooth unbroken wall of vacuum chamber.

several methods are available. Rod heaters may be clamped between the "ears" on the extruded chambers as in the PETRA design[1]. A direct electrical heating method has been successfully tried for bakeout by passing 3500 amp through the extrusion. This appears to be a better method for use in the ring, where an entire sector of half-cells between gate valves may have to be baked out. Other sections of the vacuum chamber and auxiliary equipment can be baked out with resistance heaters.

Ceramic chambers will be used in sections of the injection/extraction system (e.g., fast kicker magnets). Prototype ceramic chambers have been obtained and tested in the prototype fast kicker magnets. Thin metallic coatings on the chamber walls are used to minimize leakage of beam-induced RF fields.

b) High Vacuum Pumps

The conductance of the vacuum chambers in the bend sections limits the minimum pressure attainable using "lumped" pumps at the straight sections. "Distributed" sputter-ion pumps of the type used at SPEAR[2] will be installed in the bend sections of the vacuum chamber, and will use the field of the bending magnets for their pumping action. Prototypes of the distributed sputter-ion pump have been made and the pumping characteristics for different gases have been studied at various magnetic fields and at several pressures in the range (10^{-6} Torr-10^{-9} Torr). The final design for mass produced pumps is almost complete, and some parts have been ordered. A long section (3 meters) of pump has been made for insertion in the prototype bend magnet. Figure 6-7 shows a section of pump protruding

---

[1] Updated version of PETRA proposal, February 1976.

[2] U. Cummings et al., Journal of Vacuum Science of Technology 8, 348 (1971); D. Bostic et al., SLAC-Pub.-1547 (1975).

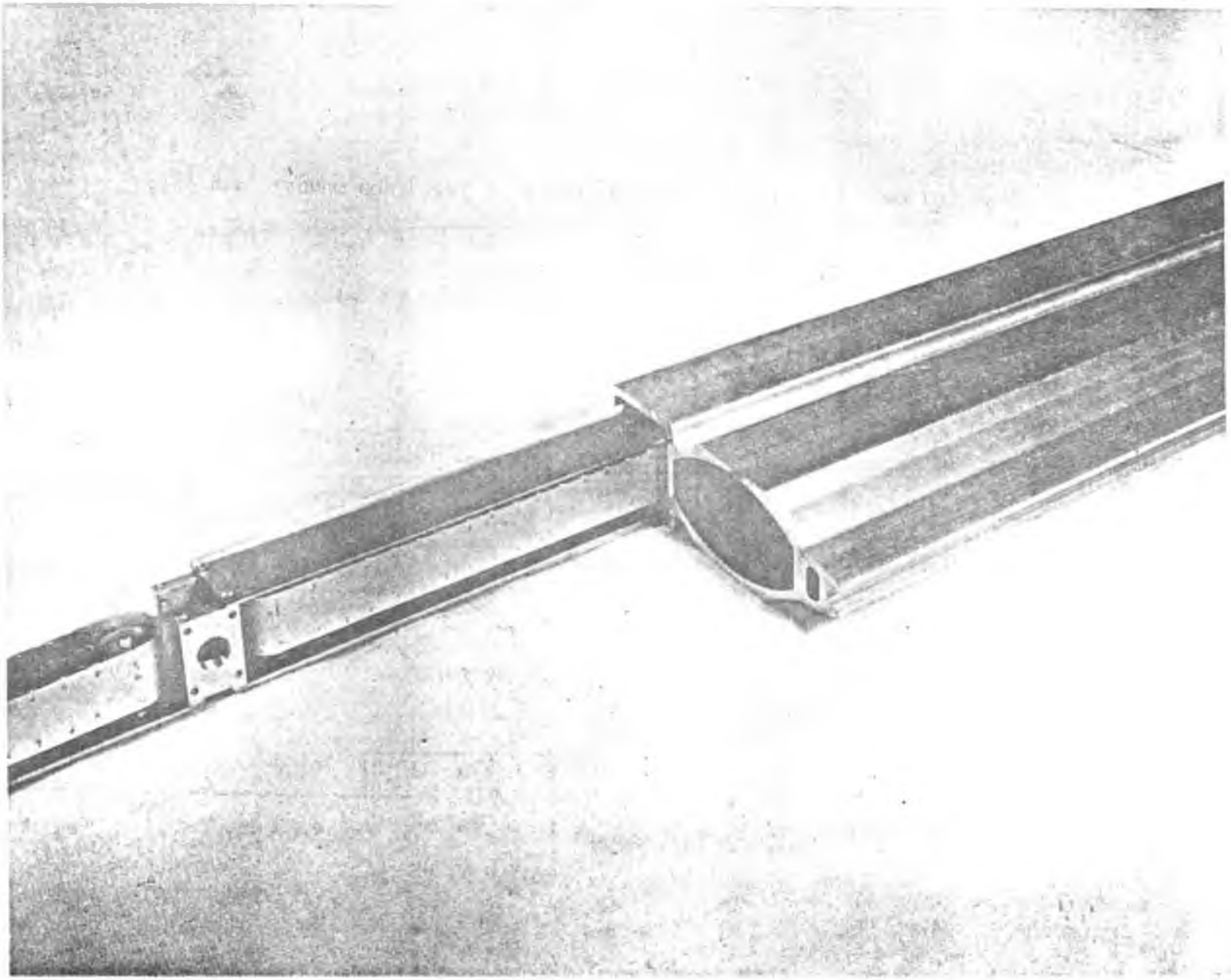

Fig. 6-7 A section of the distributed sputter-ion pump protrudes from a vacuum chamber.

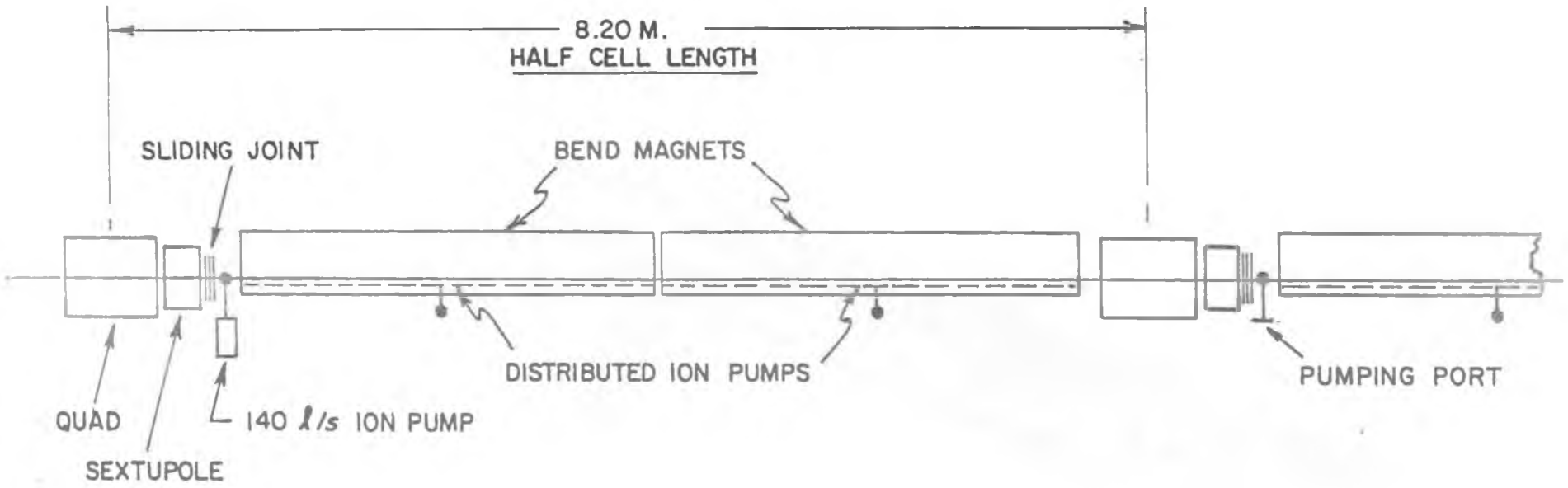

Fig. 6-8 Vacuum equipment of a typical half-cell in the bend regions.

from an extruded aluminum chamber. The pumps in the normal lattice will have three rows of anode cells of 12.5 mm diameter. Anode cells of larger diameter will be used in the low field magnets.

Commercial 140 ℓ/sec ion pumps will be installed at each quadrupole section as holding pumps when the magnets are switched off, and at the long straight sections to maintain an average pressure of 10^{-8} Torr during beam operation. For initial operation, these pumps will be installed at every alternate half-cell in the normal lattice. Additional pumps will be installed only if required for low energy operation, e.g., at 2 GeV. Fig. 6-8 shows a schematic representation of a typical half-cell in the normal bend regions.

To achieve pressures below 10^{-10} Torr in the interaction regions, special degassing methods will be used to pretreat the stainless steel vacuum chamber. At each end of each region, large titanium-sublimation pumps (3500 ℓ/sec) as well as several ion pumps will be used to maintain a high differential pumping speed. If necessary, cryogenic pumping will be used to maintain very low pressures. All equipment will be bakeable up to 200°C. Figure 6-9 shows the arrangement at one end of an interaction region.

c) Roughing Pumps

Each sector of the ring and each transfer line will have a roughing system attached at one pumping station. In addition, rough-out ports with manual valves will be provided at each ion-pump station, where a portable roughing system may be attached.

A typical roughing system will consist of three cryogenic sorption pumps, chosen to pump down a typical sector within a reasonable time ($\sim$ 30 min.) from atmospheric pressure. Manual valves and a thermocouple

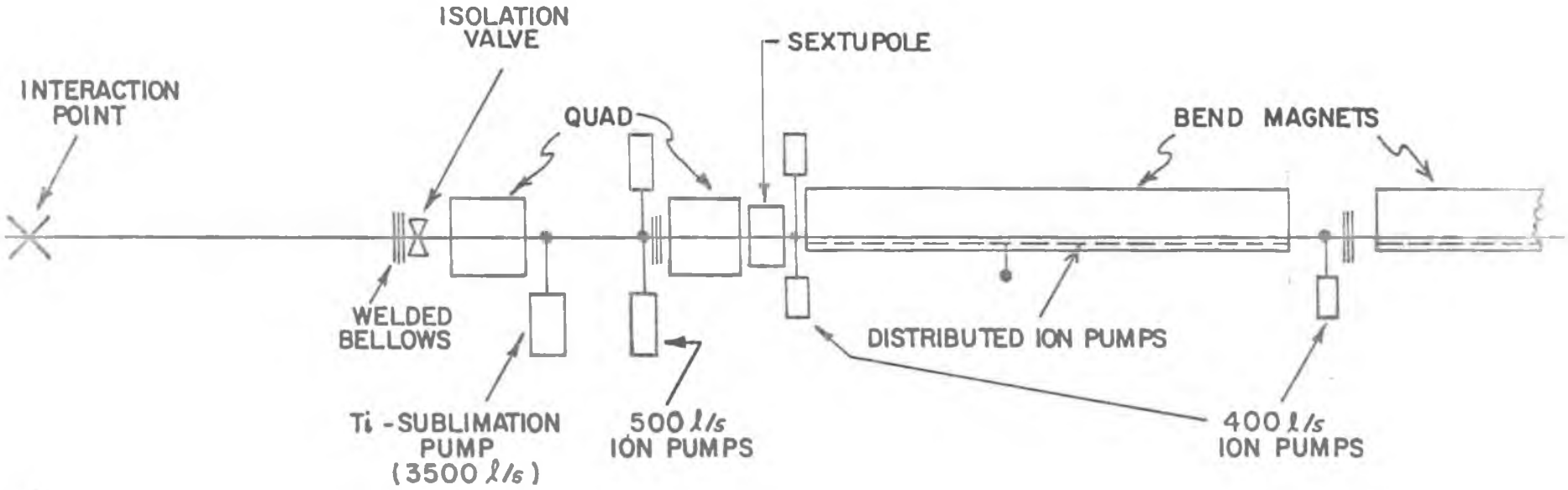

Fig. 6-9 Vacuum equipment at one end of an interaction region.

gauge are provided to optimize the closing off of the three pumps in a proper sequence. An in-line molecular sieve is provided to trap pump oil vapours in case mechanical pumps need to be attached for initial pump-down.

d) Vacuum Monitoring and Instrumentation

The currents in the distributed and lumped ion-pumps will normally serve to monitor the pressure. These will be read locally and centrally through the main multiplexing system. Additional monitoring is provided through nude UHV gauges installed in each section and transfer line. A quadrupole gas-analyzer tube will be attached at each interaction region sector, and one additional tube will be available for general use. Thermocouples are installed in each sector for monitoring pump-down rates. Pressure rise in any sector will automatically close all the fast-acting sector isolation valves.

7. Injection and Stacking

Crucial to the achievement of adequate luminosity in the storage ring is the ability to inject the requisite numbers of electrons and positrons in a time which is short compared to the useful beam lifetime. At 8 GeV, the method we propose will allow us to fill with positrons and with electrons at the rate of 0.7 mA per second and with electrons at the rate of 2 mA per second giving filling times of 2.4 minutes for each. To avoid the complexities of extra collisions with multiple bunches, electrons and positrons will be stored in single bunches. Briefly, the injection and stacking process will proceed as follows. Positrons will be made by converting an intense electron beam at a target at the midpoint of the linac. The positrons are accelerated to an energy of approximately 200 MeV and injected into the synchrotron. The electron beam in the linac will be

modulated so that 60 evenly spaced bunches of positrons are injected into the synchrotron. These 60 bunches will be accelerated to 8 GeV, whereupon they will be extracted from the synchrotron in a single turn and injected into the storage ring. This process is repeated at 60 Hz, successive bunch trains from the synchrotron being laid on top of the 60 bunches circulating in the storage ring. When the total charge in the storage ring reaches the value required, the linac is turned off and the 60 bunches circulating are coalesced into one by a vernier phase space compression technique to be described.[1] This gathering of the total charge into one bunch takes two seconds.

To avoid detrimental effects of beam-beam collision during injection, electrons and positrons should be separated from each other during injection of electrons. As it is economical to do this only at the regular interaction regions, only the properly phased bunch of electrons may circulate in the storage ring once the positrons are stored in a single bunch. This circumstance necessitates the use of a method for electron injection different from that for the positrons. Electrons will be accelerated in the linac to approximately 200 MeV and transported to the synchrotron injection point. During electron injection the linac beam will be modulated such that the synchrotron is filled with one bunch. The bunch is then accelerated to 8 GeV, extracted and stacked in the storage ring. In spite of the relative inefficiency of this method, the filling time for electrons is about the same as that for positrons because of the copious supply of electrons available from the linac. For operating energies in the range of 7 to 10 GeV the filling time will be approximately independent

---

[1] CLNS-299, Laboratory of Nuclear Studies, Cornell University, Ithaca, N.Y.

of whether the beam is injected at 8 GeV and accelerated to the energy of use or whether it is injected directly at the oeprating energy. The reason is that the damping time for betatron oscillations is short enough in this energy region that the maximum repetition rate of the synchrotron can be used. The damping time for betatron oscillations at 8 GeV is 8.2 m sec. While it may prove possible to decelerate the beam from 8 GeV to energies below 7 GeV without sacrificing optimum luminosity, the most straightforward method is to inject at an energy close to the desired operating energy. At 3 GeV, for example, the damping time is about a factor of 8 larger than at 8 GeV while the number of particles required is three eighths that at 8 GeV, giving a net increase of a factor of three in the required injection time. The details of the injection and stacking equipment and procedures are described below.

a) Injection Linac

Since the rate at which positrons can be generated is proportional to the linac beam power, it is important to be provided with a linac capable of high beam power. Additionally, in the parameter range of interest, the fraction of the positrons created at the conversion target that can be captured in the synchrotron is proportional to the energy at which the positrons are injected into the synchrotron. This means that in a given length of linac about half the length should be used for acceleration of the positrons.

The original synchrotron linac was a 3 klystron, six section, S-band machine capable of 220 MeV unloaded energy. To increase the linac power available, arrangements were made to secure the 5 section, 5 klystron 225 MeV linac that was used previously at the Cambridge Electron Accelerator. This linac is equipped with a positron target and accelerating

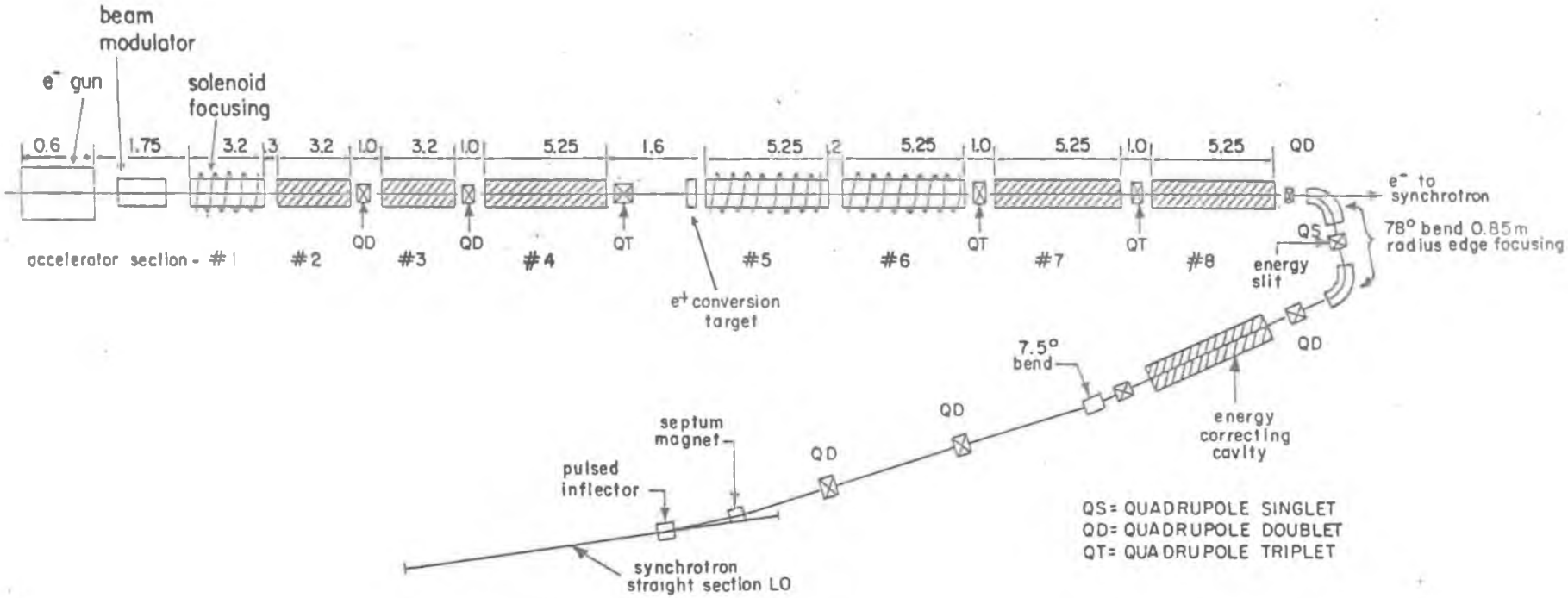

Fig. 7-1a Schematic of e^+e^- linac, formed by combining the original Cornell linac and sections of the CEA linac, with e^+ injection into LO long straight section of synchrotron.

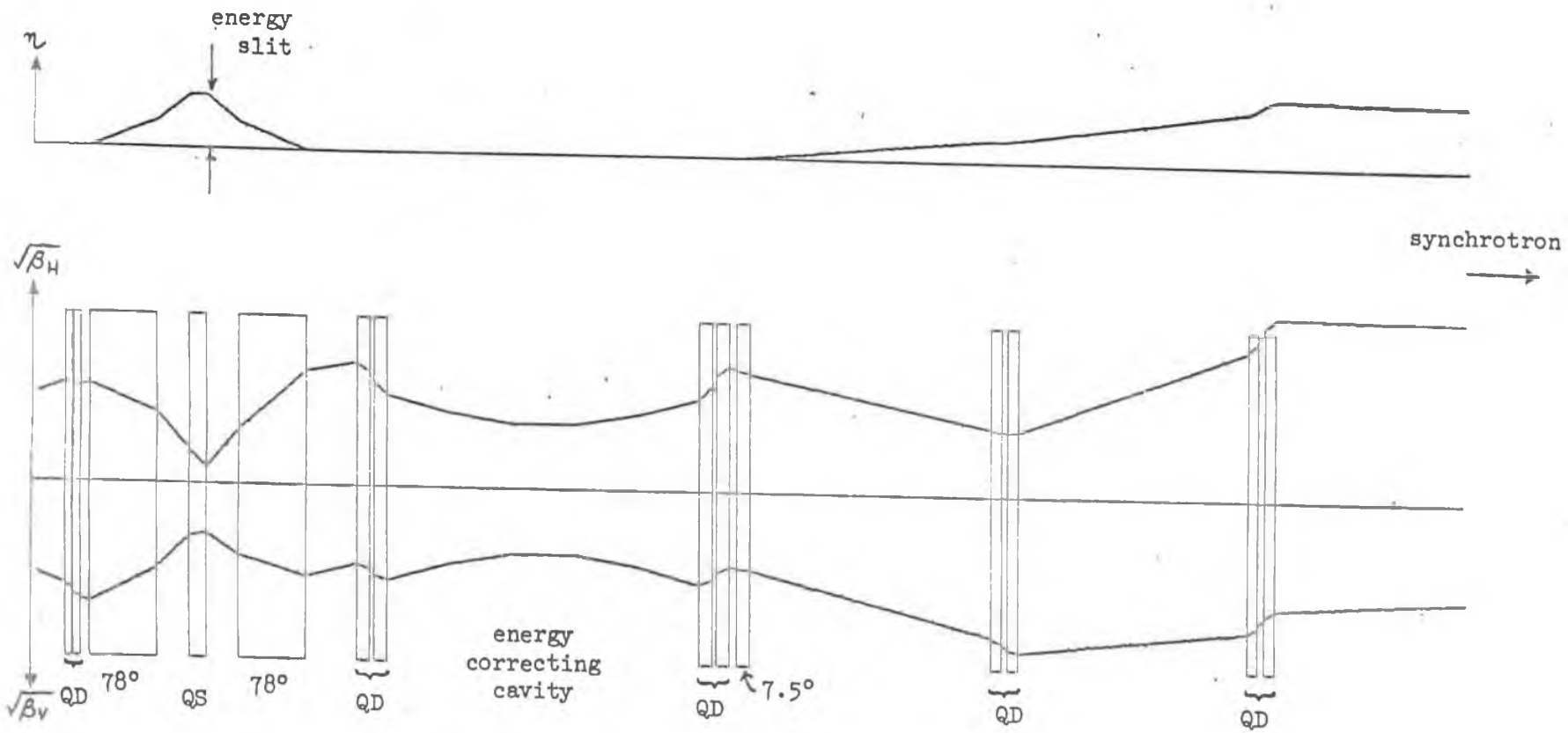

Fig. 7-1b e^+ injection optics, shown straightened out along central beam trajectory. The horizontal and vertical amplitude functions, $\sqrt{\beta_H}$ and $\sqrt{\beta_V}$, and the dispersion function η, are matched to the values which obtain at the injection point into the synchrotron.

sections with built-in positron focusing solenoids. By arranging 8 of the 11 available sections, as shown schematically in Fig. 7-1, it will be possible to accelerate electrons to 175 MeV before striking the positron converter and to accelerate the positrons emerging from the target to 200 MeV. The accelerated positrons are then bent in an asynchronous bend and passed through a final cavity to reduce the energy spread in the beam by a factor of 5, thus enhancing capture in the synchrotron.[2]

In computing the positron injection rate, a pulse averaged electron current of 30 mA is assumed. While this is a modest figure, it must be noted that because of the modulation of the beam required (all charge carried in 60 bunches), the space charge effects in the modulator and bunching section will be those corresponding to a 1 ampere pulse averaged current. While it may be possible to exceed this figure by a factor of two, to be conservative, we have chosen the lower value.

The special modulation of the linac, high current electron acceleration in the linac and synchrotron, and positron production and acceleration in the linac and synchrotron are techniques crucial to the success of CESR. For this reason, we have launched a development program to ensure that the necessary technology is in hand. This development program is centered around reconditioning the former CEA linac, modifying it as described above, and design and fabrication of the necessary modulation and beam transport equipment. The complete linac is now installed and operating for normal synchrotron injection. Figure 7-2 is a photograph of the portion of the linac containing the positron converter.

---

[2] See, for example, H. Herminghaus & K. Kaiser, Nucl. Inst. and Methods, 113 (1973) 189-194.

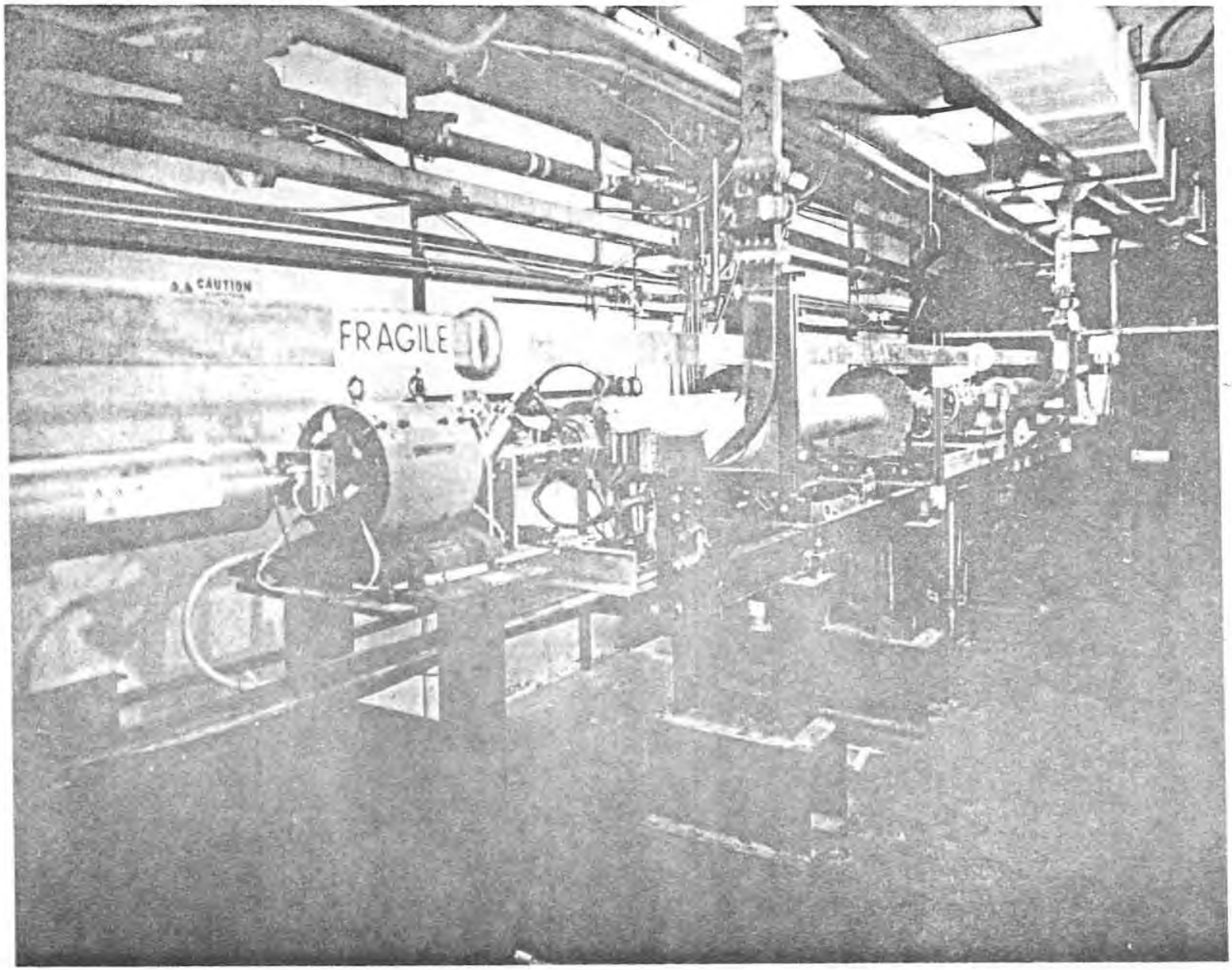

Fig. 7-2 A portion of the new Cornell electron-positron linac.

Since spring 1976, we have been designing and fabricating the linac beam modulation equipment. The CEA electron gun was set up in its final position and the modulation equipment installed for test. The test set up is shown in the photograph of Fig. 7-3. The basic modulation is accomplished by three sets of transverse deflector plates and a subharmonic pre-buncher. For positron production the DC electron beam from the gun must be modulated into a train of 60 bunches, each 42 ns apart in time. Each of the 60 bunches must be contained in a single S-band linac bunch for optimum efficiency. Coarse modulation is accomplished by applying rf to two pairs of deflection plates which produce deflections orthogonal to each other. Each of the plates is connected to a quarter wave resonant line. The resonant lines can be seen projecting upwards in Fig. 7-3. Two different frequencies are applied to the two pairs of plates so that the beam executes a Lissajous pattern on a down stream collimator. The beam sweeps across the collimator hole at twice the beat frequency of the 2 rf frequencies. The chopped beam emerging from the collimator is then velocity modulated in a 238 MHz prebuncher and a 2856 MHz prebuncher before injection into the linac. The advantage of this type of chopping is that very little rf power is required.

For electron injection, the linac beam is modulated into 1, 2 or 3 S-band bunches evenly spaced over the 2.5 μsec synchrotron revolution time. To accomplish this a pair of deflection plates upstream of the Lissajous plates is biased to prevent the beam from passing an upstream collimator. One, two or three bursts of beam are allowed to pass at the appropriate time by grounding the upstream plates with a fast tetrode (Eimac x 540) mounted directly to the plates. The components for the

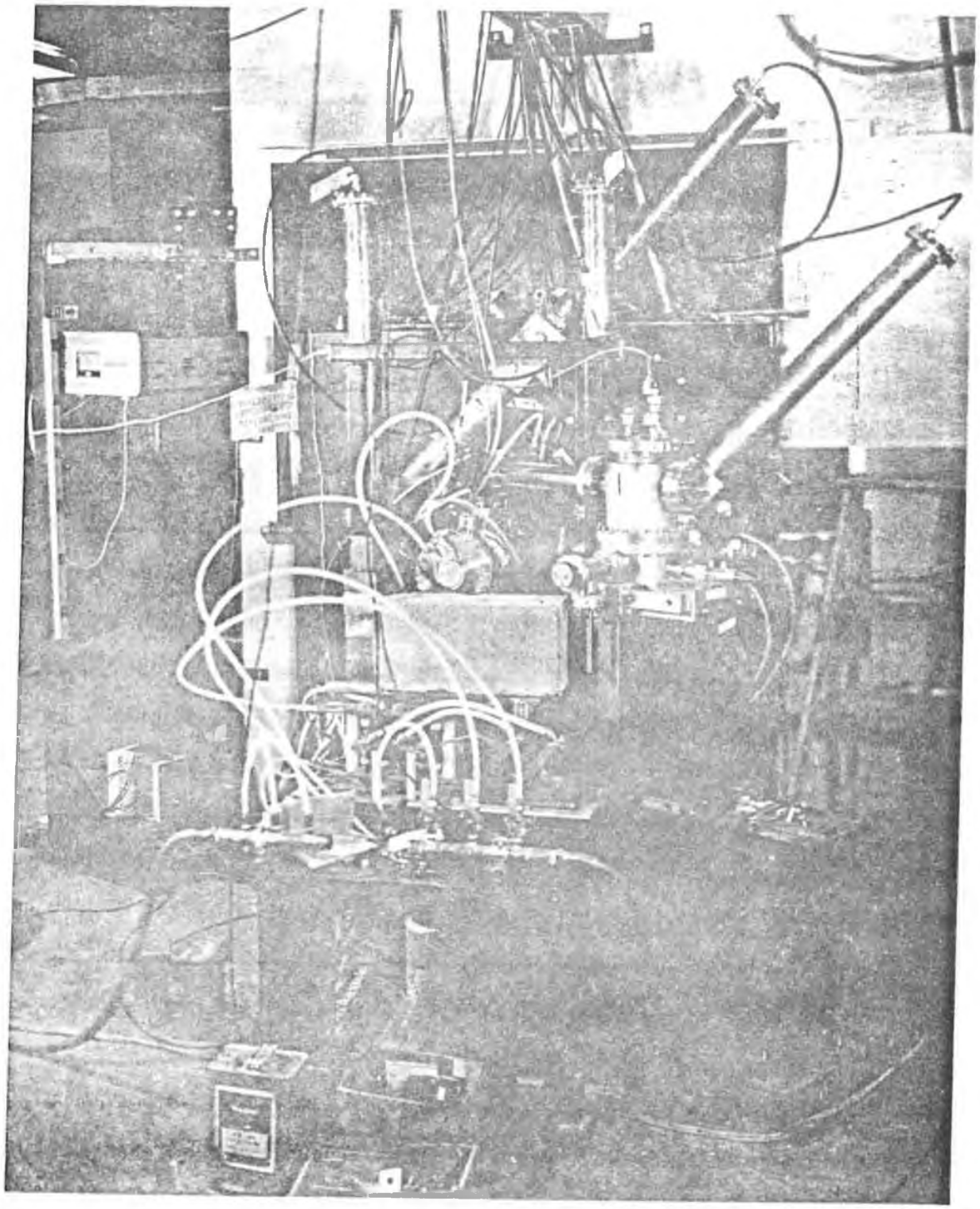

Fig. 7-3 Electron gun with modulation equipment.

system have been assembled and preliminary tests show that the designed modulation has been achieved. As soon as shielding is complete positron production tests will begin.

b) Positron Filling

The first step in filling the storage ring with positrons is to accumulate the required number of positrons (1.5×10^{12}) in 60 bunches circulating in the storage ring. Positrons are injected into the synchrotron and accelerated to the appropriate energy. Every 30th synchrotron bucket is filled. The linac and linac beam modulator are synchronized with the synchrotron rf system. The positrons are extracted in a single turn and injected into the storage ring. (Refer to Fig. 7-4 to identify components). Kicker K249W in the synchrotron kicks the beam over the septa S248W, S247W, and into the exit line Q305, Q304, etc. Injection into the storage ring is performed using septa S241W, S240W in conjunction with an orbit bump effected by bumpers B226W, B228W, and B236W. This bump reamins on for one revolution period (2.5 μsec) and is then shut off in the course of the next three revolutions so that the injected particles may continue to miss the septum. This process is repeated on subsequent synchrotron cycles. Extraction optics of the synchrotron is shown in Fig. 7-5. The time interval between cycles is long enough for damping of the horizontal betatron oscillations engendered by the injection process. Successive injections must of course be properly rf phased so that incoming bunches fall into the occupied buckets in the storage ring. The master rf oscillator will be used as the reference clock. This initial stage of filling will be complete after about 10^4 synchrotron cycles with 2×10^{12} positrons divided into 60 equal bunches circulating in the storage ring. Since the storage ring circumference is 21λ (λ = storage ring rf wave

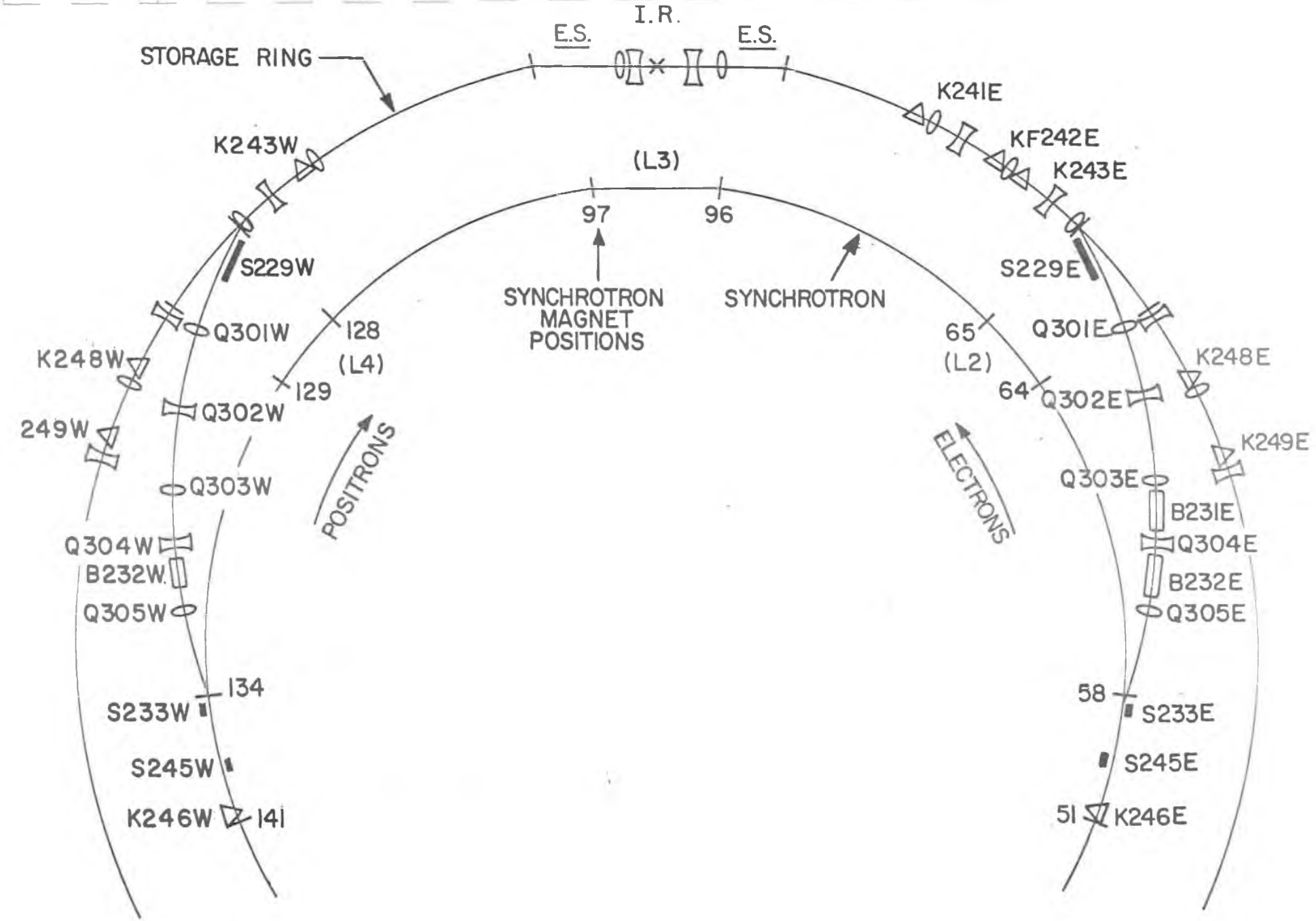

Fig. 7-4 Schematic of components for filling storage ring with positrons and electrons.

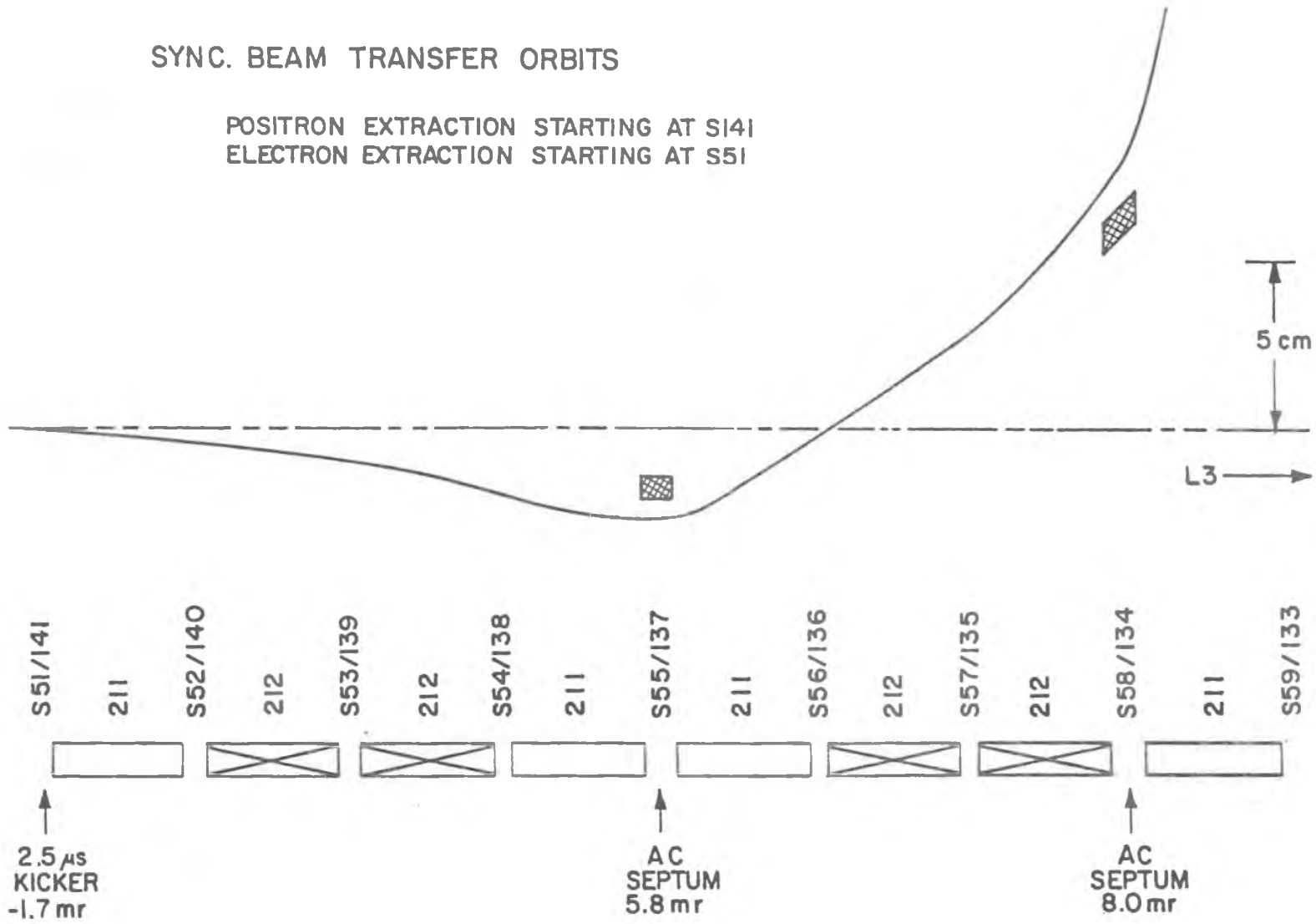

Fig. 7-5 Synchrotron extraction optics.

length) larger than that of the synchrotron, there will be an additional gap of 21λ between the first and last bunch in the storage ring. This situation is shown schematically in Fig. 7-6a.

The 60 bunches are next coalesced into a single bunch during the second stage of positron injection. At the beginning of this process, bunch number 1 alone is extracted from the storage ring over septum S240E by a fast kicker KF236E in concert with an orbit bump engendered by B238E, B236E, B232E, B230E, B228E, and B226E. The orbit bump brings the equilibrium orbit close to the septum but not so close that there is significant beam loss during the 3 revolution duration of the bump. KF236E kicks the single bunch over the septum and is off before the trailing bunch arrives. Since the temporal bunch spacing is 42n sec, then rise and fall times of KF236E of 30n sec are adequate to ensure that only the desired bunch is kicked over S240E. The extraction optics for the single extracted bunch are shown in Fig. 7-7. The bunch travels around the synchrotron until it reaches K249W where it is extracted and reinjected into the storage ring in the same manner in which the positrons were initially injected.

After the completion of this sequence the bunch has advanced in phase as compared with its initial position. This is shown in Fig. 7-6b.

The advance is due to the path difference along the equilibrium orbits in the storage ring and synchrotron. Since the first bunch kicked out transverses only a fraction of the synchrotron circumference, its position advance over its original position is somewhat less than the 21λ difference in circumference between the storage ring and synchrotron.

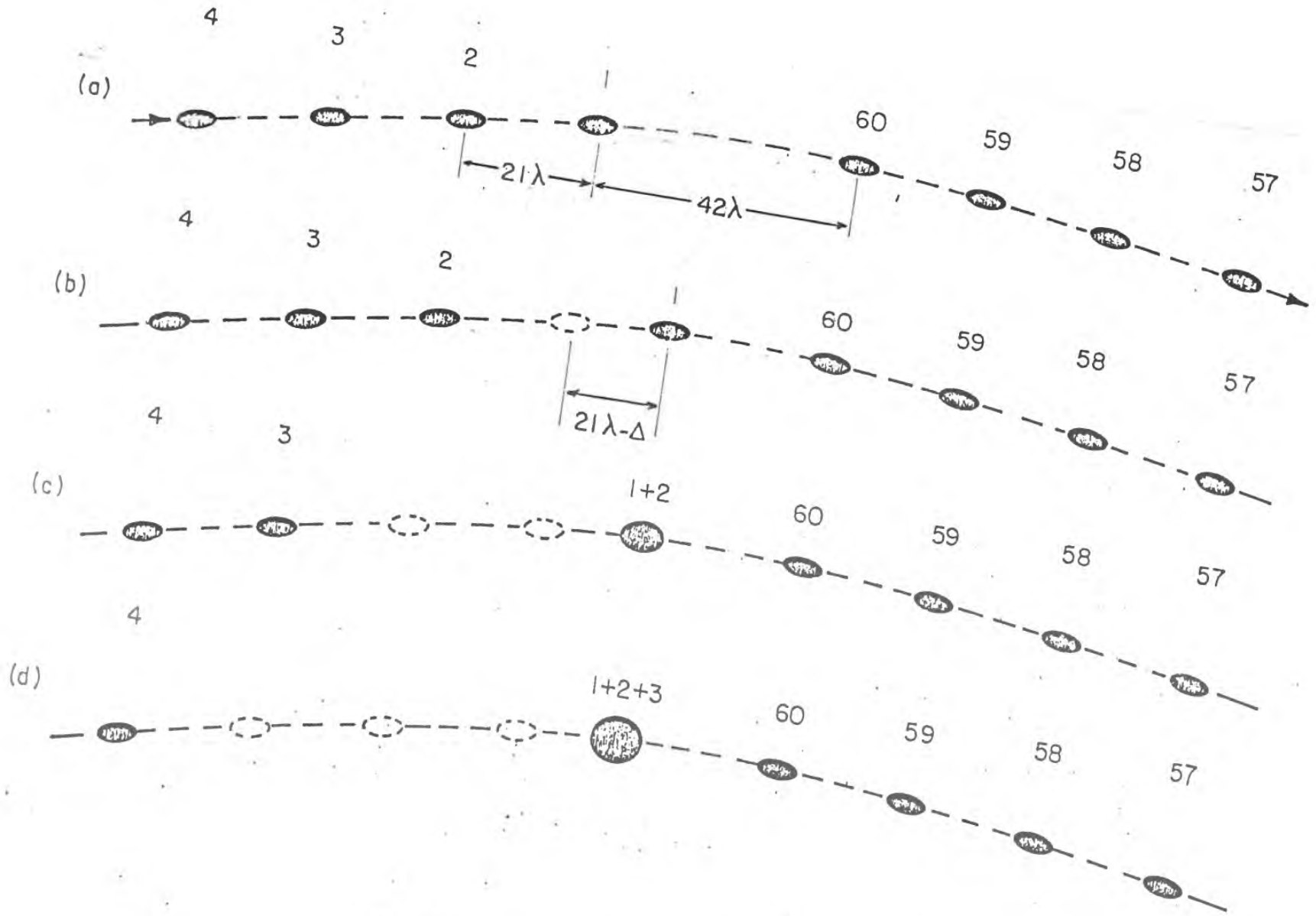

Fig. 7-6 Positron bunch compression

CESR ORBITS FOR POSITRON EXTRACTION
(drawn for 8 GeV, ν=11.38, lattice N1138.81A)

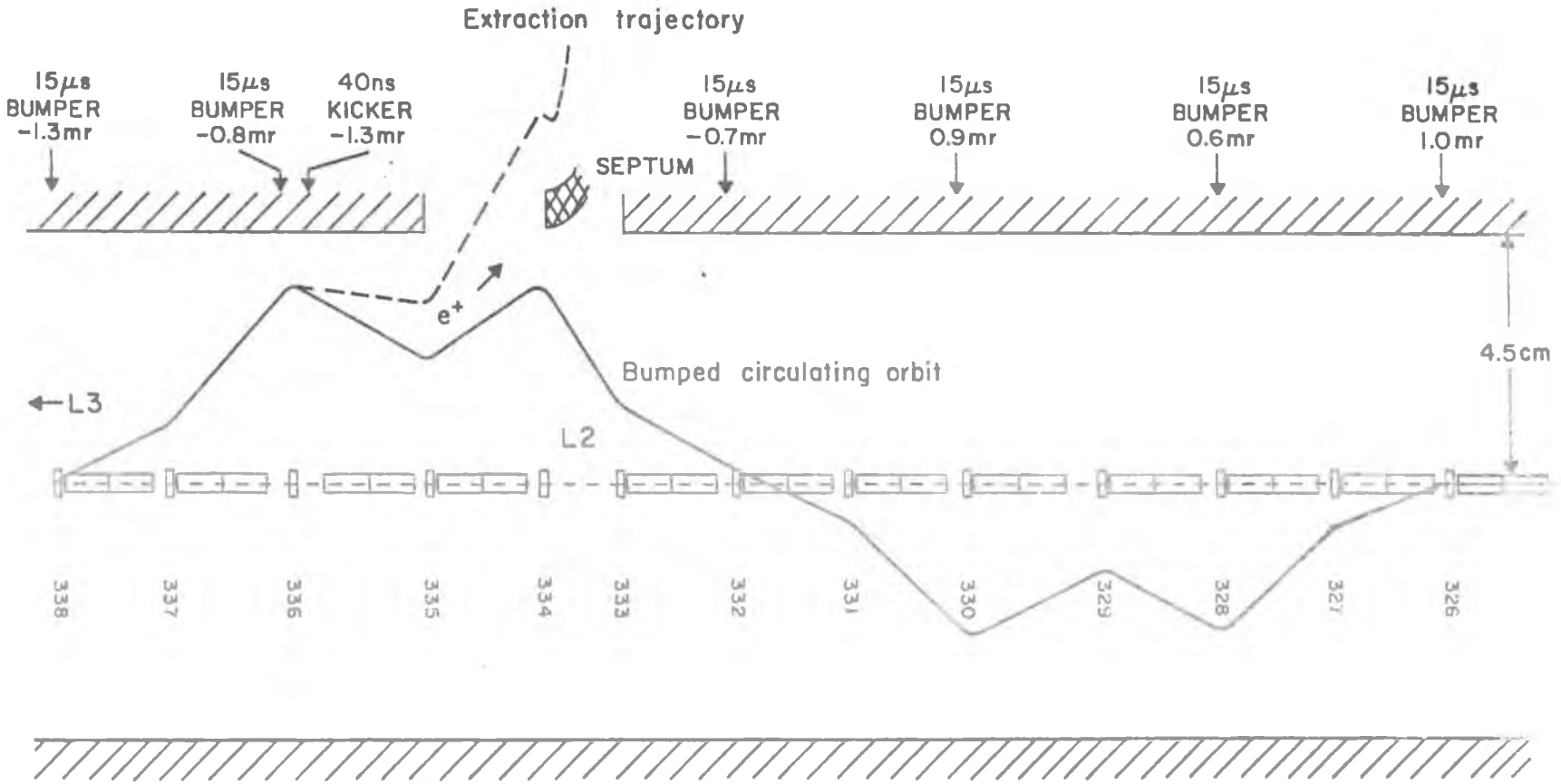

Fig. 7-7

CESR ORBITS FOR POSITRON (L4) OR ELECTRON (L2) INJECTION
(drawn for 8 GeV, $\nu = 11.38$ lattice N1138.81A).

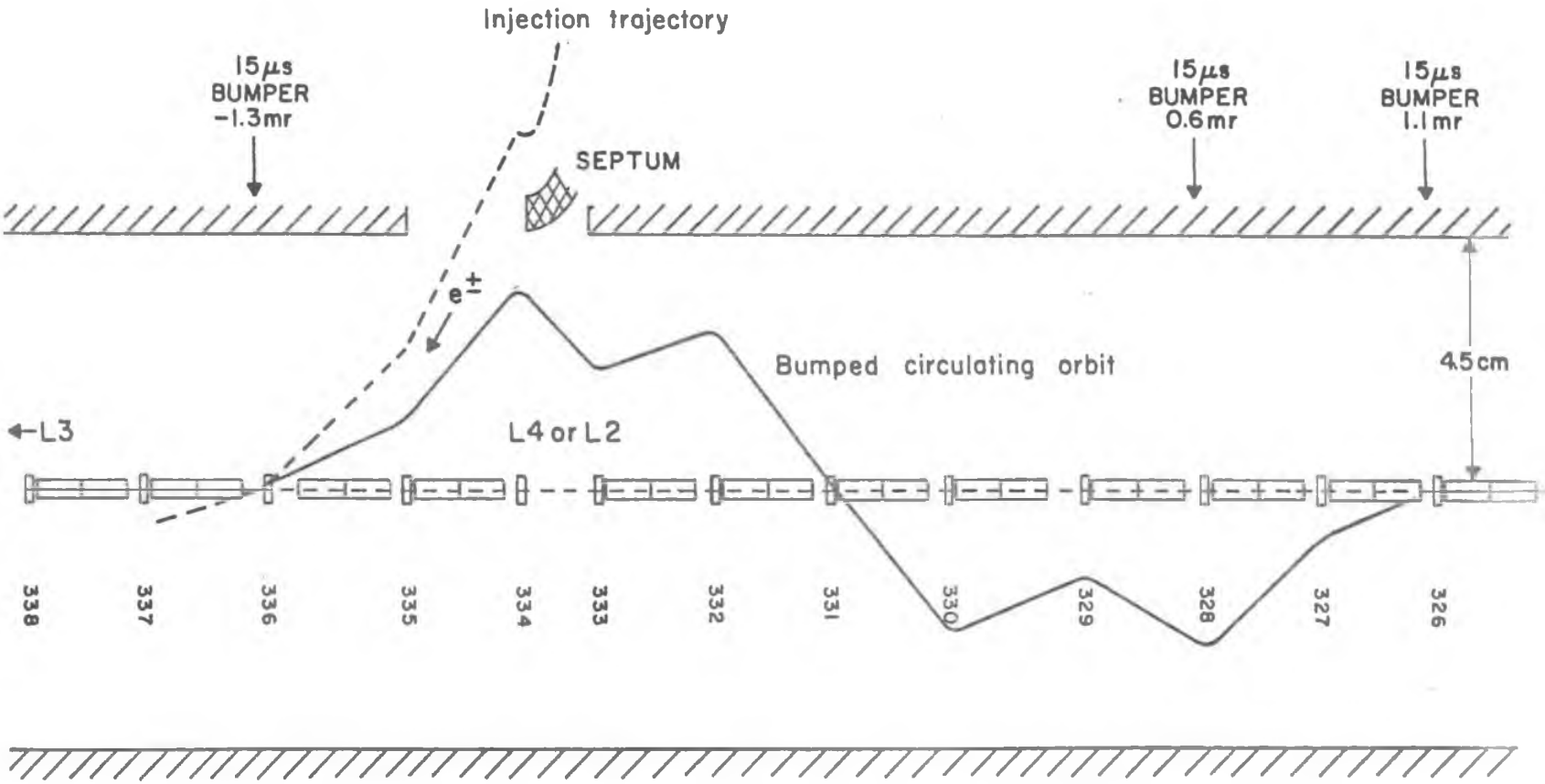

Fig. 7-8

Taking into account the detailed geometry of the extraction and reinjection lines this decrement (called Δ in Fig. 7-6b) turns out to be 6λ. Note that the extraction and reinjection of the positron bunch occurs at the peak of the synchrotron cycle.

On the next synchrotron cycle, bunch number 2 is fast extracted from the storage ring and reinjected into the synchrotron in the same manner as for number 1. However, bunch number 2 is allowed to pass K249W and make an additional full circuit of the synchrotron. The next time it arrives at K249W it is extracted from the synchrotron and injected into the storage ring. Upon arriving back in the storage ring, bunch number two will have advanced in position compared to its original station by $21\lambda - \Delta + 21\lambda$ so that it now coincides in phase with bunch number 1. The situation obtaining at this point is shown in Fig. 7-6c. Now bunch 3 is fast extracted and gets the same treatment as bunch 2 with the exception that an additional circuit of the synchrotron is allowed before reinsertion into the storage ring. It thus advances over its original position by $3 \times 21\lambda - \Delta$ and is coincident in phase with bunches 1 and 2 as shown in Fig. 7-6d. This routine is repeated 60 times, the last bunch making $\sim$ 60 circuits of the synchrotron in order to advance to the position of the first bunch[3]. In order to allow very thorough damping of the betatron oscillations between bunch advancements, these manipulations are carried out at a 30 Hz rate (i.e., four damping time constants between cycles). Thus the total time required for bunch compression is two seconds.

Details of the positron transfer optics and the component dispositions for accomplishing it are shown in Figs. 7-7, 7-8, 7-9, and 7-10 and Table 7-1. Alternatively, it has been suggested by R. Talman (CBN 76-30) that a

---

[3] If desired, the compression sequence can be reversed, thereby relaxing the fall time requirement for KF242E, to 70n sec.

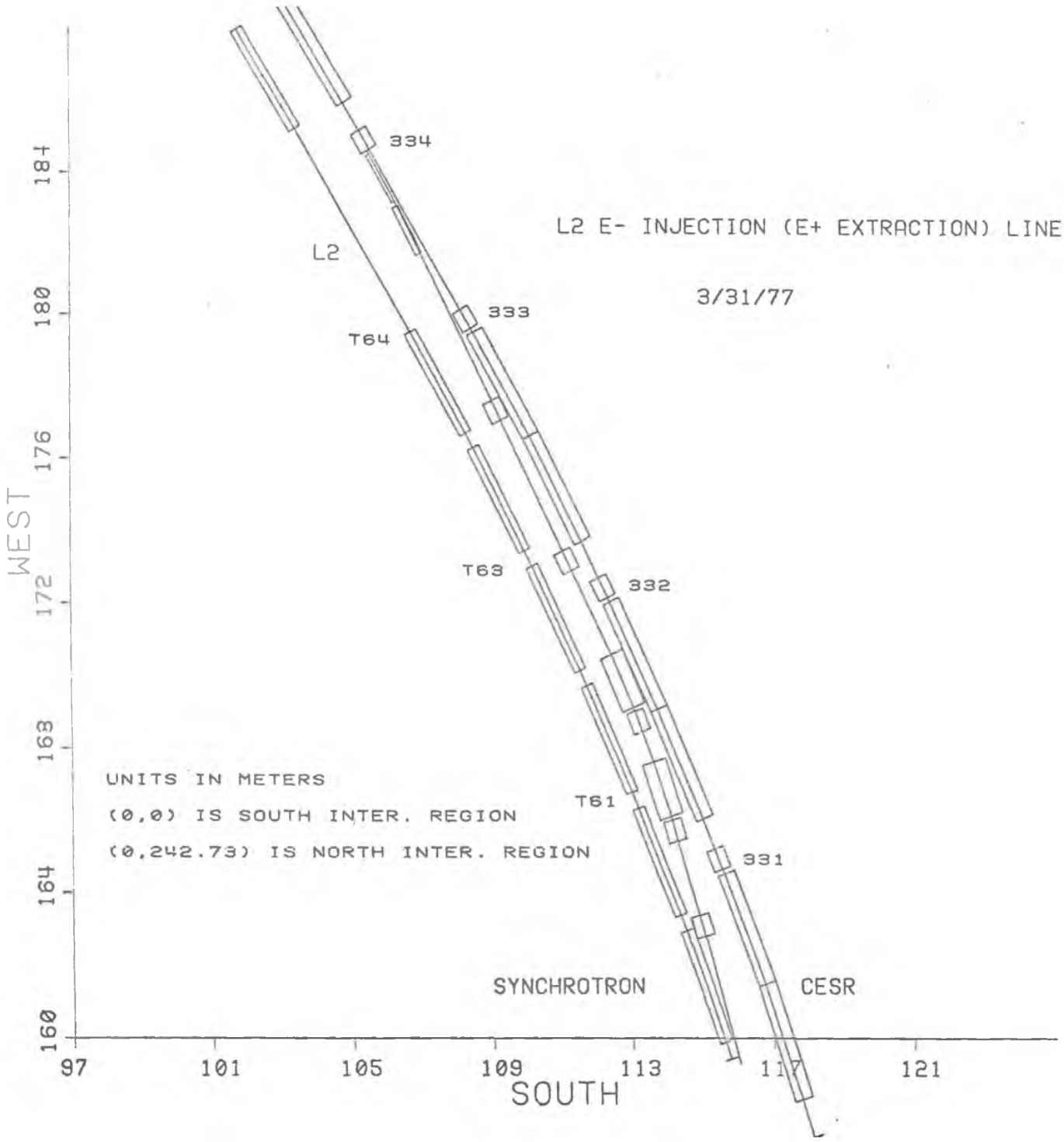
L2 E- INJECTION (E+ EXTRACTION) LINE
3/31/77
L2
334
333
332
331
T64
T63
T61
UNITS IN METERS
(0,0) IS SOUTH INTER. REGION
(0,242.73) IS NORTH INTER. REGION
SYNCHROTRON
CESR
WEST
SOUTH
160
164
163
172
176
180
184
97
101
105
109
113
117
121

Fig. 7-9

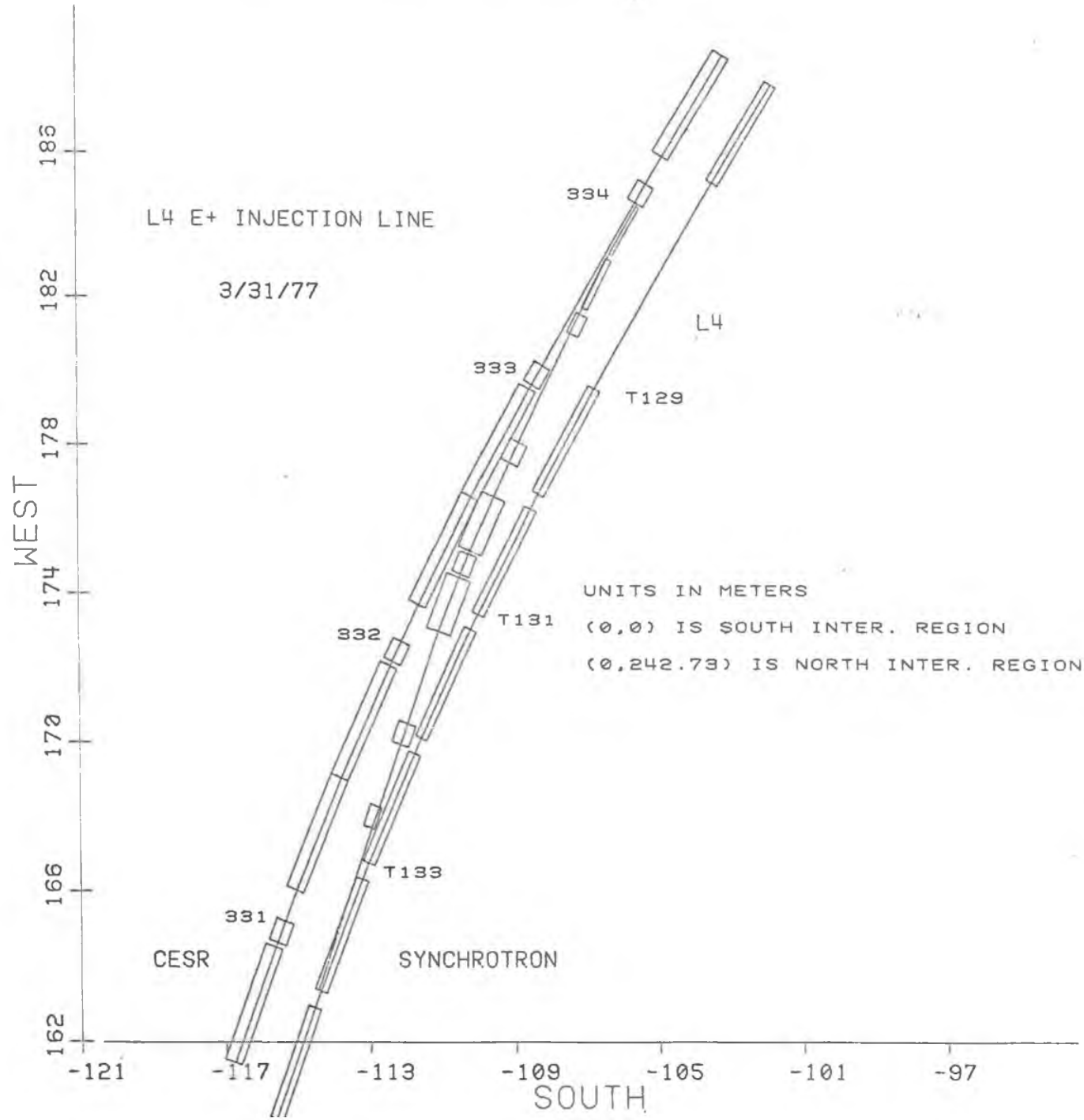
L4 E+ INJECTION LINE
3/31/77
L4
334
333
T129
332
T131
T133
331
UNITS IN METERS
(0,0) IS SOUTH INTER. REGION
(0,242.73) IS NORTH INTER. REGION
CESR
SYNCHROTRON
WEST
SOUTH
186
182
178
174
170
166
162
-121
-117
-113
-109
-105
-101
-97

Fig. 7-10

Table 7-1

Magnetic elements used in CESR injection

	Number required	Max mr bend at 8 GeV (*or k^2 in m^{-2})	B_{max} in T (* or B'_{max} in T/m)	length in m
Synchrotron kicker	2	1.5	.1	.46
Synchrotron septum	4	8	.5	.46
Tunnel quad	8	.5*	40*	.60
Tunnel half-quad	2	.5*	40*	.60
Tunnel bend	4	90	1.5	1.60
1" CESR septum	2	40	.7	1.70
$\frac{1}{4}$" CESR septum	2	40	.7	1.50
CESR bumper	9	1.3	.17	.20
CESR kicker	1	1.3	.023	1.50

form of longitudinal phase space stacking be used. In this method both betatron and energy oscillations help to miss the injection septum while up to perhaps 20 synchrotron bunches are inserted into a single storage ring bucket. This method takes 3 times as long as the coalescence method but avoids the coalescence process. The injection hardware will be built in a fashion compatible with both injection methods.

c) Electron Filling

The stage of injection and stacking of electrons, is begun by switching on the electrostatic separator plates, ES of Fig. 7-4. These generate a half wave vertical bump which separates the electrons and positrons at the interaction points. This avoids complicating effects of the beam-beam interaction during stacking, provided that the electrons are loaded only into the bucket which coincides with the positron bunch at the designated interaction points. After acceleration to peak energy, the bunch will be extracted using the combination K249E, S248E, S247E. This bunch will be injected into the proper bucket in the storage ring by way of Q305E, D243E, etc., and an orbit bump generated by B236E, etc.

Based upon present synchrotron performance and taking account of the beam modulation that is required, we can expect to accelerate 3×10^8 electrons per pulse. At 50% injection efficiency into the storage ring this gives a net filling rate for electrons of 0.6 mA per second at 8 GeV.

The most difficult technological component employed in the positron injection scheme is the fast kicker. For this reason, we have spent considerable effort in its development. As a result of this development we feel the element is entirely feasible. The kicker will be in the form of a C-shaped, ferrite loaded transmission line. To avoid

problems of ferrite in vacuuo and beam induced fields in the ferrite, the kicker will be off to one side of the beam and separated from the beam vacuum by a metal coated ceramic vacuum chamber. The metal coating must be thin enough to allow the kicker field to penetrate the vacuum chamber wall but thick enough to prevent radiation of significant energy from the beam. Figure 7-11 is a photograph of a prototype of the kicker magnet placed over a section of the ceramic vacuum chamber. Tests to date show that the necessary field and rise time can be achieved using "Cermag-11" ferrite and a spark gap switch.

8. Synchrotron Radiation Backgrounds in the Interaction Region

The bending magnets and quadrupoles near the interaction region are potent sources of hard x-ray photons. The average power radiated in the magnet B_1 (See Fig. 8-1); e.g., is approximately 400 watts at 8 GeV when 10^{12} particles are stored in each beam, yielding about 2×10^{15} photons/sec above 25 keV in energy. Since the devices in the CESR detector, particularly the drift chambers, will have some sensitivity to these photons,

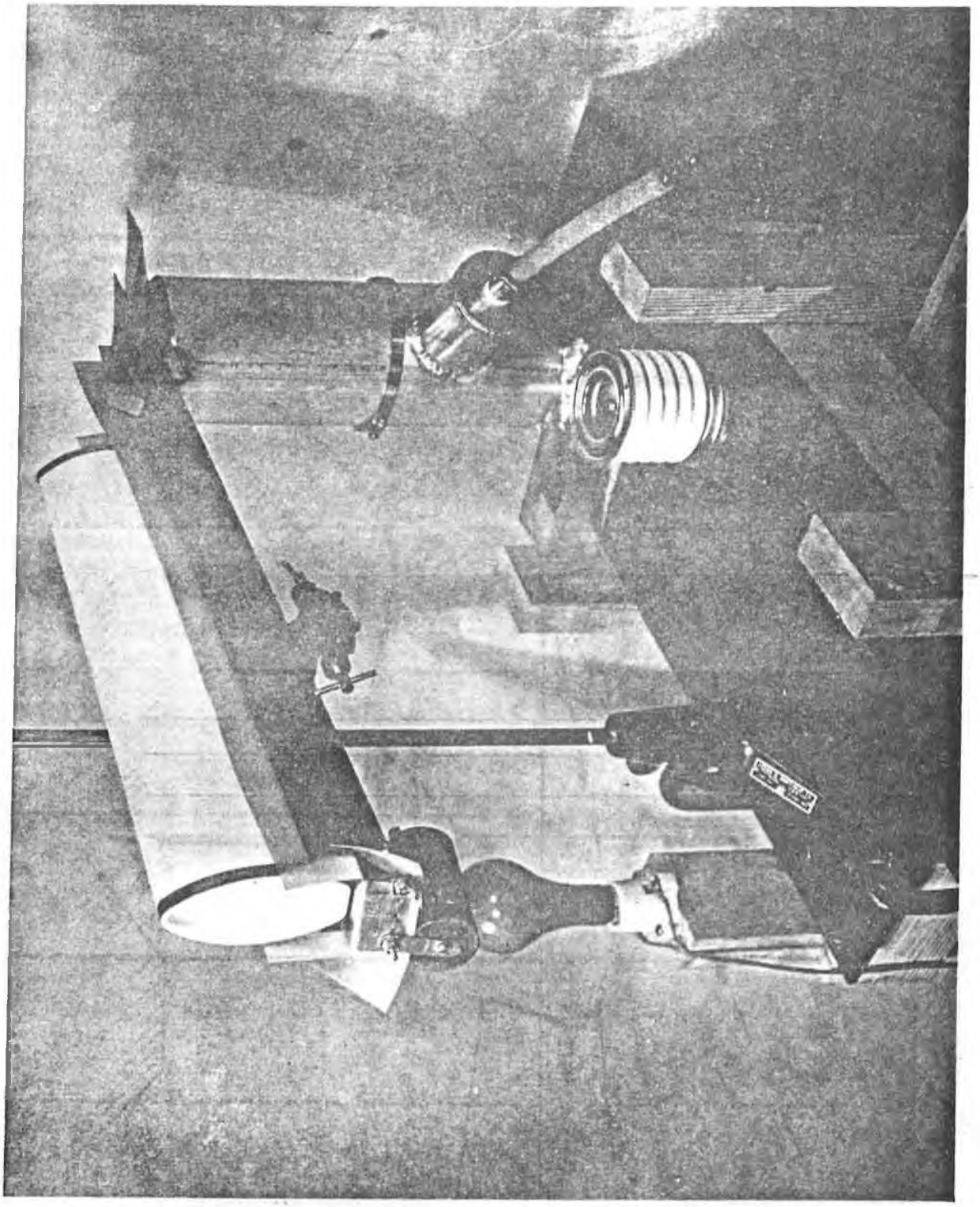

Fig. 7-11 Prototype of kicker magnet with metal coated ceramic vacuum chamber and spark gap switch

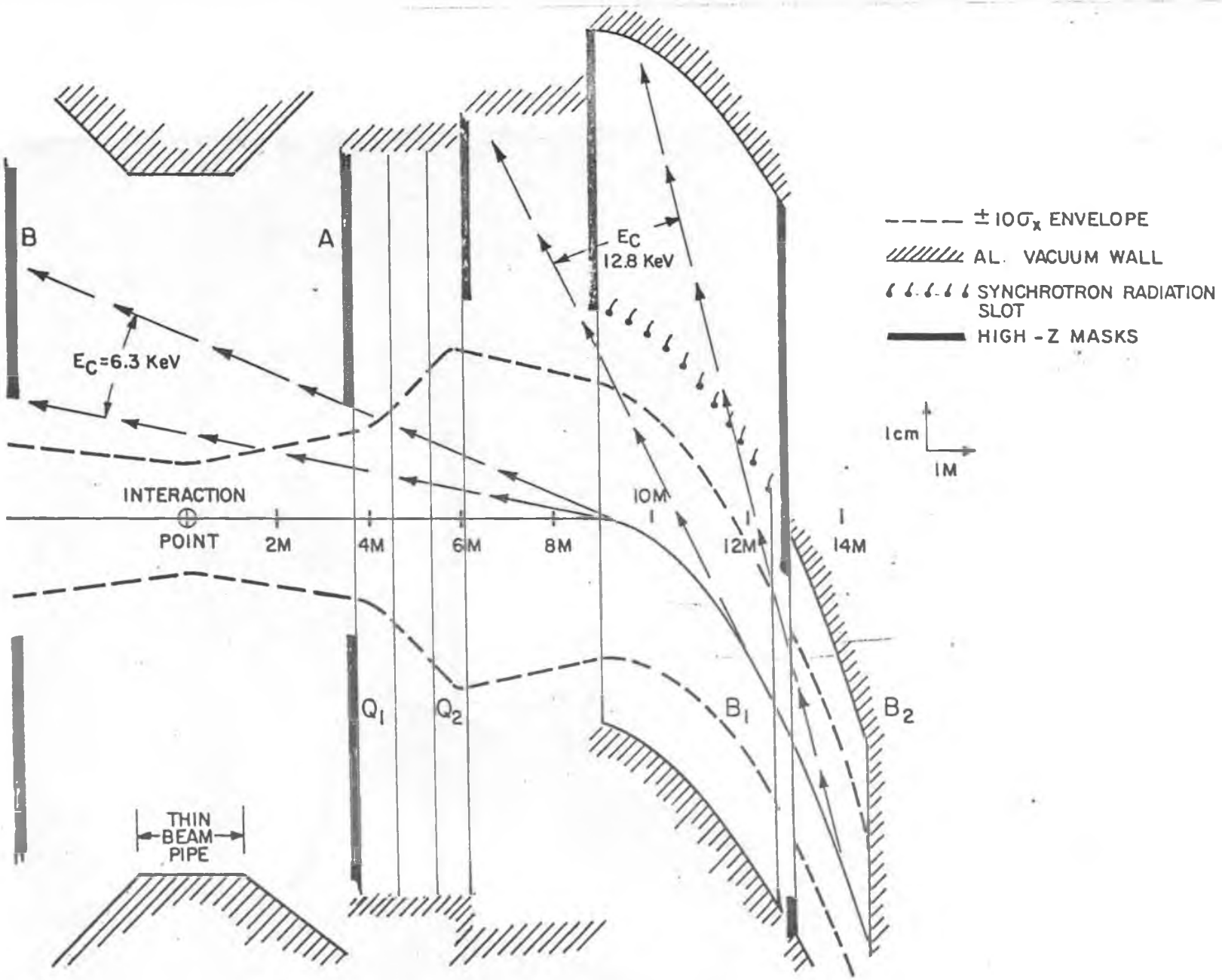

Fig. 8-1 Horizontal schematic of elements near interaction region 8 GeV beam energy.

it is vital that the number emerging from the thin-walled beam pipe be reduced from the incident flux by factors approaching 10^{10} or more.

In the past few months, we have made considerable progress in conceptual design of a system of baffles and vacuum chamber modifications which achieves this goal. Figure 8-1 shows a horizontal section of the elements near the interaction region along with the ±10 standard deviation horizontal beam envelope for the case of 8 GeV beam energy. The thin section of beam pipe is taken to be 15 cm in diameter, 2 meters long, and 0.16 gm/cm^2 of stainless steel in thickness.

The mask labelled A intercepts the synchrotron radiation from the "soft bend" magnet B_1 and will be made of high-Z material, such as Ta. The radiation which passes A may strike the symmetrically disposed mask, B, and Compton scatter into the beam-pipe, or may produce fluorescent K- x-rays which reach the beam pipe. Likewise, radiation which grazes the tip of mask A may be a source of background. These sources have been investigated and found to produce tolerable background in the detector (see below).

The high-Z masks before and after the drift region and at exit of B_2, in conjunction with the oversized vacuum chamber in B_1 (formed by welding together two Al extrusions), serve to remove a potentially disastrous source of background photons. They render "invisible" those parts of the vacuum chamber walls illuminated by the synchrotron light from B_1 and B_2. No photons can reach the beam pipe by means of a single Compton scattering in the Al wall.

At present, the dominant sources of background are found to be Compton scattering from, and fluorescence of mask B by radiation from B_1 and quadrupoles Q_1 and Q_2. This radiation typically leaves the beam

pipe after Compton scattering and is estimated to produce about five single clusters in a one-meter thick Argon drift chamber array at each beam crossing (8 GeV). Work is proceeding on methods of further attenuating this background as well as evaluating more exotic (e.g., multiple scattering) sources.

9. Higher Mode Loss Measurements

Experience with SPEAR[1] at SLAC has shown that one must make provision for the energy lost by the beam into cavity modes other than the fundamental and into all modes of incidental cavities formed by parts of the Vacuum System. This energy can cause severe local heating and produce fields, both longitudinal and transverse, which may affect beam stability. Due to the rather short natural bunch length of CESR, we will need to minimize this interaction and to provide auxiliary cooling where necessary. To be able to do this we must be able to evaluate the higher mode losses in detail for each piece of beam line vacuum hardware. Sands[2] and Rees have devised an experimental method for making this evaluation. Briefly, the item in question is threaded by the center conductor of a coaxial line. A sharp current pulse, having the anticipated beam shape, is sent down this coax line and the size and shape change of the emerging pulse recorded. From the difference between the pulse in and pulse out a measure of the energy loss of a similar beam bunch can be computed. The method agrees well with calculation for simple cavities. By this means, then, we are evaluating individual

---

[1] M. Allen, J. Paterson, J. Rees, P. Wilson, Beam Energy Loss to Parasitic Modes, 1975 Particle Accelerator Conference Proceedings.

[2] M. Sands, J. Rees, A Bench Measurement of the Energy Loss of a Stored Beam to a Cavity. PEP-95.

Fig. 9-1 Higher mode loss measuremen

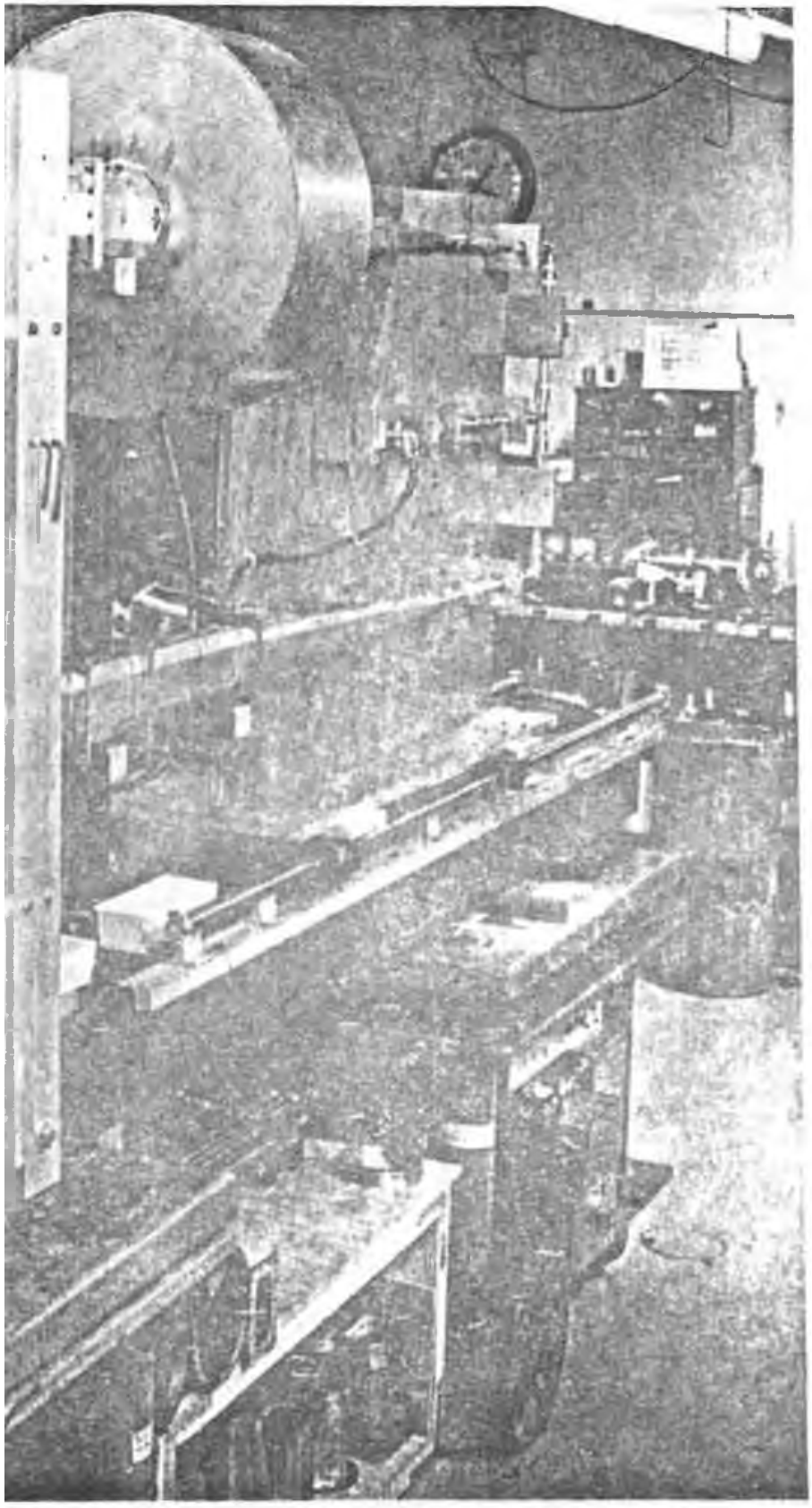

t apparatus with simple cavity in place.

hardware parts. Figure 9-1 is a photograph of the apparatus with a simple cavity in place. In the apparatus the input pulse is split in to equal parts. One half is sent down a smooth line having the cross-section of the vacuum chamber. The other half is sent down a similar line into which the test piece has been inserted. One of the pulses is then inverted in a transmission line transformer and added to the pulse from the smooth line. The difference pulse is displayed directly on a sampling oscilloscope connected to a chart recorder.

This device has been particularly valuable in evaluating the thin metallic shielding (100Å) used in the ultra fast kicker magnet. Without this ability to measure the beam interaction with a coated ceramic chamber one would be dependent upon very difficult theoretical computations whose validity would at best be approximate. As it is, the measurement indicates that this method of isolating magnetic elements from the beam vacuum and rf fields is entirely feasible.

10. Controls and Instrumentation

a) Controls

CESR's control system is centered on computers. This choice is dictated by the complexity and precision required in the operating systems; it also offers a degree of flexibility which promises to permit the controls to evolve as the machine's requirements become more refined and extensive.

There are two problems often associated with computer control: (1) if the system is too indirect, it may become difficult to diagnose whether a malfunction is due to the controls or to the equipment itself; (2) the overburden of programing ("software") may become such as to

vitiate much of the flexibility originally anticipated. Taking advantage of some of the experience gained elsewhere, we are emphasizing attention to these problems from the start. Some of the consequent choices are outlined below.

First, it should be stated that all equipment will have the capability of functioning, without the computer controls, in a "stand-alone" fashion. Thus, by substitution of a few signals which mimic the commands normally derived from the computer, an operator should be able to check the operation of each separate item. Local on/off controls and safety interlocks are contained within each equipment block; the safeties are hard-wired and follow normal industrial practice. Modular control cards have been developed for this purpose. They use relays and fixed wiring, but they also provide standardized input and output points for interconnection with the computer. In this way, although the computer is not required for control, it can nevertheless be used for status monitoring and remote operation -- which will, of course, be the normal mode.

The organization of the computer system itself is simplified both by vertical division (into virtually autonomous functional groupings) and by horizontal layering (by level of sophistication of the control tasks). The outline of the resulting arrangement is shown in Fig. 10-1.

The vertical division is into functions associated with the linac injector, the synchrotron accelerator, the colliding beam magnetic elements, and the colliding-beam RF system. At the individual-component level these systems are quite independent. This is not to imply that coordinated control will not be needed: it occurs at a higher level, however.

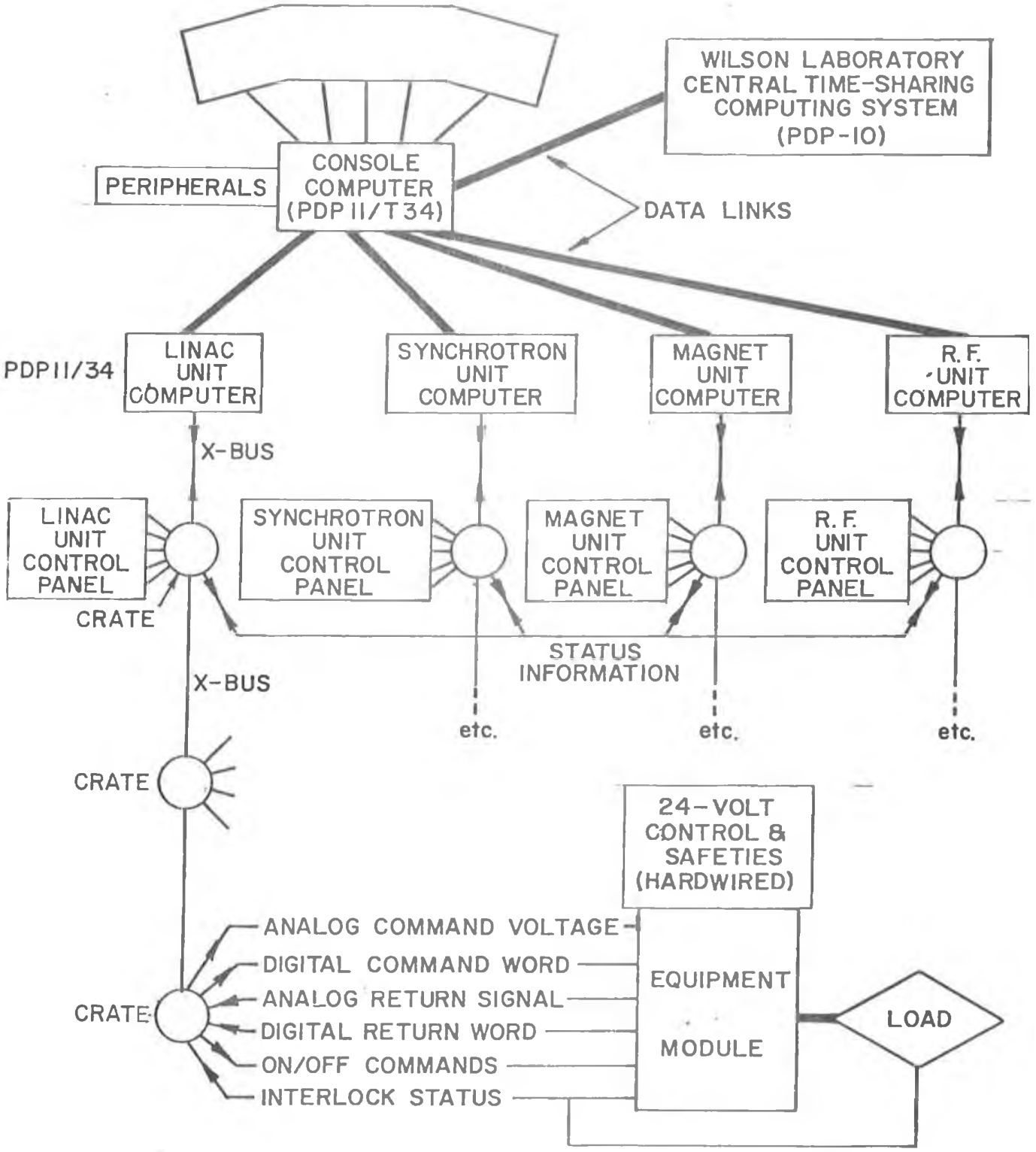

Fig. 10-1 Organization of CESR computer control system.

Each subsystem is controlled by a PDP-11/34 computer, which we call a Unit Computer. Its functions are the normal housekeeping routines. It communicates with the equipment via a two-way data bus called the X-bus. At suitable locations along the X-bus there are card crates, housing the interfacing cards which connect to the equipment. The X-bus design pays special attention to rejection of interference and to self-checking procedures. The first X-bus implementation is underway for the Linac unit system, with many of the interface cards designed and the X-bus hardware developed and checked. Figure 10-2 shows some of this hardware with the 11/34.

Each unit computer can function alone; in this case it receives and delivers information via a Unit control panel, not part of the general machine control console. Any device connected to the unit computer can be accessed from the unit panel. Such a localized control system has been designed for the linac already, and the linac is now under computer control. Since the linac is a complicated accelerator in its own right, and there may be occasions when it is to be run alone as a system and not just as an assemblage of individual components, its unit panel is more sophisticated than some of the others. This will be especially important during the transition period when the linac continues to serve the synchrotron, but before computer control has been implemented overall. A prototype unit panel and display for the linac is shown in Fig. 10-3.

Some small amount of information may need to be exchanged between

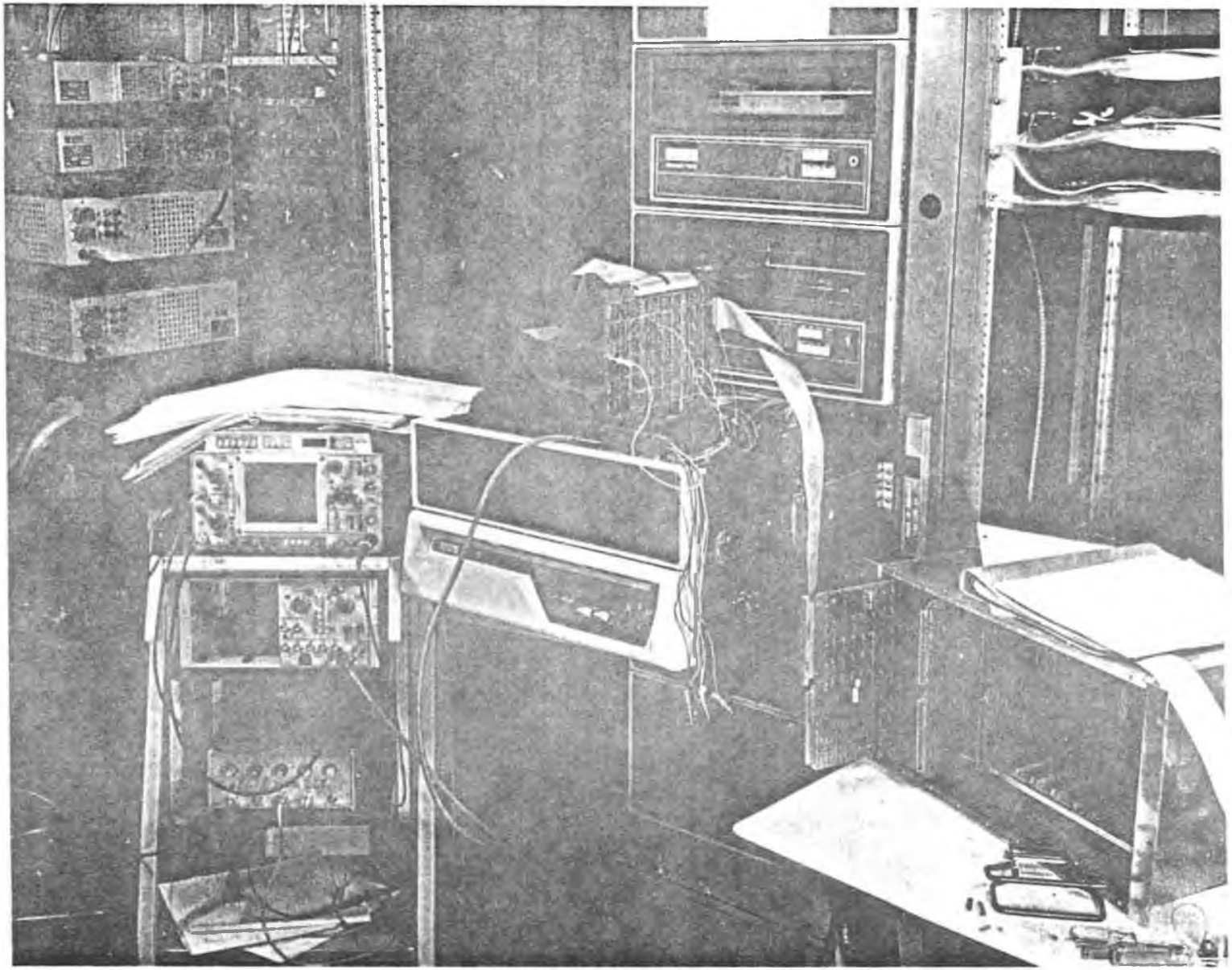

Fig. 10-2 PDP11/34 unit computer and interface development work

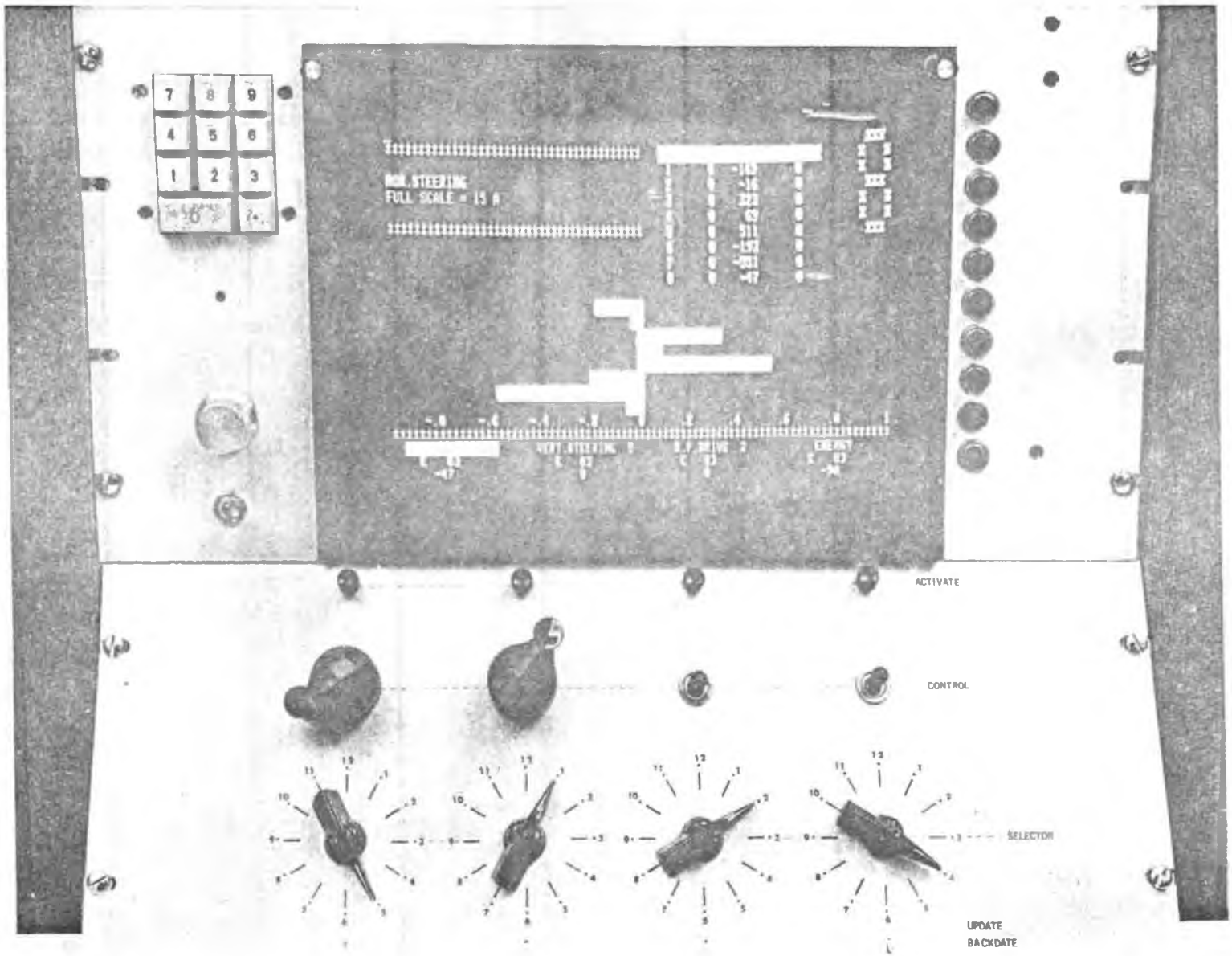

Fig. 10-3 Prototype unit panel and display for the linac.

unit computers even when they are running independently. This information, mostly status signals for equipment interlocks, will be exchanged between the various X-buses directly and will thus be available even without the higher-level computers.

The coordinated control of all unit systems is carried out with the Console computer, a PDP-11T34. All control and display elements in the central control console communicate with this computer. It will have considerable data-storage facilities, several terminals on the console, a small line printer, and the ability to handle routine coordinated control tasks. It will also be our record keeper and alarm supervisor.

When operations not yet considered routine are desired, the console computer can call upon the Laboratory's central PDP-10 computing system for help. Here sophisticated lattice calculations, minimization procedures, and track mapping can be done whenever new ground needs to be broken. In general we anticipate that such computations will yield data that can be stored for future use without necessarily invoking the central computer again. However, experience will tell what load the PDP-10 will need to carry for such tasks: since it will time-share such loads with the physics computational needs, it may turn out that the machine-development and physics analysis tasks do not overlap too often, resulting in a considerable economy of investment.

All the computers communicate with each other via data links whose specifications have not yet been finalized. We anticipate that experience with the linac control system, which will go into operation within a few months, will help provide a realistic perspective on what the final requirements are likely to become. At the same time we will be able to determine

whether the system standards adopted so far are actually efficient and convenient. The proposed implementation by stages will permit some early revisions to be made in the light of actual experience.

b) Instrumentation

In addition to the instrumentation necessary to monitor and control the functioning of the various subsystems such as magnet, rf, vacuum, etc., an extensive instrumentation system for measuring beam parameters will be installed.

Pairs of beam pickup electrodes will be located at 60 places around the ring to measure the equilibrium orbit position and thus allow its adjustment for optimum use of the aperture. The signals will be digitized locally and transmitted to the nearest data acquisition computer. Intercalibrations will be done by switching the pickups onto a set of common coax lines running around the ring. Some of the pickup electrodes will be optimized for high frequency response for analysis of instabilities.

One hundred photoscintillator detectors will be distributed around the ring for the location of sites of abnormal loss which may occur during injection or operation. In our experience with the 12 GeV synchrotron, this technique has proved to be very powerful.

The magnitude of the circulating beam current will be measured by integrating toroid signals and by phototubes viewing the synchrotron light.

Four multipurpose synchrotron light viewing stations will be installed, one at each side of each interaction region. These stations will permit measurement of beam dimensions of both beams and aid in the precision positioning of the orbit at the interaction points. Light from these ports will be viewed both with fast photodiodes and by television cameras. Additional

light viewing ports will be provided to allow the independent measurement of longitudinal and transverse phase space distribution of the beams.

Means will also be provided for the measurement of betatron and synchrotron frequencies by means of low level resonant excitation.

An energy discriminating counter telescope arrangement for measuring Bhabha scattering will be set up permanently as a luminosity monitor.

11. Plant Modifications

In addition to the tunnel flare on the east side of the South experimental flare, which includes a modest area below ground for synchrotron radiation research, some increases in electric power and cooling capacity are necessary.

The present connected power is sufficient for all storage ring purposes with the exception of the rf. To serve the rf (approximately 4 MW) we propose to bring one additional feeder, underground through an existing conduit, from an already existing transformer and switch module at the University substation (Kite Hill). This feeder will have enough capacity to allow expansion to 10 GeV operation. The existing transformer pad is sufficient for all necessary additions.

To serve the anticipated cooling needs for 8 GeV operation, two evaporative water cooling units of 3 MW nominal cooling capacity each will be needed. These units will be located adjacent to the South area and will be screened from view by a brick structure. Figure 11-1 shows how these cooling units will be used to supplement the existing cooling capacity.

12. A Synchrotron Radiation Facility

The utility of synchrotron radiation in many areas of research in physical and biological sciences is well documented in terms of the

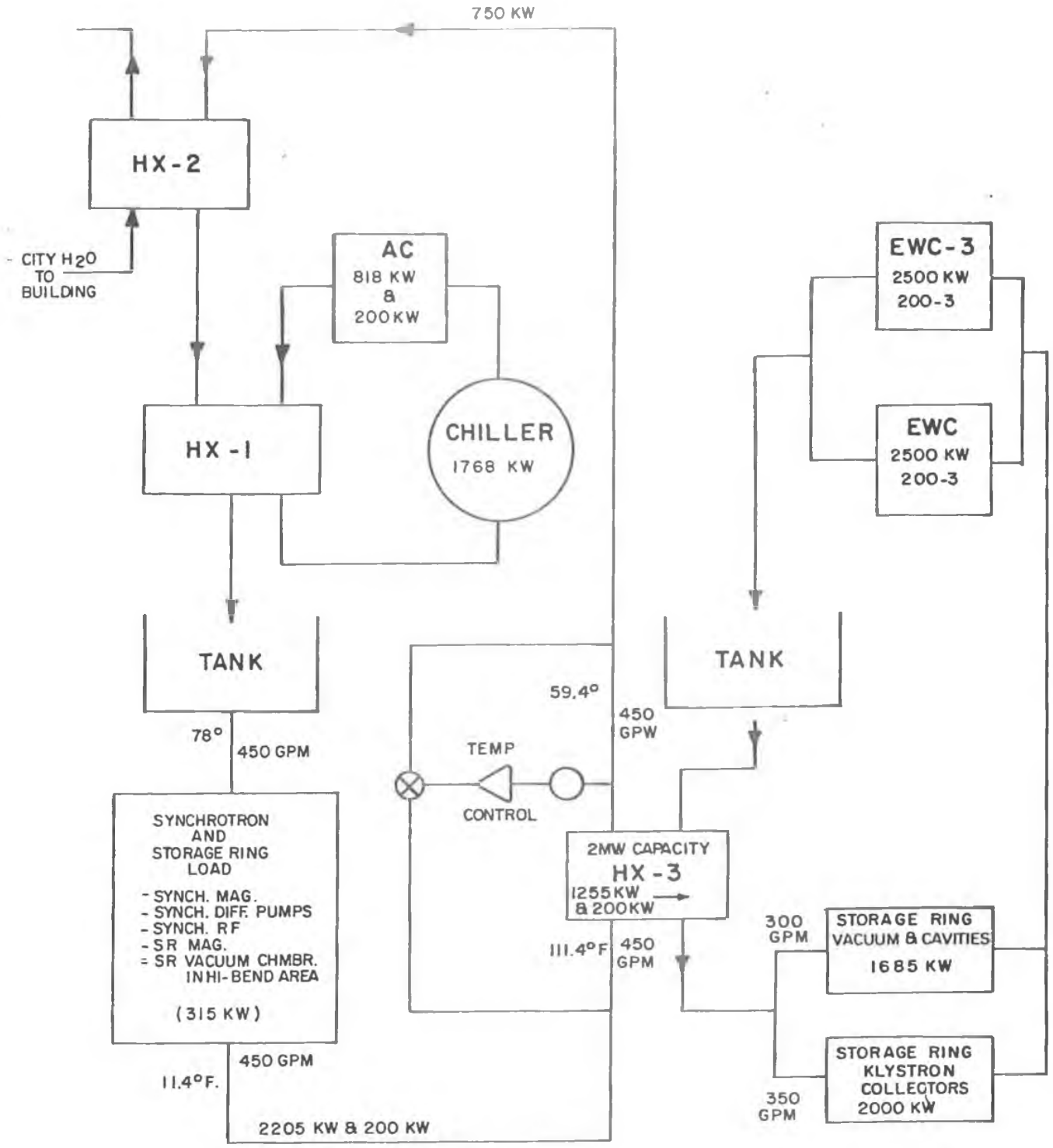

PROPOSED COMBINATION OF 65°F. AND NEW 85° WATER COOLING

Fig. 11-1

increasing numbers of workers involved in research employing synchrotron radiation as well as in the numerous reports published by panels formed by the U. S. National Research Council, the British Science Research Council, the French National Research Council, and their counterparts in other countries.

Activities in the subdisciplines of atomic and solid state physics, biology and chemistry, currently making use of synchrotron radiation, encompass the electromagnetic spectrum from the ultraviolet to X-ray regions and make use of such processes as absorption (including EXAFS), reflectance, fluorescence, the photo-effect and scattering (elastic and inelastic, as well as diffraction effects) to probe the quantum nature of matter.

It has been pointed out in a recent report sponsored by the U. S. National Research Council on the national need for facilities dedicated to the production of synchrotron radiation, that at least 60 X-ray stations providing radiation in the 1-50 keV range, and 40 VUV stations providing radiation in the 0.1-1.0 keV range will be required by 1986. (One station consists of a monochromator plus requisite beam optics and serves four full-time users.) While many of these needs can be met by dedicated facilities, CESR can make an important contribution as an alternative source in the hard X-ray, X-ray, and to a lesser extent in the VUV region as well.

Due to the high electron energy, large circulating current, regions of high magnetic curvature and small beam size in the vertical direction (< 0.2 mm in the magnets from which radiation will be extracted), CESR is a unique source of radiation in the X-ray region. The highly intense

radiation, collimated vertically to about 13 seconds of arc, can illuminate a monochromator located as close as 10 m to the source and will provide unique experimental opportunities not realized at existing or proposed storage rings. Figure 12-1 gives comparative intensities for CESR and other machines.

In the present arrangement, a minimum of three beam lines and a suitable isolated area can be provided for the synchrotron radiation facility. Each of these lines will have an angular range of about 10 mrad. and will be directly accessible at a distance of about 15 m from the source. The arrangement and location of the facility are shown in Fig. 12-2. The work area will be shielded from the storage ring so that it will be continuously accessible except while the ring is being filled. The working area can be separated into cubicles and the individual beam lines split to provide several stations. Limited office and experimental work space will be provided in the adjacent experimental hall.

In the context of this proposal, we plan to provide the shielded working area as well as ports into the vacuum system of the storage ring as part of our own construction plan. These ports will be terminated with a beam stop and valve next to the guide field magnets. The remainder of the beam transport equipment, slits, stops, controls, spectrometers, etc., as well as possible utilization of work area immediately over the accelerator floor, are not included in our proposal.

It is anticipated that the synchrotron radiation facility will mostly be operated in a symbiotic mode with the high energy physics program. It is expected that the major operating range will be between 4 and 8 GeV, and in this case the photon flux, at say 10 keV, changes by about a factor

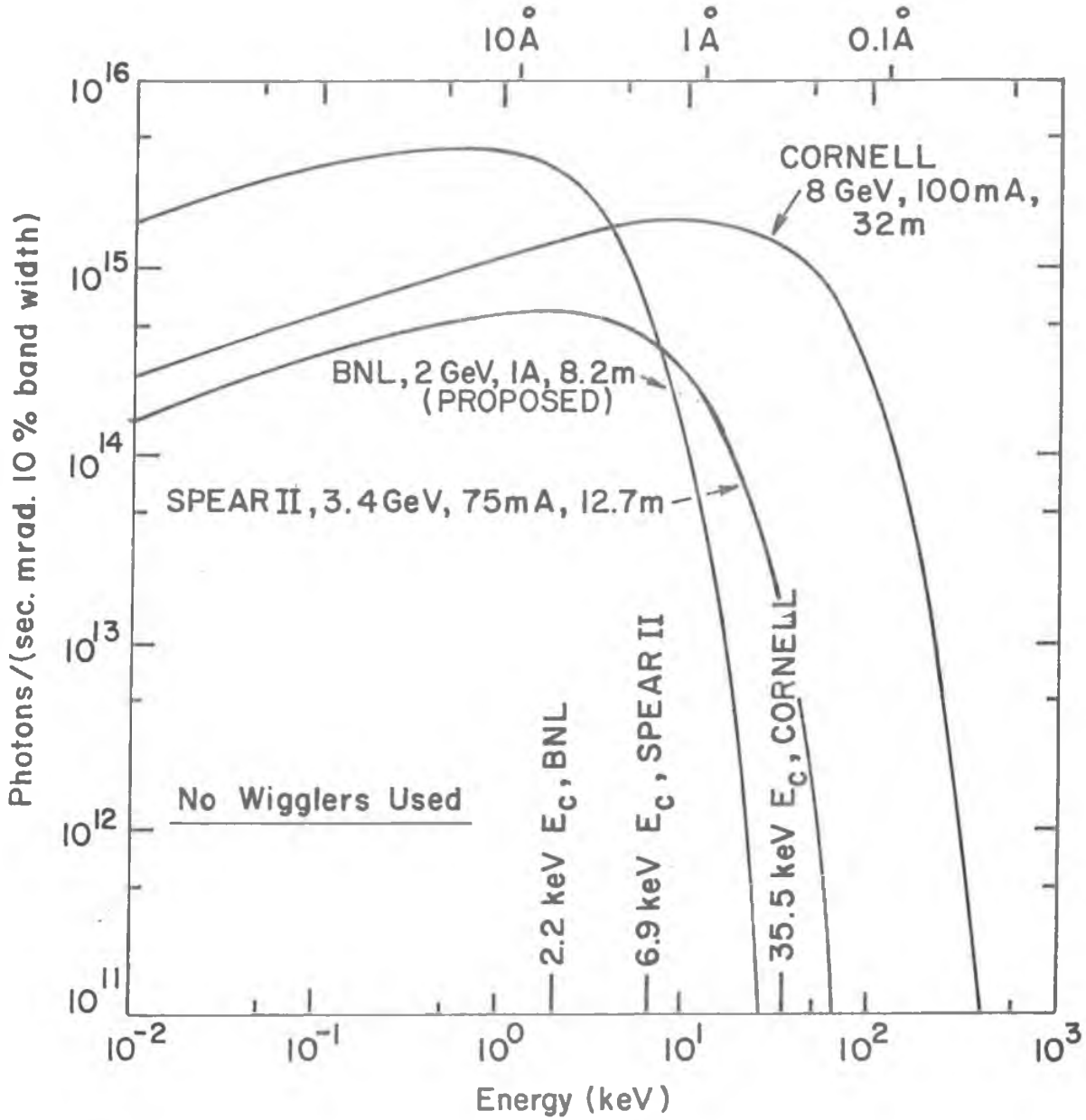

Fig. 12-1 Comparative radiation intensities in the X-ray region for CESR and other machines.

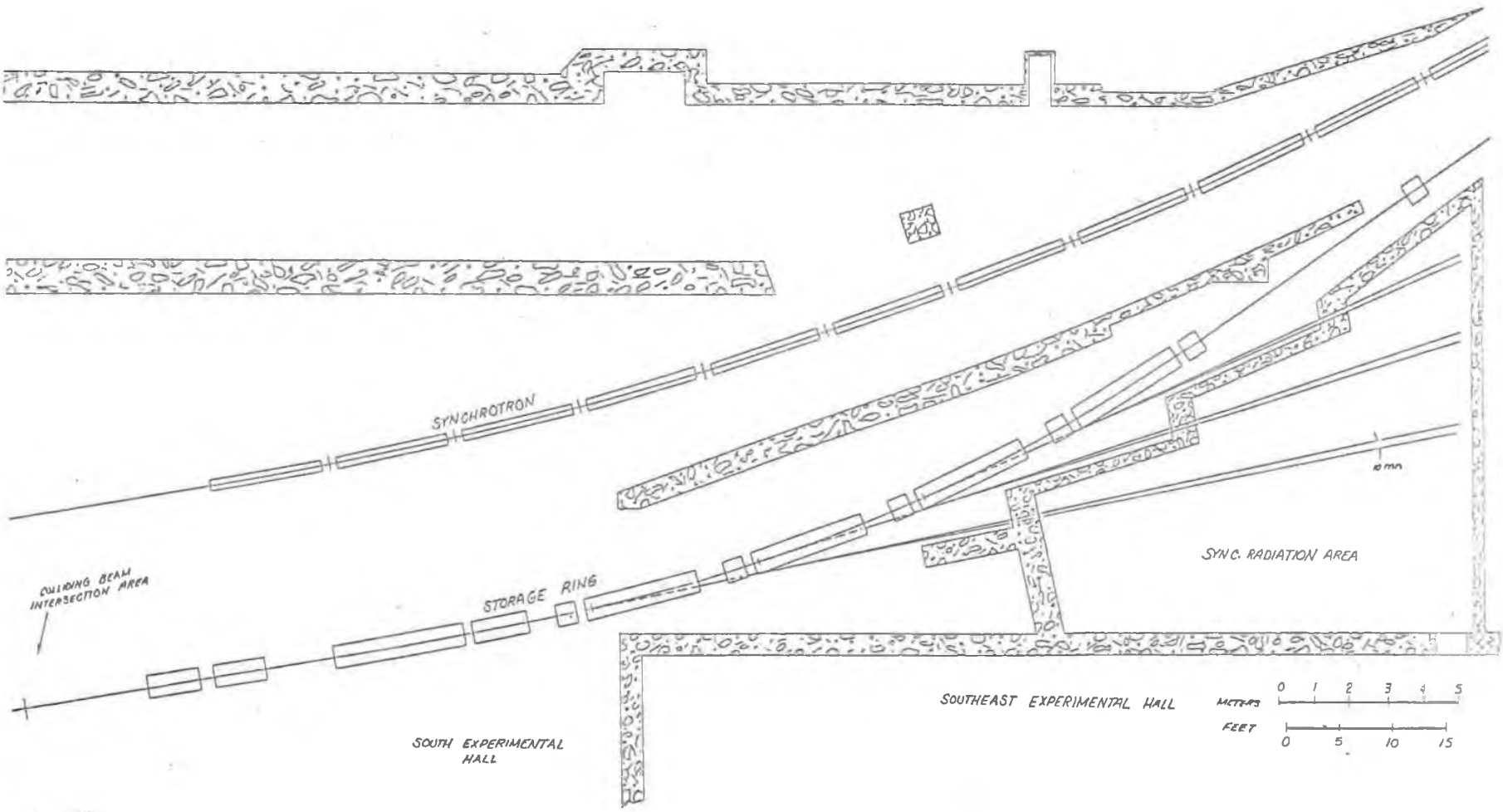

Fig. 12-2 Arrangement of X-ray beam lines.

of 7 for the same circulating current, while in the VUV range no discernible change in flux would be observed as the machine energy changes (Fig. 12-3). Thus the symbiotic mode of CESR will be almost equivalent to a dedicated mode, since sufficient intensity will be available in the typical photon energy ranges of interest. (The closest spectral distribution to CESR's at 8 GeV and 100 mA can be obtained from SPEAR II operating at 3.4 GeV, 50 mA with a 5T, 6 pole wiggler.)

A radiation facility of this scope is certainly useful to a small number of users, and as such could be accommodated without changing the scale of our project or creating new administrative problems (associated with safety, vacuum, operations, etc.). As the storage ring develops, high energy physics goals must be preserved, but every attempt will be made to maintain a compatible and productive synchrotron radiation facility.

At present, a group of prospective users are examing how the proposed synchrotron radiation facility might be organized.

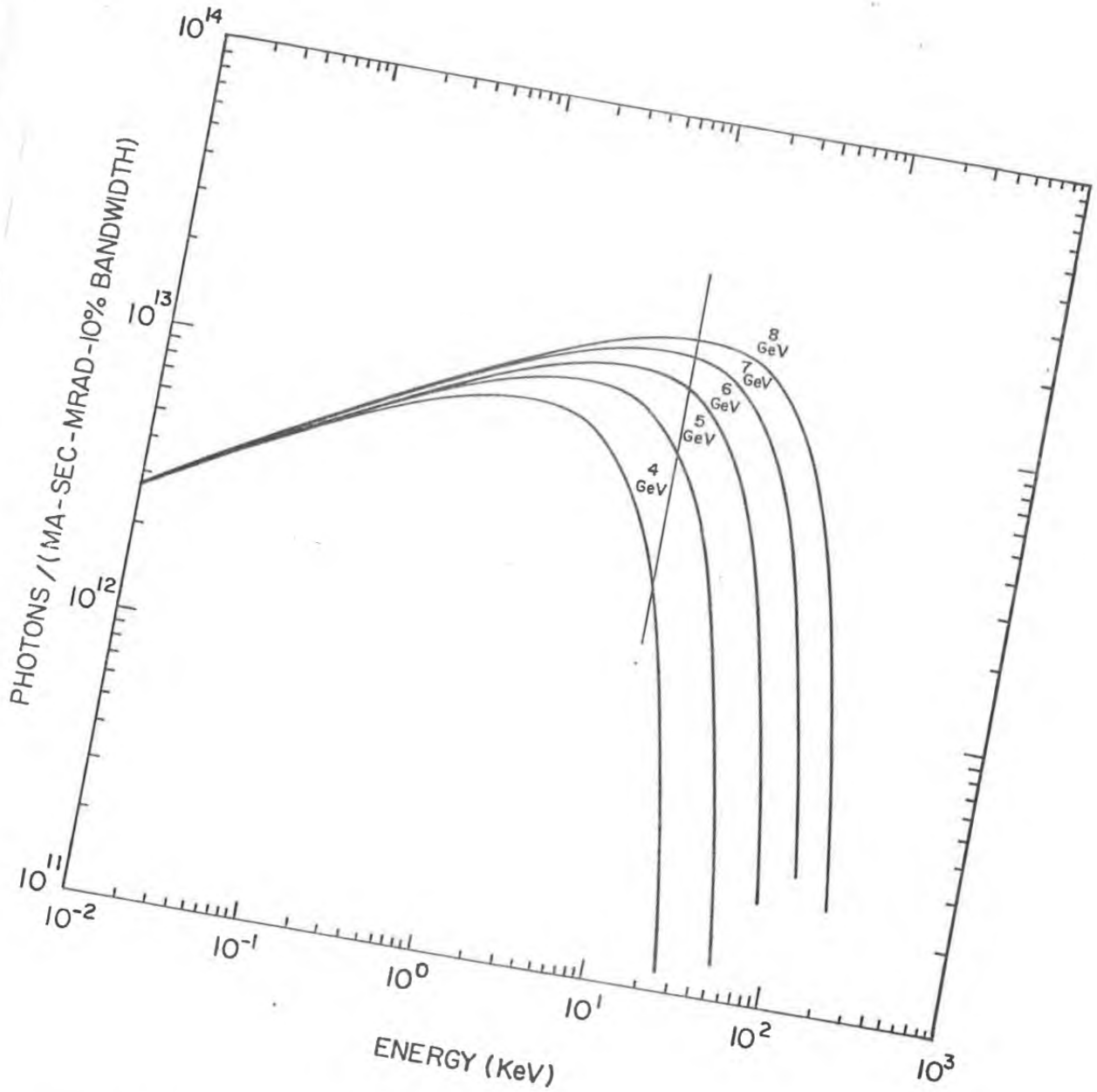

Fig. 12-3 Photon flux at various synchrotron operating energies.

13. Cost and Time Schedule

The detailed cost estimates for the construction of the facility are contained in the following pages. Many of the cost estimates for the technical components are based on prototype designs and actual quotations. The estimates for the conventional construction have been prepared by Sanders and Thomas, Consulting Engineers, Pottstown, Pa. The costs given here do not include those for the research and prototype development work which has already been done or is currently being performed with funds appropriated earlier for this purpose. In particular, the funds already appropriated for the linac modification and for the proto-sector have resulted in a substantial reduction in the totals shown.

A summary is given in Table 13-I which shows both the total cost estimates for each of the subsystems, as well as a break-down for budgetary purposes which is separated by budget year, taking the renewal date as October 1. The details for each of the subsystems is given in Table 13-II. All figures are quoted in January 1977 dollar value, except in the total lines of the summary sheet, Table 13-I, where escalation has been included at the rate of 7 percent per annum for Technical Components and 10 percent per annum for Utilities and Building Modifications.

Table 13-III shows the construction schedule we expect to follow. This schedule is based on the funding schedule shown in Table 13-I. The target date for initial colliding beam studies is October 1, 1979.

Table 13-1

CESR Cost Summary

(Thousands of Dollars - Jan. 1977 Values Except As Indicated)

	1977-78	1978-79	Total
A. Magnet system	1050	100	1150
B. Magnet power supplies	225	-	225
C. R.F.	927	820	1747
D. Vacuum	695	250	945
E. Injection and stacking	204	-	204
F. Controls & instrumentation	730	200	930
A-F. Totals	3831	1370	5201
Escalation, 7%, 10%	268	137	405
Totals with esc.	4099	1507	5606
G. Utilities & construction	1287	0	1287
Escalation 10%	129		129
Total with esc.	1416	1507	1416
A-G. Totals, escalation included	5515	1507	7022
Cornell labor related costs for above	1556	2100	3656
Grand Total, esc. incl.	7071	3607	10678

TABLE 13-II

Cost Detail

Technical Components

(Thousands of Dollars - Jan. 1977 Values)
Cornell In-House Labor Not Included

A. Magnet System	
Bending magnets (mostly in-house fabrication)	654
Quadrupoles (mostly in-house fabrication)	250
Sextupoles	80
Miscellaneous magnet fabrication materials	66
Support system and mounting in tunnel	100
	1,150
B. Magnet Power Supplies	
Quadrupole regulators (components & outside labor)	92
Sextupole regulators	20
Bus work for main supply	34
Bending supply modification and hook-up	20
Supplies for special magnets	59
	225
C. RF System	
DC power supplies	332
Klystrons and sockets	736
Klystron aux. hardware (fil. & mod. transformers, etc.)	70
Combining hardware and control	35
Accelerating structures	88
RF drive and all controls and monitoring	90
RF power distribution (circulators included)	396
	1,747

Cost Detail (Continued)

(Thousands of Dollars - Jan. 1977 Values)

D. Vacuum System	
Vacuum chambers	56
Transition pieces	222
Pumps	395
Valves	85
Instrumentation	72
Bake out and cooling	75
Synchrotron radiation ports	40
	945
E. Injection and Stacking	
Switching and septum magnets	50
Special bending and quadrupole magnets	44
Mechanical components and instrumentation	85
Controls	25
	204
F. Controls and Instrumentation	
Computer Items	
Console and backup computer	
Network lines and mag. tapes	
Unit computers	
DEC-10 Enhancement	
Unit panels and console	271
Linac control hardware	55
CESR control hardware	190
Distributed interface hardware	31
Beam monitoring devices, controls and interfaces	383
	930